

**Tooling Ball Detecting Method
Design for ABB Welding Robot in
Automatic TIG Welding Process**

by

Zhenhao Li

A thesis
presented to the University of Waterloo
in fulfillment of the
thesis requirement for the degree of
Master of Applied Science
in
Mechanical Engineering

Waterloo, Ontario, Canada, 2010

© Zhenhao Li 2010

I hereby declare that I am the sole author of this thesis. This is a true copy of the thesis, including any required final revisions, as accepted by my examiners.

I understand that my thesis may be made electronically available to the public.

Abstract

This thesis provides the design process for a new tooling ball detection method to calibrate moulds in automatic TIG welding. A mechanical component is designed to locate the tooling ball and convert the position information into analog signals. An electrical component is designed to process signals from the mechanical component and achieve the signal communication process. Finally, the computational component is designed and programmed to receive bits from the electrical component and convert information into position values for the tooling ball. The homogeneous transformation process is mathematically modeled for position computation in a robot system.

The method is significantly different from current methods that have been developed and applied. Firstly, it uses a mechanical-touch style operation to locate the tooling ball with only a one-time detection operation. Secondly, it introduces a new approach for utilizing the joystick. Rather than as a manually operated direction controller for mobile control of devices, the joystick is used as a passive detection angle sensor. In order to properly use the joystick as an angle sensor, the joystick calibration method is also designed and tested.

The designs of the three components are all implemented and tested separately. The results of these tests prove the feasibility of the new detecting method; however, the accuracy of detection is not yet acceptable and further improvements need to be made.

In addition, a vision-based detecting method is also discussed at the end of the thesis. Compared to mechanical touch-style detection, the vision-based detecting method is designed to obtain better performance in a high temperature environment and to automate the tooling ball detecting process.

Acknowledgements

I gratefully acknowledge the assistance provided to me by many people during my research.

I especially would like to thank Professor Huissoon for affording me the opportunity to spend two years in Canada as an international student. His invaluable support, knowledge and experience helped guide me through the complexities of mechatronics and Canadian culture. Without his valuable suggestions and insights, I cannot imagine how my two years' research and study would have gone.

I also wish to thank Robert for his excellent machining of all the parts. Without his hard work, all my designs would just be on paper. His experience in mechanical design was very important to my research.

As well, I wish to thank the Department of Mechanical Engineering and Ontario Centers of Excellence for providing me with a world-class study environment.

And to my friends in Canada, especially Jiheng and Zhiyue, Vladimir and Murtasim, I extend a big thank-you for the advice on my research and assistance in my day-to-day life. They have made my time here full of happiness and pleasure.

Finally, I owe my sincere appreciation to my parents. No words could describe how much I love them and no words could describe they've shown their love for me over the past twenty-five years of my life.

I thank everyone for all their help, I truly appreciate it.

Contents

List of Tables	ix
List of Figures	xiii
1 Introduction	1
1.1 Automatic TIG Welding Project	2
1.1.1 Mould Modification and TIG welding	2
1.1.2 Project of Automatic TIG welding	3
1.1.3 Direction of the research	12
1.1.4 Requirements for the New Tooling Ball Detecting Method	15
1.2 Current Methods for Position Measurement	16
1.2.1 Methods Currently Applied in the Project	16
1.2.2 Other Developed Methods	17
1.3 Chapter Summary	19
1.3.1 Brief conclusion of Chapter 1	19
1.3.2 General Description of Other Chapters in the Thesis	19

2	Tooling Ball Detecting Method Design	20
2.1	Basic Rule for Tooling Ball Detecting Method Design	20
2.2	Cell System Design	22
2.3	Mechanical Component Design	23
2.3.1	Analog Biaxial Joystick	24
2.3.2	Detecting Part	27
2.4	Implementation of Mechanical Component	27
2.4.1	Version 1	30
2.4.2	Version 2	33
2.5	Electrical Component Design	36
2.6	Computational Component Design	38
2.6.1	Compute Deflection angles of joystick	41
2.6.2	Compute position of tooling ball in joystick coordinate system	43
2.6.3	Transformation process in tooling ball detecting process	43
2.6.4	Coefficients for Computation	46
2.7	Cell System Integration	46
2.8	Chapter Summary	48
3	Calibration and Detecting Test	49
3.1	NC Milling Machine with Indexing Head & Tooling Ball	50
3.1.1	NC Milling Machine with Indexing Head	50
3.1.2	Tooling Ball	51

3.2	Joystick Calibration	52
3.2.1	Method for Joystick Calibration	54
3.2.2	Result of Joystick Calibration Experiment	68
3.3	Detector Calibration and Testing	72
3.3.1	Objectives of Detector Calibration Experiment	72
3.3.2	Detector Calibration Procedure	75
3.3.3	Transformation Process	78
3.3.4	Method for Data Processing	80
3.3.5	Detector Testing	83
3.3.6	Results of Data Processing	84
3.4	Evaluation and Analysis	89
4	An Extension: Optical Detecting Method Design	95
4.1	Hardware Setting	96
4.2	Optical Characteristics of Tooling Ball	98
4.3	The Reflection Phenomenon	98
4.4	Vision-Based Tooling Ball Detecting Method Design	100
4.4.1	Pre-described Concepts	100
4.4.2	Procedures for Acquiring Position of Tooling Ball in Photos	106
4.4.3	Transformation from Photo Coordinate System to World Coordinate System	107
4.5	Experiment and Result	108
4.6	Chapter Summary	109

5 Conclusion	112
5.1 Thesis Summary	112
5.2 Future Work	115
APPENDICES	116
A Technical Specifications of Joysticks and Tactile Switch	117
B Programs	121
B.1 Program in Microprocessor	121
B.2 RAPID Code for Computational Component	130
Bibliography	137

List of Tables

3.1	Results of Joystick Calibration Experiment	68
3.2	Amplitudes and Phases Offsets of Data in Group 1	71
3.3	Amplitudes and Phases Offsets of Data in Group 2	71
3.4	Ideal Detecting positions of TCP (mm)	78
3.5	Actual Detecting positions of TCP (mm)	81
3.6	Voltage Signal Outputs	81
3.7	Results of Deflection Angle Computation	85
3.8	Results of Detector Calibration Experiment	86
3.9	Average Values of $\delta\theta$, L and Δz at Calibration Positions	86
3.10	Results of Detector Calibration Experiment	88
3.11	Errors of Tooling Ball Position Detection (mm)	89

List of Figures

1.1	Robot Cell Setting for TIG Welding	5
1.2	Working Flow of Robot Automatic Welding in General	8
1.3	Differences Computation	9
1.4	General Description of the Mould Calibration Process	11
1.5	Vertices of the mould	13
1.6	Mould with tooling balls	14
2.1	Cell System for Tooling Ball Detection	22
2.2	Illustration of Tooling Ball Detecting Process	25
2.3	Joystick	26
2.4	Shaft Deflection of the Joystick	28
2.5	Tooling Ball Locating	29
2.6	Mechanical Component of Version 1	31
2.7	the Broken Shaft of Joystick	33
2.8	Mechanical Component of Version 2	34
2.9	Signal Transmission Flow of Tooling Ball Detecting Process	36

2.10	LPC2131 ARM7 Microcontroller with the Development Board EasyARM 2131	37
2.11	Program Flow Chart of ARM7 Microprocessor	39
2.12	RAPID Program Flow Chart	40
2.13	Joystick Coordinate system	42
2.14	Transformation Process in Robot System	44
3.1	Milling Machine	50
3.2	Tooling Ball	51
3.3	Dimension of the Tooling Ball	51
3.4	The output voltage of joystick is proportional to the deflection angle.	52
3.5	Configuration Example of Joystick Coordinate System	53
3.6	Mechanism for Joystick Calibration	55
3.7	Center the tool holder on the steel rod.	57
3.8	Three Coordinate Systems in Joystick Calibration Process	59
3.9	Deflection Angles of Joystick in Calibration Process	62
3.10	Output Voltage Values of Joystick at Two Heights in Joystick Calibration Process	69
3.11	Fit to the Data of Joystick Calibration Experiment	70
3.12	The relationship between L and d	74
3.13	Obtain z value of the tooling ball center by the chuck.	76
3.14	Coordinate Systems in Detector Calibration Process	77
3.15	Positions of TCP for Tooling Ball Detection	79

3.16	Consistency of Angle Computation	84
3.17	$\delta\theta$	87
3.18	L	87
3.19	Δz	88
3.20	Errors of Tooling Ball Position Detection	90
3.21	Relationship between $(\theta_{x1} - \theta_{x2})^2$ and $(\theta_{y1} - \theta_{y2})^2$ and Correspondent Positions of TCP	91
3.22	Relationship Between $\delta\theta$ and Correspondent Positions of TCP on X_m	91
3.23	Relationship Between L and Correspondent Positions of TCP on Y_m	92
3.24	Relationship Between Δz and Correspondent Positions of TCP on Y_m	92
3.25	Relationship between Errors of Position Detection and Correspondent Positions of TCP	93
4.1	Partial Ring Shaped Light Source	96
4.2	Position Relationship among the Camera, Light Source and the Tooling Ball	97
4.3	Reflection Image	99
4.4	Pixel in Photo Coordinate System	100
4.5	Dark Region	104
4.6	Dark Region at the Gap of 'C' Shape	105
4.7	8 Dark Points	105
4.8	9 Types of Same Photos	108
4.9	A Sample Image for Describing Center Deviation	110
4.10	Center Deviation	110

A.1	J1R6AAA00 Copied from: Elobau Sensor Technology	118
A.2	J6R6AAA00 Copied from: Elobau Sensor Technology	119
A.3	B3F5000 Tactile Switch Copied from: Omron Electronic Components LLC	120

Chapter 1

Introduction

In the ABB welding system for automatic TIG welding, the spherical centers of tooling balls can be considered as reference points in robot working space. Place tooling balls on the mould; detect positions of spherical center of tooling balls in robot working space; then, position information can be applied by robot for calibrating the position and orientation of the mould in robot working space. Applying a fast tooling ball detecting method in mould calibration procedure can increase the efficiency.

A fast one-time mechanical touching tooling ball detecting method is developed and the method will be introduced in this thesis. This chapter introduces the background and direction of the research. The automatic TIG welding process for mould modification is first described, and then the mould registration and calibration processes are outlined in detail. Several methods which have been previously applied or developed are considered and compared. Next, a tooling ball detection method designed for use with an ABB welding robot in the mould registration process is proposed. Finally, a brief conclusion of the chapter is provided, together with an outline of the following chapters.

1.1 Automatic TIG Welding Project

1.1.1 Mould Modification and TIG welding

In the mould fabrication industry, moulds are commonly machined from a large billet of expensive tool steel using NC machining, programmed to remove material based on a CAD model of the desired mould cavity. According to the requirements of practice, mould machine always need adjustment. This is because a mould may be not be made to specifications due to a machining error. Materials that are over-machined need to be added and excess materials should be removed. Also when a previous mould design is not suitable and needs to be improved, the mould machined has to be adjusted. Moreover, when an old unused mould is similar to a new mould designed, doing a mould adjustment for the old mould is obviously an efficient choice for time- and cost-saving. As a result, mould adjusting, including removing excess materials and adding missing materials, is necessary and unavoidable in the mould fabrication industry, and the techniques for the mould adjusting process have a great impact on production efficiency. [1]

The mould adjusting process can be achieved by NC machines to remove excess materials and by welding techniques to add missing materials. TIG (Tungsten Inert Gas) welding, also known as GTAW (Gas Tungsten Arc Welding), is a commonly used welding technique. In the TIG welding process, metal is melted by the heat from a current passing between the non-consumable tungsten electrode and the workpiece. During the welding process, inert gas (e.g. argon) is continually provided, preventing materials from reacting with atmospheric contamination. By applying this technique, almost all types of materials can be welded by TIG welding, and the weld is clean and of high quality. Unlike MIG (Metal Inert Gas) welding, there are no pinholes in the welds and no sparks during the welding process. However, tungsten electrodes cannot sustain a high current, the welding speed is limited and becomes time-consuming. According to data from experienced

welders, the speed of MIG welding is about 6lb/hour while the speed of TIG welding in manual operation mode is only 0.5lb/hour. Another reason that limits the efficiency of TIG welding is that it requires skilled welders as it is a labor-intensive process. As a result, in order to increase the efficiency of production while still maintaining the high quality of the weld, methods for automatic robotic TIG welding are now being considered and developed. [2]

1.1.2 Project of Automatic TIG welding

A project called 'Automatic TIG Welding based on ABB Welding Robot' is being developed by Tool-Tec Welding Inc.¹ The project is set up based on automotive mould adjusting task. The automotive mould is made of P-20 tool steel with several projections to be added, while the surface of the desired mould is required to be a Class-A tool steel surface. The actual mould and CAD data of both actual mould and desired mould in 3D CAD software (solidworks for instance) are provided by the customer.

There are three main steps in achieving the task. First, remove materials at the positions where the projections are added in order to obtain a new ground surface. Second, based on this new ground surface, materials are welded to the desired position, with the volume of materials being slightly more than the one desired. Finally, excess materials are removed and the desired surface is achieved.

The welding accuracy and efficiency of the second step are important in saving time and lowering costs. An accurate welding operation makes the excess materials to be removed at the final step as little as possible so that machining time and the cost of welding materials can be maximally reduced. In order to satisfy the requirements of surface quality, the project applies TIG welding as the welding technique used in the second step. A

¹ABB welding robot is the product from ABB company. Details of the robot can be found from <http://www.abb.ca/product/us/9AAC100735.aspx>.

programmable ABB welding robot (robot IRB4450s with robot controller IRC5) is also utilized to automate the welding operation to increase the working efficiency and accuracy.

Working Environment Setting of the Project

Figure1.1 describes the whole setting of the robot cell for TIG welding. There are seven components within the robot cell: ABB Welding Robot, Robot Controller, Mould, Heating Table, Temperature Controller, PC (Robot) and PC (Office).

- ABB Welding Robot & Robot Controller: ABB welding robot IRB4450s and robot controller IRC5 are applied for the welding task. The robot controller contains a user interface called FlexPendant, with which the operator can operate the robot and control the program flow of welding.
- Heating Table, Temperature Controller & Mould:

Tool steel TIG welding for the automotive mould requires the mould to be preheated to a temperature of about $700F^{\circ}$. This temperature should be maintained throughout the whole welding process. Therefore, the mould to be worked on is placed on a heating table designed by Tool-Tec Inc. The heating table generates a flame for heating the mould and the temperature of the mould is reflected to the temperature controller through a temperature sensor. The temperature controller controls the power of the heating table and, according to the temperature setting and mould temperature sensed, the temperature of the mould can be controlled.

The heating table is used to maintain the temperature of the mould instead of heating the mould to the required temperature. The heating table is not able to heat the mould to $700F^{\circ}$. The reason is that the speed of heat missing from large areas of the mould surface is higher than the speed of absorbing heat from the heating table.

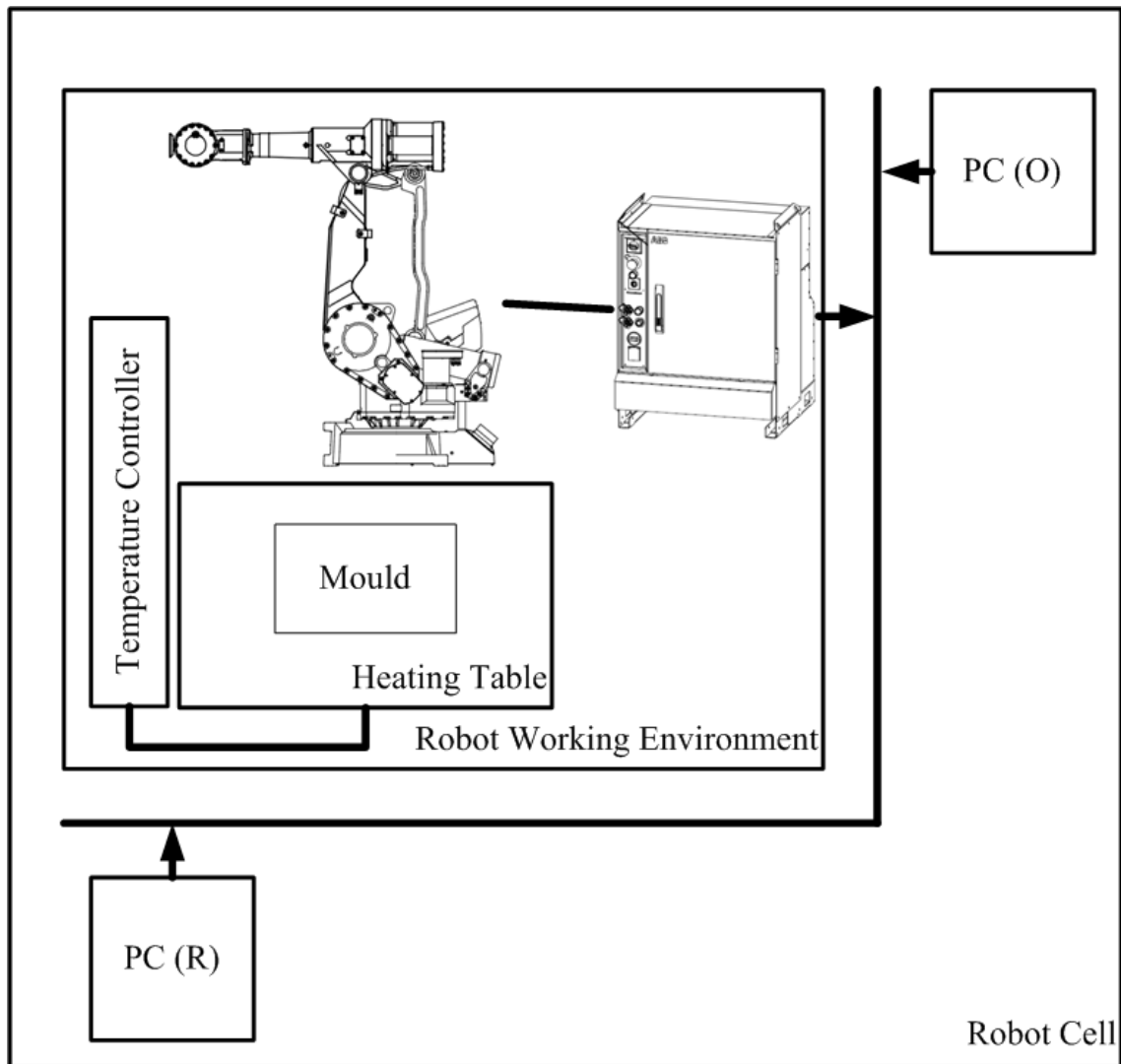


Figure 1.1: Robot Cell Setting for TIG Welding

As a result, the mould is heated in an oven until $700F^{\circ}$ is reached, after which, the mould is moved to the heating table to be worked on.

- PC (Robot) and PC (Office): PCs are used for robot programming, welding tool path planning and welding parameters controlling. There are two PCs: one is placed in the robot's working environment for direct robot programming and control, and the other one is placed in the office (for engineers) for off-line programming, simulating and working status monitoring.

Spaces and Coordinate Systems in ABB Robot System

There are two spaces in a robot system: one is robot space representing the actual working space of the robot and the other is CAD space which is a virtual space in 3D CAD software. Space can be numerically described by a coordinate system in the form of coordinate values (x, y, z) . There are five coordinate systems defined in the ABB robot system: the base coordinate system, the world coordinate system, the tool coordinate system, the workpiece coordinate system and the user coordinate system. Definitions of each coordinate system can be found in the ABB robot user manual: they are not mentioned here. [3] The relationship among different coordinate systems in robot space can be described by homogeneous transformation. [4]

- World coordinate system and base coordinate system ($F_{world} : X_w - Y_w - Z_w$)

Since there is only one ABB robot in the project, the world coordinate system and the base coordinate system coincide with each other, and both are to be called the world coordinate system. The world coordinate system can be used to describe the position information of robot space.

- Workpiece coordinate system ($F_{workpiece\ or\ CAD} : X_c - Y_c - Z_c$)

The workpiece coordinate system located on the mould and the CAD data of workpiece (mould) in 3D CAD software are described based on the workpiece coordinate system. The workpiece coordinate system can be used to describe the position information of CAD space.

- Tool coordinate system ($F_{tool} : X_t - Y_t - Z_t$)

The robot system is able to have several different tool coordinate systems at the same time representing information of different tools applied. Take the welding task, for example. A torch for TIG welding is designed and mounted on the sixth axis of the robot, so there is a tool coordinate system representing the torch. The torch moves with the robot arm and the pose of the torch in robot space can be described by the pose of its tool coordinate system in the world coordinate system. ²

- User coordinate system ($F_{user} : X_u - Y_u - Z_u$)

The user coordinate system is located on the heating table and its pose in the world coordinate system represents the location of the heating table in the robot space.

Working Flow of Welding Task

Figure 1.2 describes the main flow of the working process for the robot's automatic TIG welding task. There are six main sections: Difference Computation, Path Generation, Welding Process Simulation, Welding Parameters Adjusting, Mould Calibration and Automatic Welding.

- Differences Computation:

Figure 1.3 describes the differences computation process briefly.

²Word 'pose' in the thesis represents position and orientation.

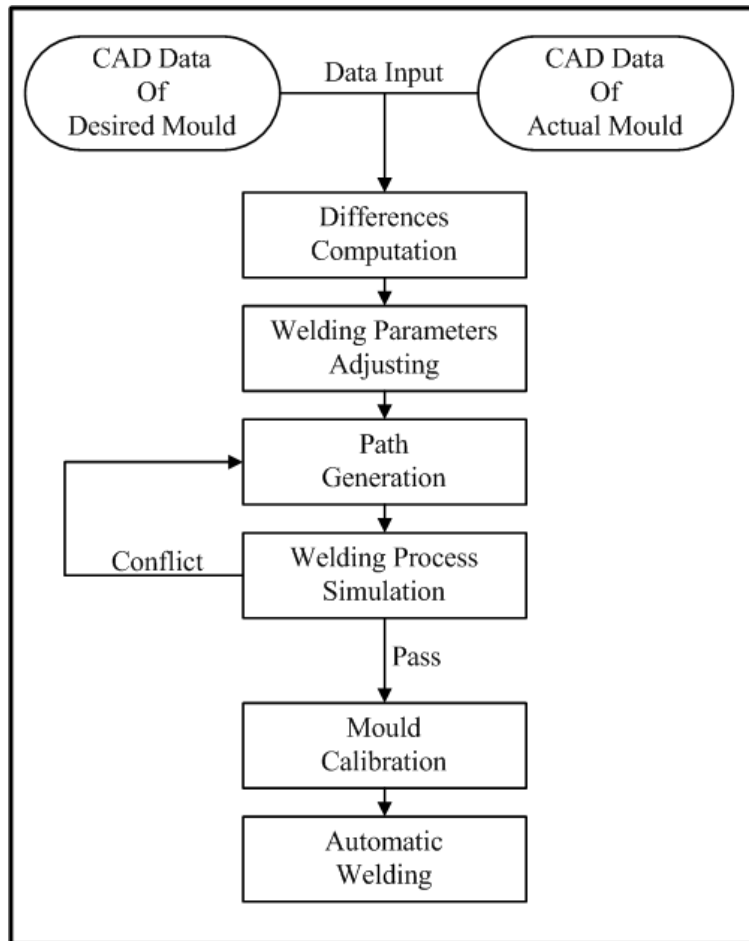


Figure 1.2: Working Flow of Robot Automatic Welding in General

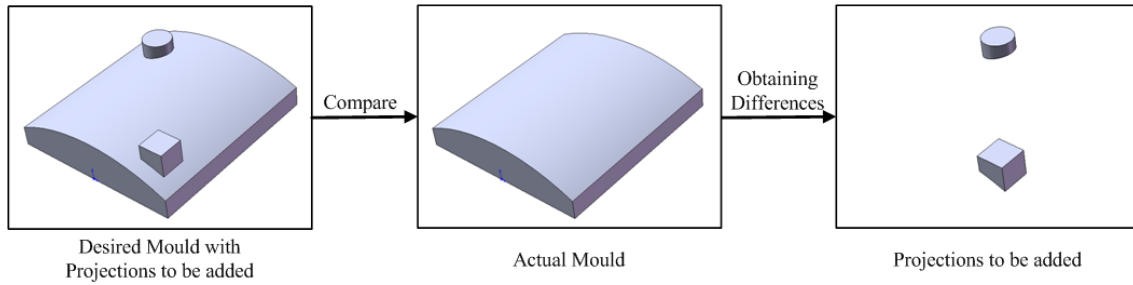


Figure 1.3: Differences Computation

Compare actual mould data with ideal mould data and obtain the differences simply by subtracting with the 3D modeling software Solidworks. There is a customized application called robot designer developed for the purpose of achieving this computing process. The data of differences are position information of materials to be welded. The position data is located within CAD space.

- Welding Parameters Adjusting:

Skilled welders achieve the TIG welding task manually using traditional manual operation mode based on experience. However, in the automatic welding process, the human experiences of welding techniques should be transferred into welding parameters for automated robot welding operation control. According to actual welding practices and manual welding experience of welders, parameters such as feed rate of filler metal, voltage and current supplied for arc generation, welding angle of the torch, moving speed of robot arm and so on are decided after large numbers of welding experiments and a mathematical model is created for the welding task. Using such a mathematical model of welding parameters, a welding tooling path can be set up in the next step.

- Path Generation:

After obtaining the differences data and setting welding parameters, the welding

paths for the robot in the welding process are generated. The differences data are usually several pieces of 3D solid parts and the can be formed by welding layer by layer. As a result, the robot designer separates the 3D solid into several layers and then separates the layers into welding paths that are connected with each other. The robot works following these paths and the solid piece can be formed.

- Welding Process Simulation:

Welding simulation is necessary for analyzing programs of robot control to avoid conflicts in the actual welding process. If conflicts arise in the simulation process, the actual welding task can not be carry out and the welding tool path should be rebuilt until the simulation pass.

- Mould Calibration:

The mould calibration process aims to obtain the transformation matrix from the CAD coordinate system in the CAD space to the world coordinate system in robot space. Within the project, the SVD algorithm based on least square method developed by Arun et al.[5] is applied in solving the calibration problem.

$\{P_i^{SpaceName}\}$ means a point set in space *SpaceName*. The first step of the mould calibration procedure is to select several reference points on the surface of the mould in CAD space, obtaining the point set $\{P_{iRef}^{CAD}\}$. Next, the operator operates the robot arm carrying the detecting tool to detect reference points in robot space and obtaining the point set $\{P_{iRef}^{robot}\}$ under the condition of existing detecting error V_{iRef} . The algorithm supposes that there is a fixed linear relationship between positions of points in robot space and in CAD space represented by Equation 1.1. R is a rotation matrix and T is a translation matrix. $\{P_i^{CAD}\}$ is the point set in CAD space and $\{P_i^{robot}\}$ is the point set in robot space corresponding to $\{P_i^{CAD}\}$. Since the existence of the detecting error, the point sets $\{P_{iRef}^{CAD}\}$ and $\{P_{iRef}^{robot}\}$ can be fitted

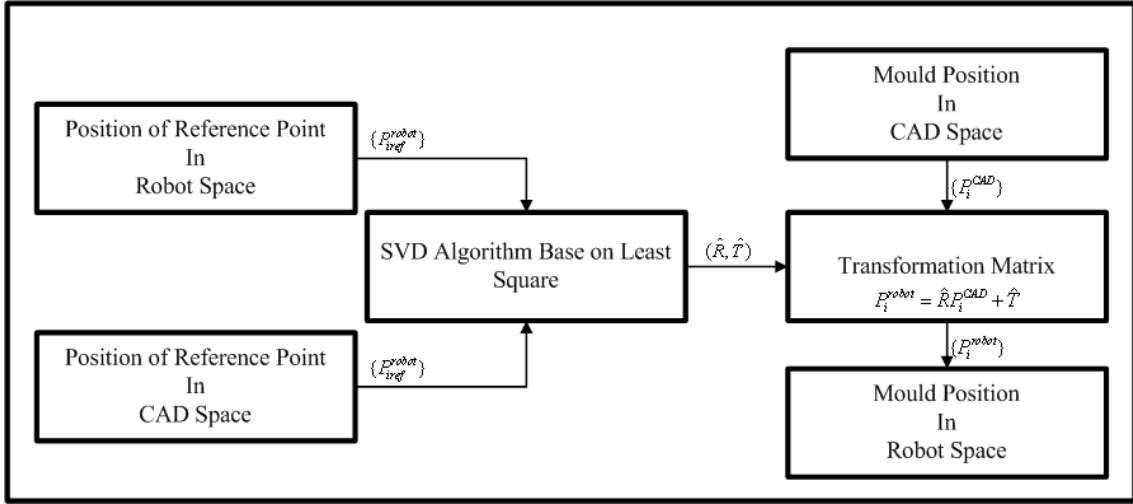


Figure 1.4: General Description of the Mould Calibration Process

into an improved Equation 1.2 in solving the optimal transformation matrixes \hat{R} and \hat{T} instead of R and T . Finally, All points in the point set $\{P_i^{CAD}\}$ can be transformed into point set $\{P_i^{robot}\}$ using Equation 1.3 and \hat{R} and \hat{T} are the target transformation matrices. The mould calibration process is illustrated in Figure 1.4.

$$P_i^{robot} = RP_i^{CAD} + T \quad (1.1)$$

$$P_{iRef}^{robot} = RP_{iRef}^{CAD} + T + V_{iRef} \quad (1.2)$$

$$P_i^{robot} = \hat{R}P_i^{CAD} + \hat{T} \quad (1.3)$$

- Automatic Welding:

After finishing all the five previous procedures, the robot knows what is to be welded and how the welding works should be carried out. Then robot starts doing the actual

welding process following the programs in the robot controller, and finishes the TIG welding task automatically.

1.1.3 Direction of the research

There are two types of reference points that are usually selected in the mould calibration process. They are spherical centers of tooling balls and vertices of the mould itself (intersection points of edges, for instance). Figure 1.5 and figure 1.6 illustrate vertices and tooling balls. In figure 1.5, *A*, *B*, *C* and *D* are four vertices of the mould. The mould is symmetric and thus, there are four vertices in another side of the mould are also required to be selected as reference points. The tooling ball in figure 1.6 is specified by figure 3.2 in page 51.

Vertices are easier to detect because they can be found directly at the point using a detecting pin. However, it may confuse the operator in the reference point detecting process when the mould surface is complicated with large quantities of vertices in high intensity. On another hand, a tooling ball is easy for the operator to capture but it can only be detected in an indirect way, as the reference point of a tooling ball is the spherical center which is a point located inside the solid. Considering the terrible working environment of welding, if a detecting tool for a detecting tooling ball with high efficiency can be applied for the mould calibration process for reference points detecting, incorrect detecting operation could be avoided and the efficiency of the calibration process will be improved.

As a result, this research aims to develop a tooling ball detecting method for the mould calibration process of automatic TIG welding system. Applying this detecting method, a robot controller should know the position of the tooling ball in the world coordinate system. The efficiency of the tooling ball detecting process should increase with the new method and the detecting accuracy should locate within the range of requirement.

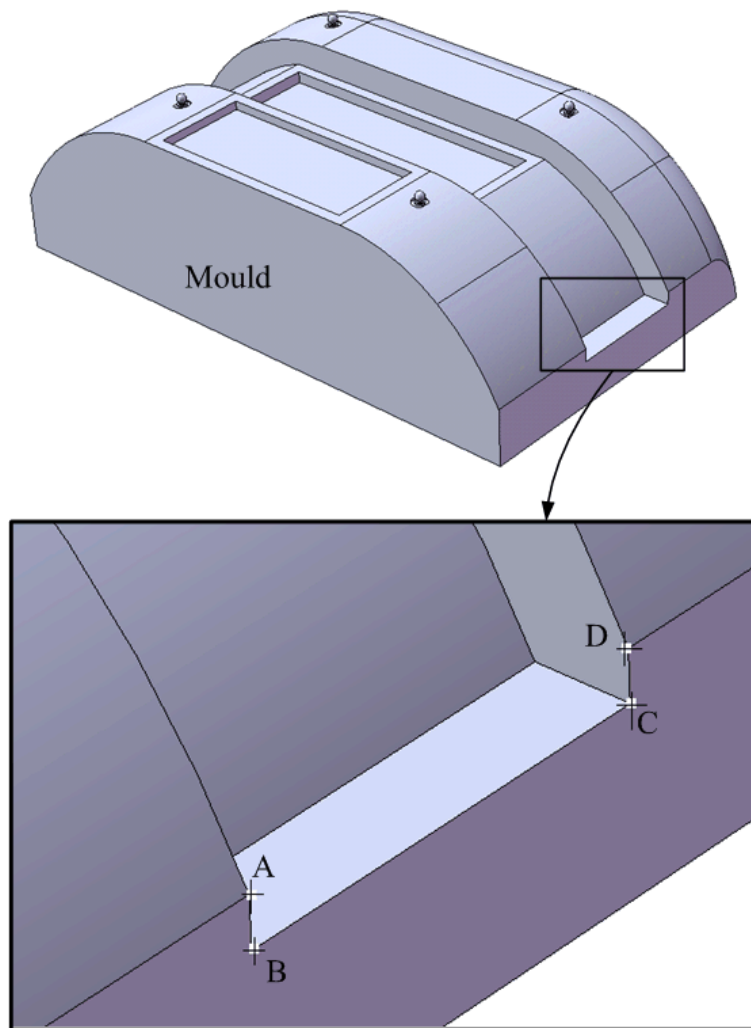


Figure 1.5: Vertices of the mould

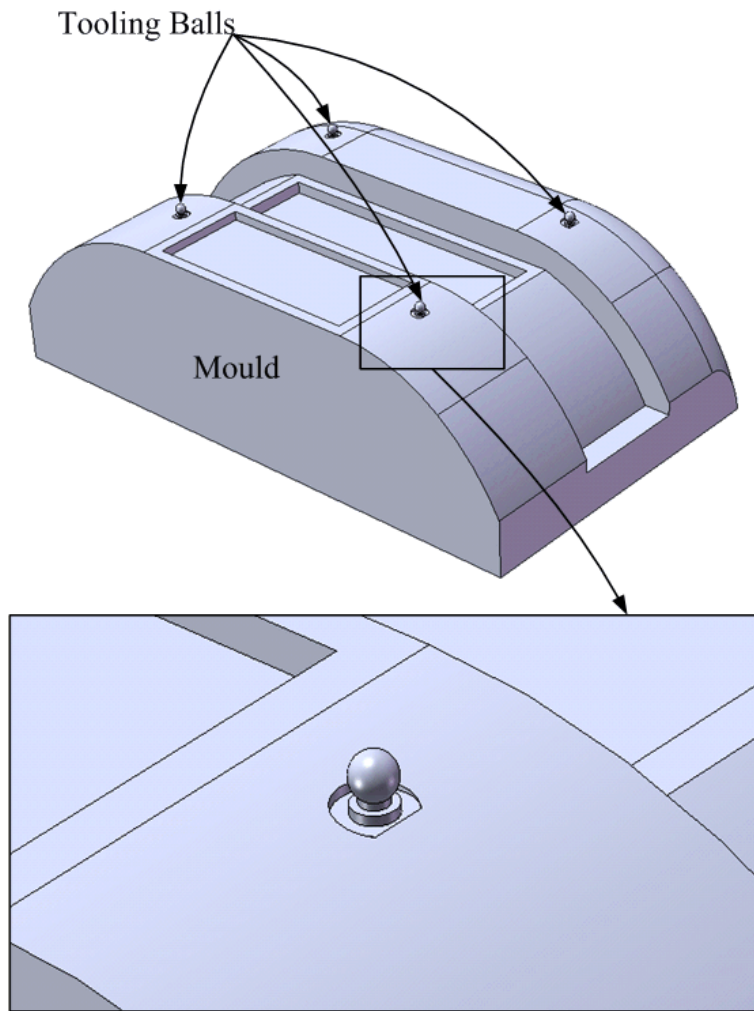


Figure 1.6: Mould with tooling balls

1.1.4 Requirements for the New Tooling Ball Detecting Method

The following requirements are considered in the research process.

- Work robustly in a heavy-duty working environment of TIG welding:

High temperature, dusty air, strong illumination from surrounding welding works, high possibility of causing impact by collision between robot arm and objects are five main factors that have negative effects on the tooling ball detection process. The new tooling ball detecting method should avoid being effected by these factors.

- Be able to be integrated with the whole system of automatic TIG welding:

The new tooling ball detecting method is designed for the Automatic TIG Welding system and therefore, the design should be able to be easily integrated into the whole system.

- Strike a balance among detecting accuracy, detecting efficiency and the cost of the product:

The accuracy of robot motion is 1mm on three axes of the world coordinate system. Base on the experimental results in the mould calibration process, calibration results which are obtained from setting a vertex as the only type of reference point is acceptable. This means that the accuracy of the new detecting method for tooling ball spherical center detection should be the same as for vertex detection by a detection needle which is still 1mm on each axis.

Currently, the tip of a tungsten electrode is used to detect the vertex and the accuracy is the same as for robot motion. Therefore the accuracy for tooling ball detection is required to be 1mm on three axes of the world coordinate system.

- Be able to be applied in a different calibration application:

As a product design, the detector should not be limited to the project of TIG welding but should be applicable to other types of applications, such as the CNC machine calibration process. As a result, the additional value of the detector itself can be increased.

1.2 Current Methods for Position Measurement

1.2.1 Methods Currently Applied in the Project

- Ball Surface Point Detecting by Tungsten Electrode Applying 4–point Method:

There is a sharp tip at the end of the tungsten electrode in TIG welding. The position of the tip in the world coordinate system can be directly read by the robot controller so that it can be utilized as a point detector. The position of the sphere can be computed by its surface points (at least four points). Therefore, if four surface points of the tooling ball can be detected by the tip of the tungsten electrode, spherical center of the tooling ball can be figured out (4–point method, [6]).

This is the easiest tooling ball detecting method that can be applied for tooling ball detection in an ABB robot system. A tungsten electrode is needed for TIG welding in the entire working process and there is no need to mount any other detecting tools. The detecting operation is simple for operators, especially when the operator is familiar with robot operation.

However, this method is time-consuming because of the four times' detecting operation required and its detecting accuracy is difficult to control because it is hard to make touching judgements (whether the tip of the electrode touches the surface or not) and also because it is difficult to control the position of surface points that are detected. According to the analysis in [6], the most accurate result of detection can

only be obtained when four detecting points form a regular polyhedron and this is impossible for operators to achieve by operating the ABB robot. On the another hand, the high temperature of the mould (about $700F^{\circ}$) is dangerous for operators working around it for long periods of time, especially for work requiring careful operation.

- High accuracy probe:

As an improvement for the 4–point method using tungsten electrode as a point detector, a high accuracy probe is applied to take the place of the electrode. The probe is able to generate touched/not-touched digital signal as feed back information to the robot controller. Once the tip of the probe touches the surface of the tooling ball, the feed back signal is generated immediately to let the robot arm stop moving. Touching status is judged by the feedback signal rather than by the eyes of operator. Though the reliability of touching status judgment is enhanced by using the high accuracy probe, time for the detecting operation is not reduced. The probe is expensive (about \$5000), and the feeding speed of the robot arm’s movement has to be set at the slowest level (0.1mm/increment) to protect the probe from collision. Also because the working temperature range of the probe is $257F^{\circ}$ (which is much lower than the temperature of the mould), the probe can be applied only when the mould is cold.

1.2.2 Other Developed Methods

Currently, methods for tooling ball detecting can be divided into three types: mechanical touching, optical sensor detecting, and vision-based object recognition. The mechanical touching method is seldom considered because of its low accuracy compared to the other two. Methods of optical sensor detecting ([7] [8] [9] [10] [11]) and vision-based object recognition ([12] [13]) have their own advantages:

- There is no contact between the device and targets so collisions are avoided.
- The detecting accuracy is higher than in mechanical touching methods.
- Detecting targets are not limited by their physical characteristics. For example, not only spherical objects can be detected but also other types of objects (cube, sheet, etc) can be recognized.

However, there are also disadvantages in the application environment of this project:

- High accuracy is always related to strict requirements about operation and working environment. The working environment and requirements about ball detecting operation cannot satisfy requirements of applying optical sensors or vision devices.
- Considering the accuracy requirement of tooling ball detection, optical sensing or vision-based methods are too accurate which is not necessary.

As a result, the mechanical touching method is chosen to be developed because of the following advantages:

- The method for position computation is deterministic.
- Mechanical components are cheaper and more robust than optical sensors and vision devices.
- Applying standard parts, the mechanical touching style detector can be easily repaired when some components are broken.

In conclusion, in light of the shortcomings of current methods that have been developed and applied, it is valuable to develop a new mechanical touching style tooling ball detector for mould calibration of the automatic TIG welding process.

1.3 Chapter Summary

1.3.1 Brief conclusion of Chapter 1

In conclusion, this research will develop a mechanical contact style tooling ball detector for an ABB welding robot in the mould calibration process of automatic TIG welding. The detector should be able to sustain a high temperature working environment within the time of operation and the position of the tooling ball's spherical center detected by the detector should be sufficiently accurate according to the requirements of the mould calibration process. The operation and cell system design of the detector should be suitable to be integrated by the whole TIG welding system. And finally, under the condition of achieving the calibration task in the project of automatic TIG welding, the adaptability of the design to other applications should be considered.

1.3.2 General Description of Other Chapters in the Thesis

Chapter 2 describes the whole designing process. The design of mechanical component, electrical component and computational component are introduced in detail. Chapter 3 describes the calibration process of the joystick and the detector. A simulation of the tooling ball detecting process based on the design in Chapter 2 is also described and, according to the results of the simulation, the new tooling ball detecting method is evaluated. As an extension and comparison between optical and mechanical detection methods, a simple optical detecting method utilizing reflection image forming of light source is given and discussed in Chapter 4. Finally, Chapter 5 concludes the research with an overall summary, conclusions, and thoughts towards future works.

Chapter 2

Tooling Ball Detecting Method Design

This chapter introduces the design of the new tooling ball detecting method for the mould calibration process of the automatic TIG welding task. First, the basic rule for designing the detecting method is given. Next, the cell system for tooling ball detection, which is the structure of whole designing process, is described. Third, three components in the cell system are described separately in detail. Finally, some points about integrating the cell system with the automatic TIG welding system are discussed.

2.1 Basic Rule for Tooling Ball Detecting Method Design

The target of research is to design a new tooling ball detecting method for an ABB welding robot in the mould calibration process of automatic TIG welding. The position of the tooling ball's spherical center in the world coordinate system is to be computed and

transmitted to the robot controller. Coordinate systems transform from one to another following the rule of homogeneous transformation, which is also the basic rule for designing the new detecting method. Coordinate systems utilized in the tooling ball detecting process are mentioned again.

- World coordinate system ($F_{world} : X_w - Y_w - Z_w$)
- Tool coordinate system ($F_{tool} : X_t - Y_t - Z_t$)

All tools that are applied in the robot system are described by their own tool coordinate system $F_{tool}^i : X_{ti} - Y_{ti} - Z_{ti}$ and every time after mounting a tool, the tool should be calibrated to let robot know the pose of the tool coordinate system in the world coordinate system. The origin of the tool coordinate system is defined as the Tool Center Point (TCP) and both of the position of TCP and the orientation of the tool coordinate system can be read by the robot controller directly.

Suppose the position of a point P in F_{world} is $P^w = \begin{pmatrix} x_P^w & y_P^w & z_P^w & 1 \end{pmatrix}^T$. A tool is currently applied in robot system with tool coordinate system F_{tool} with position of TCP in F_{world} as $TCP^w = \begin{pmatrix} x_{TCP}^w & y_{TCP}^w & z_{TCP}^w & 1 \end{pmatrix}^T$. Position of P in F_{tool} is $P^t = \begin{pmatrix} x_P^t & y_P^t & z_P^t & 1 \end{pmatrix}^T$. The robot arm is operated such that the directions of all the axes of F_{tool} coincide with the direction of the axes of F_{world} . According to homogeneous transformation, we have Equation 2.1.

$$P^w = \begin{pmatrix} x_P^w \\ y_P^w \\ z_P^w \\ 1 \end{pmatrix} = T_{wt} P^t = \begin{pmatrix} 1 & 0 & 0 & x_{TCP}^w \\ 0 & 1 & 0 & y_{TCP}^w \\ 0 & 0 & 1 & z_{TCP}^w \\ 0 & 0 & 0 & 1 \end{pmatrix} \begin{pmatrix} x_P^t \\ y_P^t \\ z_P^t \\ 1 \end{pmatrix} \quad (2.1)$$

Matrix T_{wt} is the transformation matrix from F_{world} to F_{tool} with only a translating process without rotation. The transformation matrix defines the pose of F_{tool} in F_{world} .

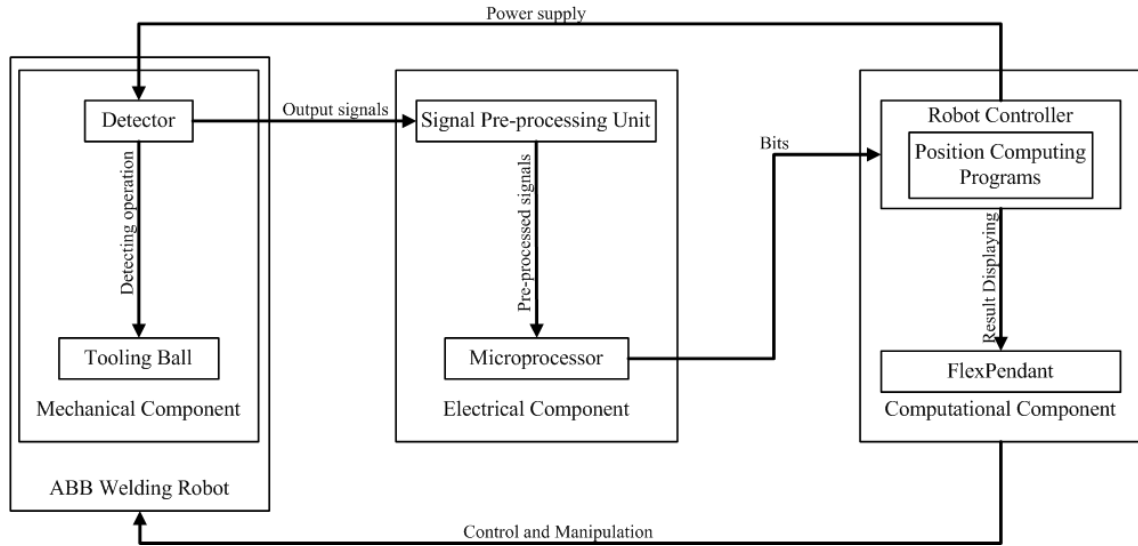


Figure 2.1: Cell System for Tooling Ball Detection

Consider the position of tooling ball in F_{world} as point P in Equation 2.1. Then if the position of the tooling ball in F_{tool} is known, the position of the tooling ball in F_{world} can be computed. This is the basic rule for the tooling ball detecting method design.

2.2 Cell System Design

The flow chart in Figure2.1 describes the cell system designed for tooling ball detecting in the robot system.

There are three components in the cell system: the mechanical component, the electrical component and the computational component. The mechanical component contains a detector that is mounted on the sixth axis of the robot arm for tooling ball detection. The power to run the detector comes from robot controller (USB port for 5 volts voltage output). The operator operates the robot arm to detect the tooling ball and the detector generates output signals describing the position of the tooling ball with respect to the

detector. Output signals are transmitted into the electrical component which contains a signal pre-processing unit and a microprocessor with a piece of development board.

The target of the electrical component is to let the robot controller know the content of the output signals, value of voltage signal outputs, for instance. Because the robot controller has a COM1 port for serials communication, output signals can be converted into bits and sent to the robot controller by serial channels. The pre-processing unit adjusts the original output signals into a suitable status for the microprocessor to receive. The microprocessor achieves both the signal conversion task and the serial communication task.

The last component is the computational component, which translates output signals into position information and computes the position of the tooling ball using programs programmed in the controller. The results of position computation are displayed on the LCD screen of FlexPendant.

The design of each component is carried out according to the flow chart in Figure2.1 described in detail in following sections.

2.3 Mechanical Component Design

The task of mechanical component design is to design a detector in order to obtain position information of a tooling ball with respect to the detector. The detector is mounted on the sixth axis of the robot arm as one of the tools applied in the robot system. It has its own tool coordinate system, detector coordinate system $F_d : X_d - Y_d - Z_d$. All the position information with respect to the detector is described in F_d .

The detector is designed as an analog biaxial joystick with a detecting part mounted on the deflection shaft.¹ The detecting part has a tactile switch that can be activated by a sliding mechanism to generate a digital signal output showing the status of detection.

¹The idea to use a biaxial joystick came from professor Jan Huissoon.

The detecting process is illustrated in Figure 2.2 and details of the joystick and detecting part are given in the following paragraphs. Before detecting the ball, the detector is set vertical to the plane $X_w - O_w - Y_w$ of the world coordinate system and moved to a position that allows the tooling ball to be located within the detecting range. Next, the detector is dropped down as a ball detecting process. The tooling ball tangent contacts with the cone's inner surface of the detecting part and slides to the center position. Finally, once the spherical center of the tooling ball coincides with the center axis of the joystick's shaft, the tangent points between the cone's inner surface and the ball surface forms a tangent circle and the tooling ball is properly located. In order to ensure the locating status, the detector keeps being dropped down until the tactile switch is activated by a sliding mechanism and the detecting process is finished. A compressing spring is applied to the sliding mechanism to ensure the cone's inner surface keeps contact with the ball's surface.

2.3.1 Analog Biaxial Joystick

An analog biaxial joystick is a type of sensor that converts mechanical values (deflection angles of the shaft) into analog voltage signals. As the joystick coordinate system shown in Figure 2.3, the shaft deflects about X_j, Y_j and the origin of the coordinate system O_j is the deflection center. Z_j coincides with the center axis of the shaft when the shaft locates at the center position with no deflection. Once the shaft is deflected, the joystick emits voltage signals representing deflection angles of the two axes. The shaft deflects about each axis in a range of $[-\alpha, +\alpha]$ and there is a linear input-output relationship that is described by Equation 2.2.

$$V_{out} = k\theta_{in} + V_c \quad (2.2)$$

k is the slope of the line and there is $k = (V_{max} - V_{min})/2\alpha$. V_{out} is the output voltage, V_{max} is the maximal output voltage when the shaft is deflected to angle $+\alpha$ and V_{min} is

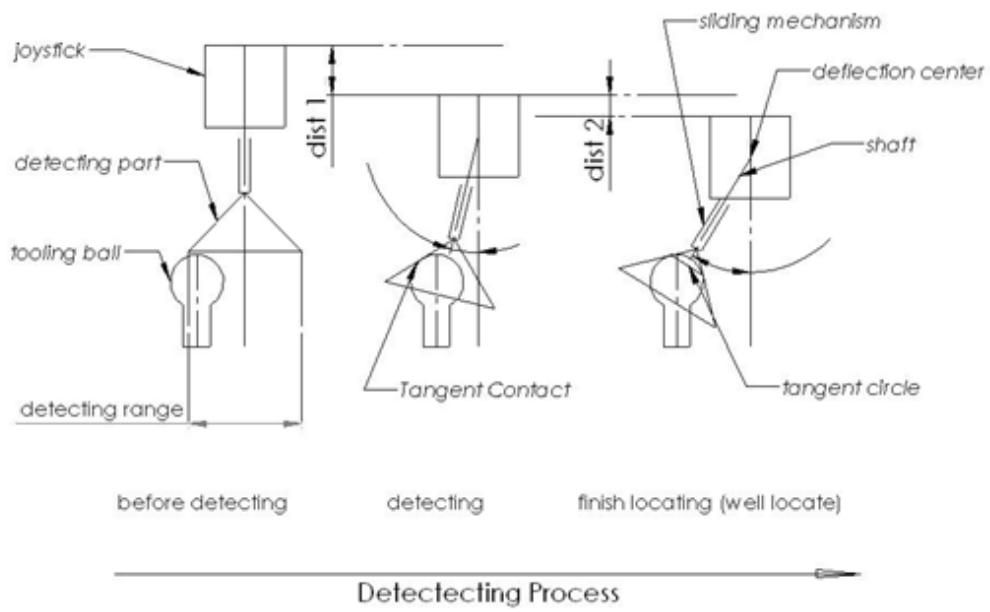


Figure 2.2: Illustration of Tooling Ball Detecting Process

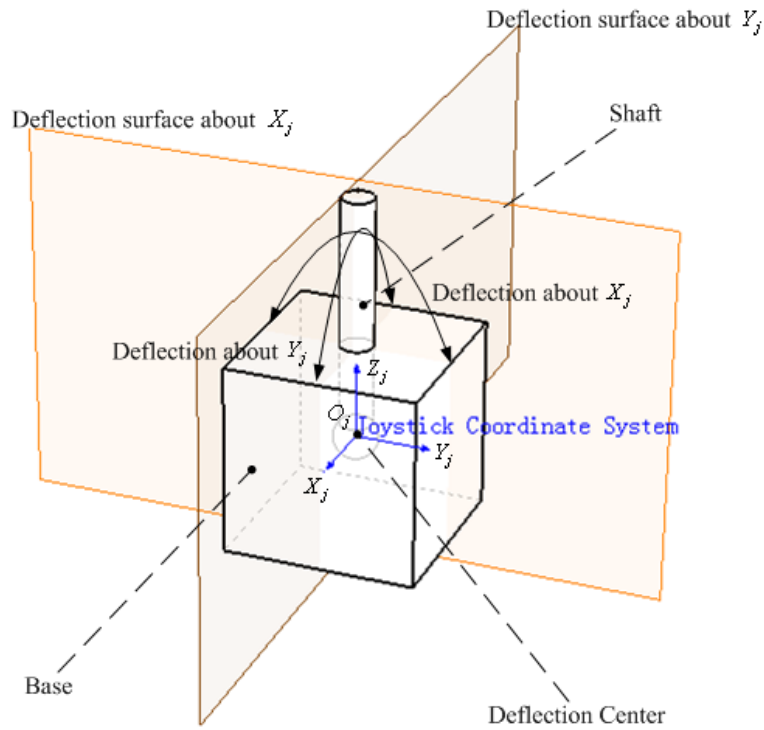


Figure 2.3: Joystick

the minimal output value when the shaft is deflected to angle $-\alpha$. V_c is the output voltage when the shaft is not deflected.

According to the voltage outputs that represent deflection angles of the shaft about X_j and Y_j , it is easy to compute the position of a point that locates on the center axis of the shaft. As shown in Figure 2.4, θ_x and θ_y are deflection angles of about X_j and Y_j that are obtained from output voltage signals. P is a point located on the center axis of the shaft and the distance from O_j to P is L . (L is positive when P located on X_j^+ , vice versa.) The position of P in joystick coordinate system can be computed by Equation 2.3.

$$P^j = \begin{pmatrix} x_P^j \\ y_P^j \\ z_P^j \\ 1 \end{pmatrix} = \begin{pmatrix} L \cos(-\theta_x) \sin \theta_y \\ L \cos \theta_y \sin(-\theta_x) \\ L \cos(-\theta_x) \cos \theta_y \\ 1 \end{pmatrix} \quad (2.3)$$

If we let the spherical center of a tooling ball be located on the center axis of the shaft which is the same condition as the point in Figure 2.4, according to Equation 2.3, the position of the tooling ball's spherical center within the joystick coordinate system can be computed. Also, the transformation from the joystick coordinate system to the detector coordinate system is decided when the whole detector is manufactured and assembled, and the position of the tooling ball in the detector coordinate system can be figured out. Locating the ball to the center axis of the shaft is the task of the detecting part, as described in next paragraph.

2.3.2 Detecting Part

Figure 2.5 illustrates the tooling ball locating method of the detecting part. Only when the tooling ball is properly located can the compressing spring start being compressed until the digital signal is activated. After finishing the detecting process and lifting the detector, the compressing spring is released and goes back to the original status.

2.4 Implementation of Mechanical Component

There are two design versions of design for implementing the mechanical component, as discussed below.

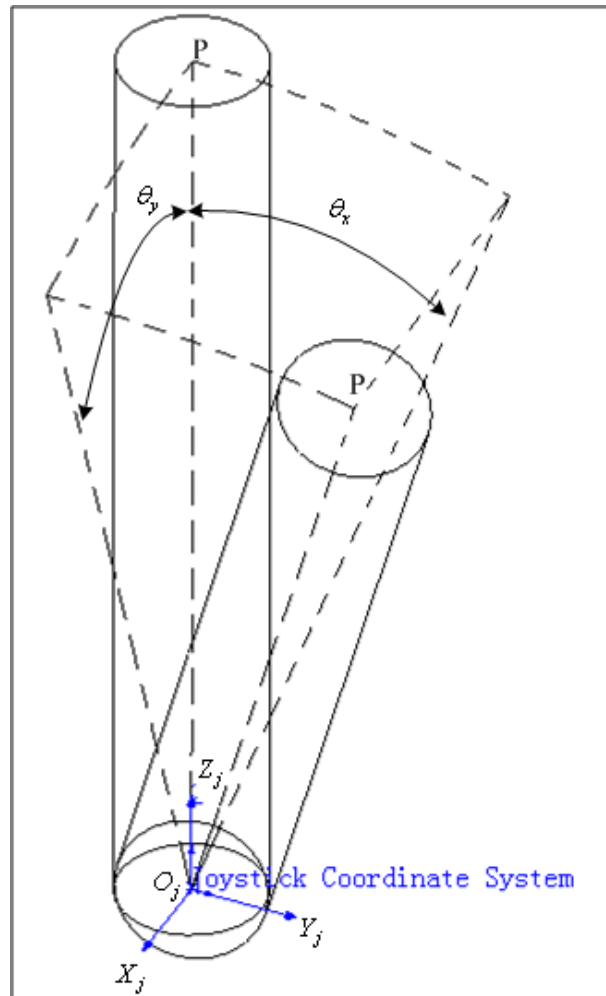


Figure 2.4: Shaft Deflection of the Joystick

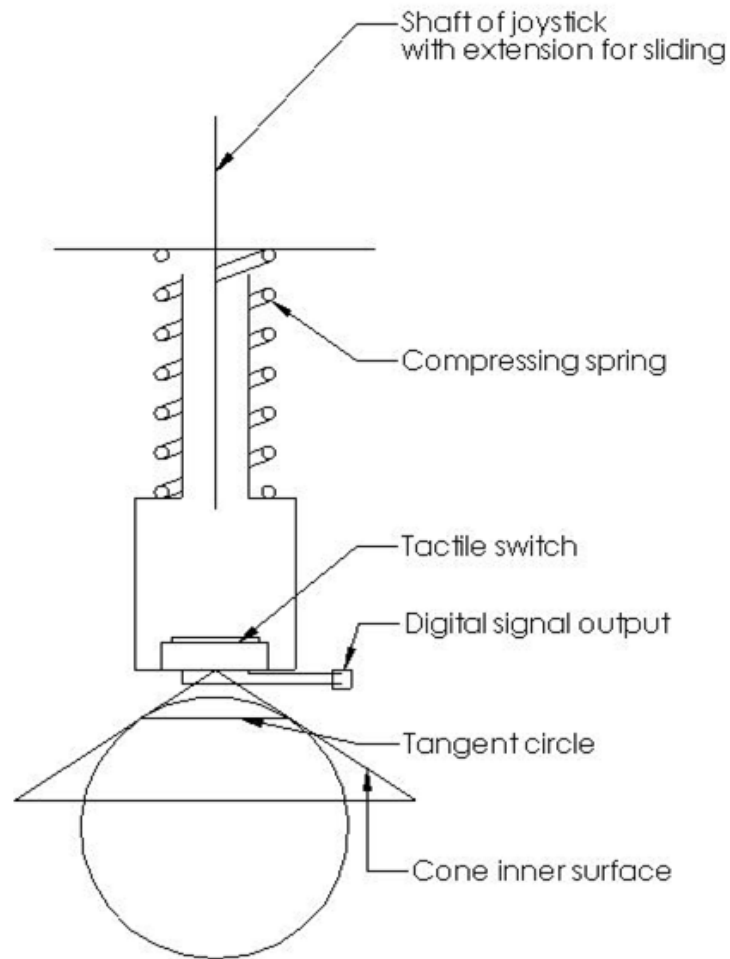


Figure 2.5: Tooling Ball Locating

2.4.1 Version 1

Figure 2.6 illustrates the mechanical component of version 1.

Parts within Figure 2-6 are listed below:

Part 1: Joystick Mounting Base

Part 2: Joystick

Part 3: Connecting Cap

Part 4: PCB

Part 5: Tactile Switch

Part 6: Distance Fixing Part

Part 7: Locking Nut 1

Part 8: Locking Nut 2

Part 9: Linear Motion Bearing

Part 10: Cone Part

Part 11: Outer Compressing Spring

Part 12: Outer Spring Position Fixer

Part 13: M3 Nut

Part 14: M3 Washer

Part 15: M3-40 Socket Head Cap Screw

Part 16: Inner Compressing Spring

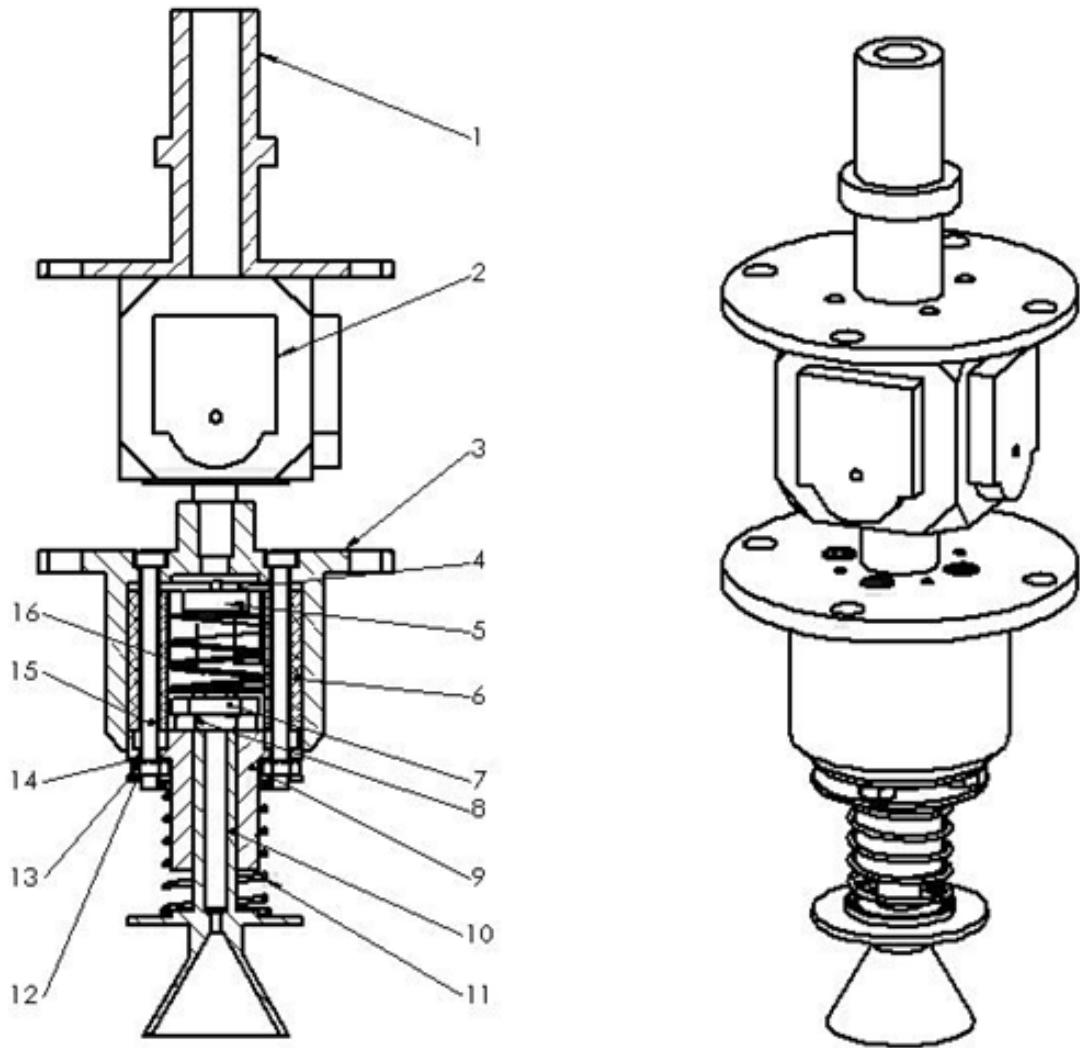


Figure 2.6: Mechanical Component of Version 1

Joystick that is applied in version 1 is J1 series joystick purchased from Elobau Sensor Technology. The technical specifications of the joystick are provided in AppendixA. Part 5, the tactile switch, is the B3F-5000 one purchased from Omron Electronic Components LLC. Its technical specifications are provided in AppendixA.

Feature description

The joystick mounting base is made of brass and thread-connected with the sixth axis of the robot arm. The angular operating range of the joystick is $\pm 15^\circ$. The joystick is fixed to the joystick mounting base through thread holes at the bottom of the base. The shaft of the joystick is threaded and the connecting cap is thread-connected with the shaft.

A linear motion bearing is applied to achieve a sliding movement. The cone part is made of steel and inserted into the bearing to enable the sliding movement. The space in the connecting cap for the cone part to slide is kept at a distance by a distance fixing part. The inner compressing spring is applied to activate the tactile switch which is soldered onto the PCB. Once the cone part slides in, the spring is compressed until the elastic force of the spring reaches the activating force of the switch and the digital signal is generated. Another compressing spring is applied outside the bearing to enable it to return to a sliding position. The bearing, the connecting cap and the distance fixing part are connected by four pairs of M3 Socket Head Cap Screws and M3 nuts.

Analysis of the design

Generally speaking, the design of version 1 achieve the target function. However, two defects regarding assembly, detecting durability and detecting accuracy are not able to be overlooked. Firstly, the shaft of the joystick is not strong enough to sustain repeated tooling ball detecting operation and assembly tasks. The shaft was broken already when

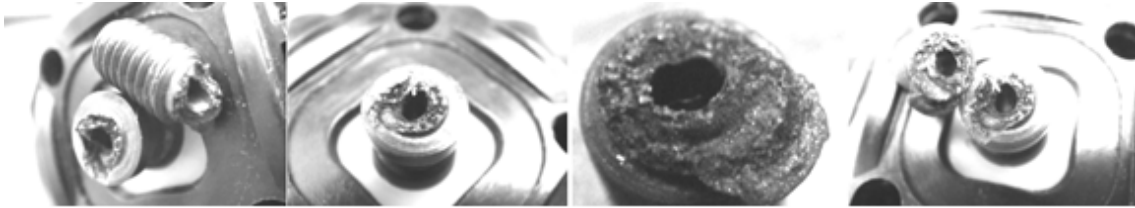


Figure 2.7: the Broken Shaft of Joystick

it was threaded with the connecting cap in the assembling process. The broken position is at the shoulder of the shaft which can be seen in Figure2.7.

When the connecting cap is connected with the shaft, the threaded connection generates axial tension force and tangential force on the shaft by the connecting cap. When the connecting cap stops at the shoulder of the shaft, the tension force will increase sharply if the tread keeps being tightened. The shaft is made of engineering plastic and the increased force is much higher than the maximal force allowed of the shaft. However, the design is not able to control the tightness of threading to avoid the increased force.

The other defect is a weakness related to distance control. The distance between the deflection center of joystick and the ball center is a very important coefficient for ball position computation. However, the threaded connection between the shaft and the connecting cap is not able to control the tightness of the threading so that the distance is not fixed. This will have negative effects on computing the position of the tooling ball.

As a result, improvements should focus on these two defects. The second version of the mechanical component design is given in the next section, with improvements on the defects.

2.4.2 Version 2

Figure2.8 illustrates the mechanical component of version 2.

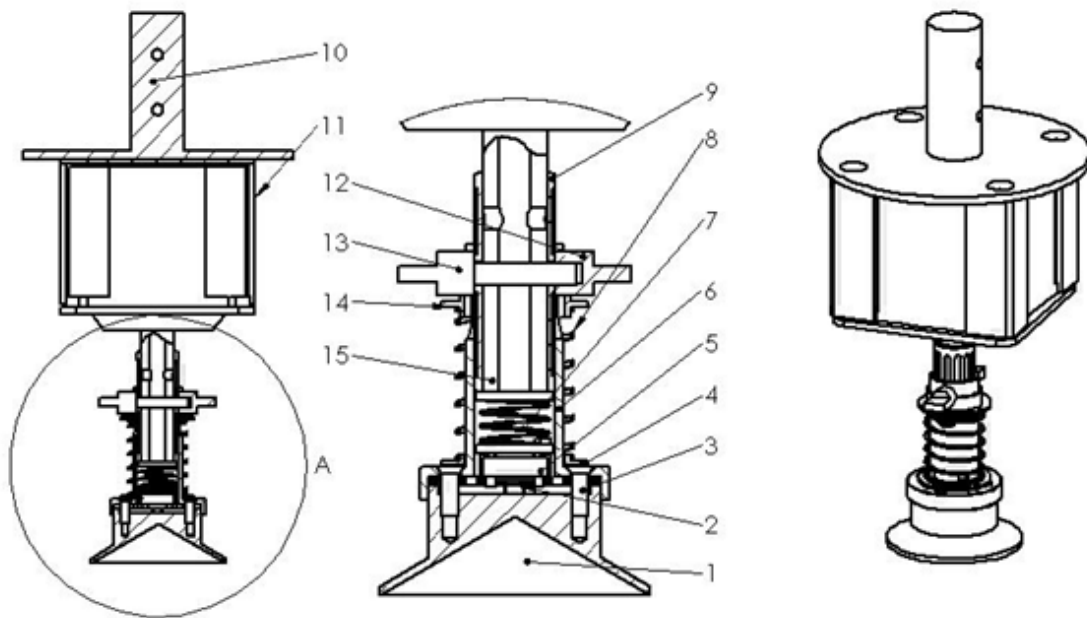


Figure 2.8: Mechanical Component of Version 2

Parts within Figure2.8 are listed below:

Part 1: Cone Part

Part 2: PCB

Part 3: M3 Counter Sunk Screw

Part 4: Bottom Spring Fixer

Part 5: Tactile Switch

Part 6: Sliding Part

Part 7: Inner Compressing Spring

Part 8: Outer Compressing Spring

Part 9: Brass Pushing

Part 10: Joystick Mounting Base

Part 11: Joystick Mounting Post

Part 12: Stopper 1

Part 13: Stopper 2

Part 14: Top Spring Fixing

Part 15: Joystick

Joystick that is applied in version 2 is J6 series joystick purchased from Elobau Sensor Technology. The technical specifications of the joystick are provided in AppendixA. Part 5, the tactile switch, is the B3F-5000 one purchased from Omron Electronic Components LLC. Its technical specifications are provided in AppendixA.

Feature description

The joystick mounting base is made of 1045 steel and connected with the sixth axis of the robot arm through the cylinder. The position of the joystick mounting base with the robot arm is fixed by those two threaded holds. The angular operating range of the joystick is $\pm 25^\circ$ and the joystick is fixed to the joystick mounting base and the joystick mounting post through four M5 counter sunk screws at the four corners of the joystick. A pusher made of brass is fixed to the shaft of joystick by stopper 1 and 2. The sliding part slides on the pusher and its position is fixed by the outer compressing spring and two stoppers. The cone part is connected to the sliding part by three M3 counter sunk screws and the PCB is fixed between the sliding part and the cone part with the tactile switch soldered on. The method for generating the digital signal is the same as the method in version 1.

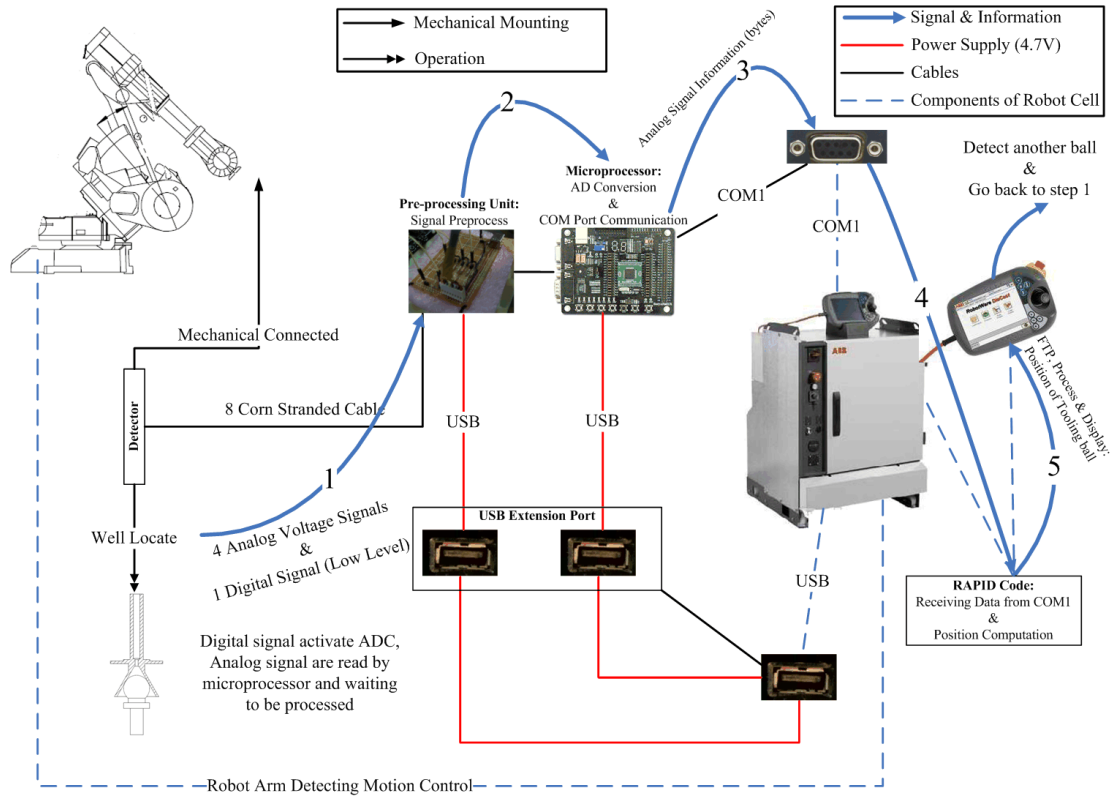


Figure 2.9: Signal Transmission Flow of Tooling Ball Detecting Process

Analysis of the design

The design of version 2 achieves the target functions without the deficiencies which occurred in version 1. The tooling ball is properly located and the satisfactory performance of the J6 joystick increased the effects of the ball locating operation. The experiments and testing process of the J6 joystick and the detector of version 2 will be introduced in Chapter 3.

2.5 Electrical Component Design

Figure 2.9 illustrates the signal transmission flow of the tooling ball detecting process.

From the Figure 2.9, we can see that there are five output signals of the mechanical

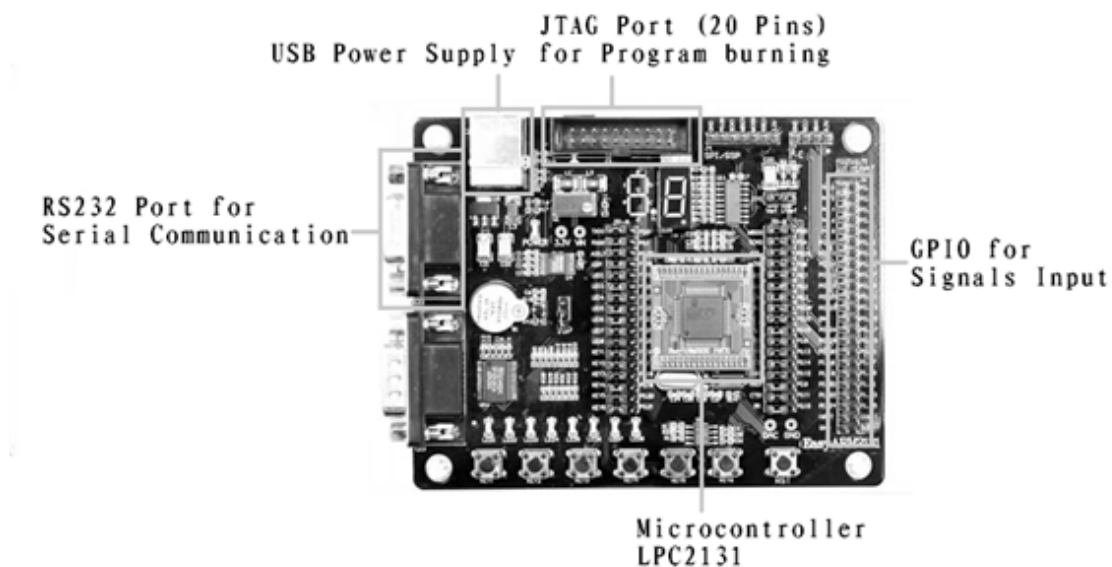


Figure 2.10: LPC2131 ARM7 Microcontroller with the Development Board EasyARM 2131

component: one digital signal from the tactile switch and four analog voltage signals from the joystick. The electrical component should let the robot controller know the value of the four voltage signals when the digital signal is generated. Therefore, two processes are required to achieve the target: the AD conversion process and the communication process. They are to be implemented by a Philips LPC2131 ARM7 microprocessor based on the development board EasyARM 2131 which is developed by Zhouligong Microcontroller Development Co. Ltd (Figure2.10).

Voltage signals are input into the development board from GPIO (General Purpose I/O) and converted into bits by the AD converter that is integrated into the microprocessor. From the serial port of the development board, bits are sent to the robot controller through the COM1 port and read by programs within the robot system.

The values of four voltage signals range between 0.55V and 4.95V when the supply voltage is 5.5V (the maximal input voltage of the joystick). The convertible voltage value

of the AD converter is from 0V to 2.48V because the reference voltage of the development board is 2.48V [14]. As a result, output voltage signals from the joystick should be decreased into half (0.275V to 2.475V) before being input into the microprocessor from GPIO. This is achieved by the pre-processing unit.

The digital signal from the detecting part is considered as the External Interrupt to the microprocessor. Once the interrupt is activated, the detector stops detecting the ball and AD converter starts converting the voltage signals into bits.

UART (Universal Asynchronous Receiver/ Transmitter) that is integrated into the microprocessor can be utilized for serial communication. There is also a COM1 port in the robot controller for serial communication. The microprocessor and the robot controller can communicate with each other through RS232 Cables, and bits converted by the AD converter can be obtained by the robot controller.

The program that is burned in the microprocessor is provided in AppendixB and the program flow chart is shown in Figure2.11.

2.6 Computational Component Design

The computational component designed contains two layers. The first layer is designed for data processing, which is implemented by programs programmed in the robot controller. The second layer is the computing layer which is designed for position computing utilizing known parameters. The second layer is inserted into the first layer. The first layer's operating data that is required in the second layer. The program flow chart is given in Figure2.12 and details of the program are provided in AppendixB.

In order to compute the position of the tooling ball in the second layer, bits representing output voltage values of the joystick received from the microprocessor are first read and translated into the deflection angles of the joystick. Next, according to Equation 2.3, the

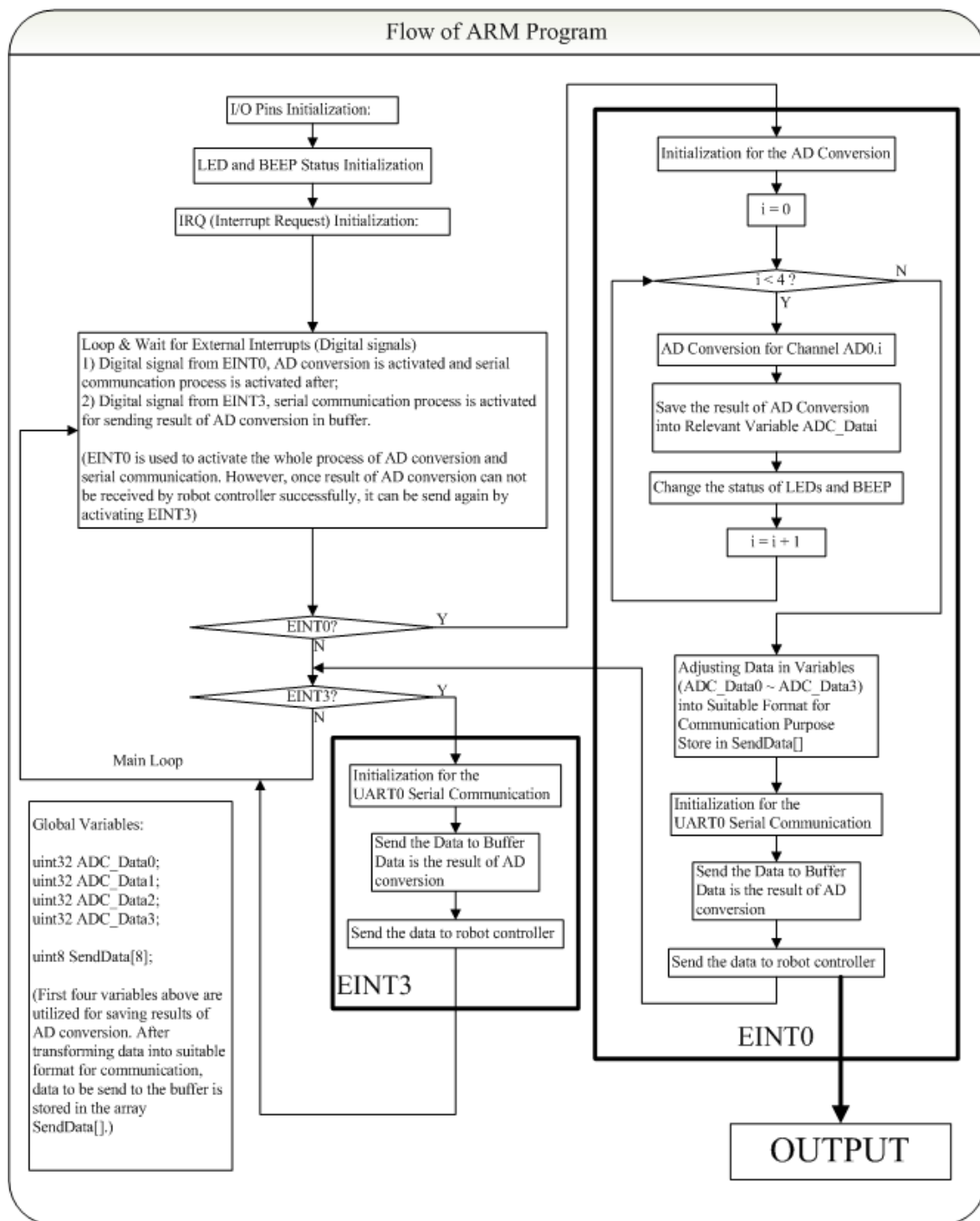


Figure 2.11: Program Flow Chart of ARM7 Microprocessor

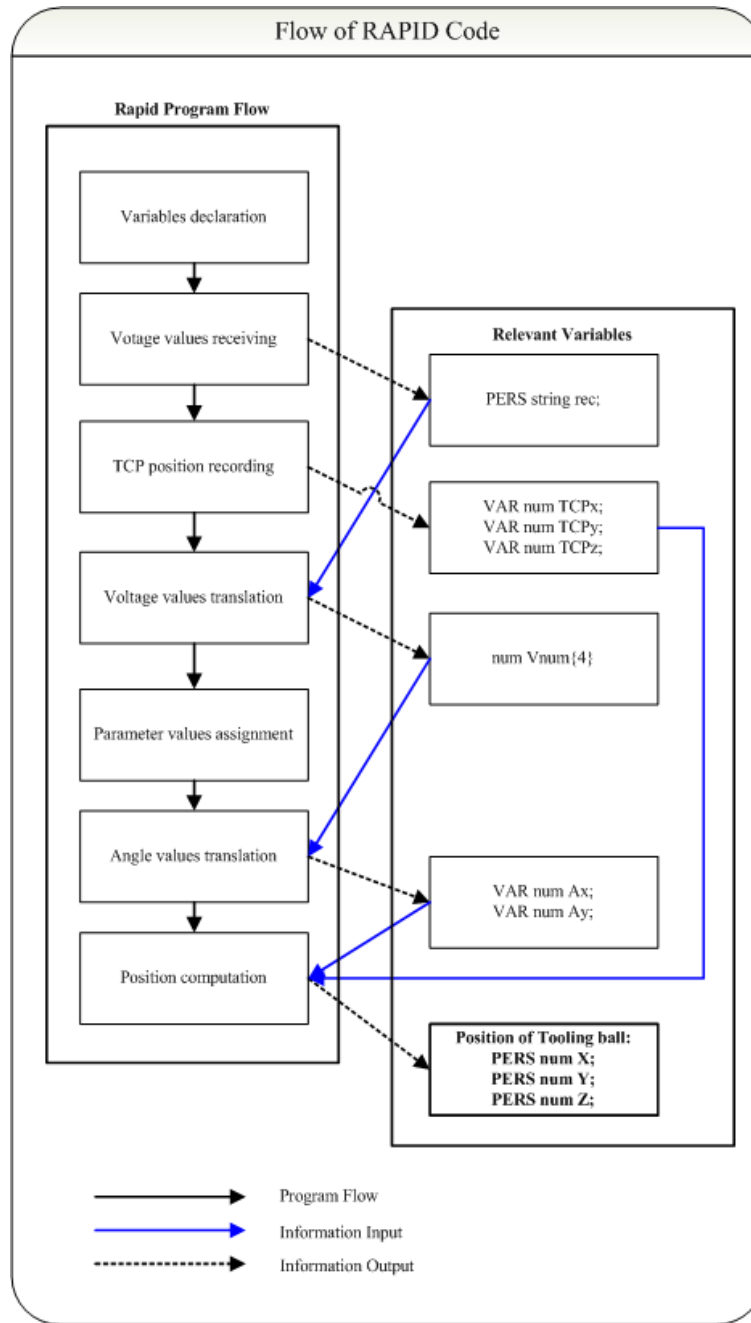


Figure 2.12: RAPID Program Flow Chart

position of the tooling ball in relation to the joystick is computed according to the values of deflection angles. Third, according to the transformation in the tooling ball detecting process, the position of the tooling ball in the world coordinate system is computed as the final result. The final result of computation is saved into memory for the mould calibration process of TIG automatic welding and, the results display the result on the screen of FlexPendant to be checked by the operator.

2.6.1 Compute Deflection angles of joystick

Values of four output voltage signals of joystick are firstly read from the microprocessor. Define joystick coordinate system as which is shown in Figure2.13. There is a group of output voltage signals V_{out}^{x1} , V_{out}^{x2} , V_{out}^{y1} and V_{out}^{y2} for a detecting process received from microprocessor. V_{out}^{x1} is the voltage value of signal 1 for X_j and V_{out}^{x2} is the voltage value of signal 2 for X_j . V_{out}^{y1} is the voltage value of signal 1 for Y_j and V_{out}^{y2} is the voltage value of signal 2 for Y_j .

Output voltage values are proportional to the deflection angle. Slopes of each signal k_{x1} , k_{x2} , k_{y1} , k_{y2} and output voltage values at center position V_c^{x1} , V_c^{x2} , V_c^{y1} , V_c^{y2} are obtained from joystick calibration experiment which is described in Chapter 3. Then according to Equation 2.2 we have:

$$\theta_{x1} = (V_{out}^{x1} - V_c^{x1})/k_{x1} = \Delta V^{x1}/k_{x1} \quad (2.4)$$

$$\theta_{x2} = (V_{out}^{x2} - V_c^{x2})/k_{x2} = \Delta V^{x2}/k_{x2} \quad (2.5)$$

$$\theta_{y1} = (V_{out}^{y1} - V_c^{y1})/k_{y1} = \Delta V^{y1}/k_{y1} \quad (2.6)$$

$$\theta_{y2} = (V_{out}^{y2} - V_c^{y2})/k_{y2} = \Delta V^{y2}/k_{y2} \quad (2.7)$$

θ_{x1} is the deflection angle about the axis X_j computed from signal 1 and θ_{x2} is the deflection angle about the axis X_j computed from signal 2. θ_{y1} is the deflection angle

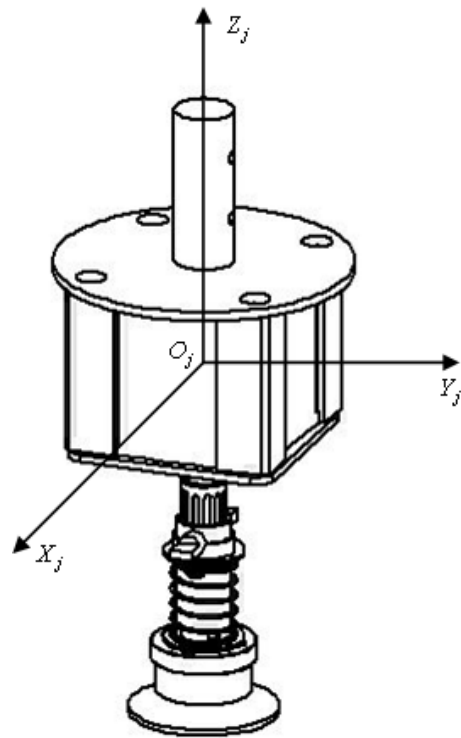


Figure 2.13: Joystick Coordinate system

about the axis Y_j computed from signal 1 and θ_{y2} is the deflection angle about the axis Y_j computed from signal 2.

Then deflection angle about the axis X_j is $\theta_x = (\theta_{x1} + \theta_{x2})/2$ and deflection angle about the axis Y_j is $\theta_y = (\theta_{y1} + \theta_{y2})/2$.

2.6.2 Compute position of tooling ball in joystick coordinate system

According to the setting of the joystick coordinate system in Figure2.13, once the tooling ball is appropriately located by the detector, Equation 2.3 can still be applied to compute the position of the tooling ball in the joystick coordination system. L is the distance form the deflection center of the joystick (the origin of the joystick coordinate system) to the spherical center of the tooling ball. It is a negative value.

2.6.3 Transformation process in tooling ball detecting process

The transformation process in the robot system among coordinate systems is shown in Figure2.14.

There are three coordinate systems in the process of tooling ball detection: the world coordinate system $X_w - Y_w - Z_w$, the tool coordinate system $X_t - Y_t - Z_t$ and the joystick coordinate system $X_j - Y_j - Z_j$. P is the spherical center of a tooling ball. The transformation process from a world coordinate system to a joystick coordinate system is described by the following two transformations.

From $X_w - Y_w - Z_w$ to $X_t - Y_t - Z_t$, there is a translation which is described by transformation matrix in Equation 2.8.

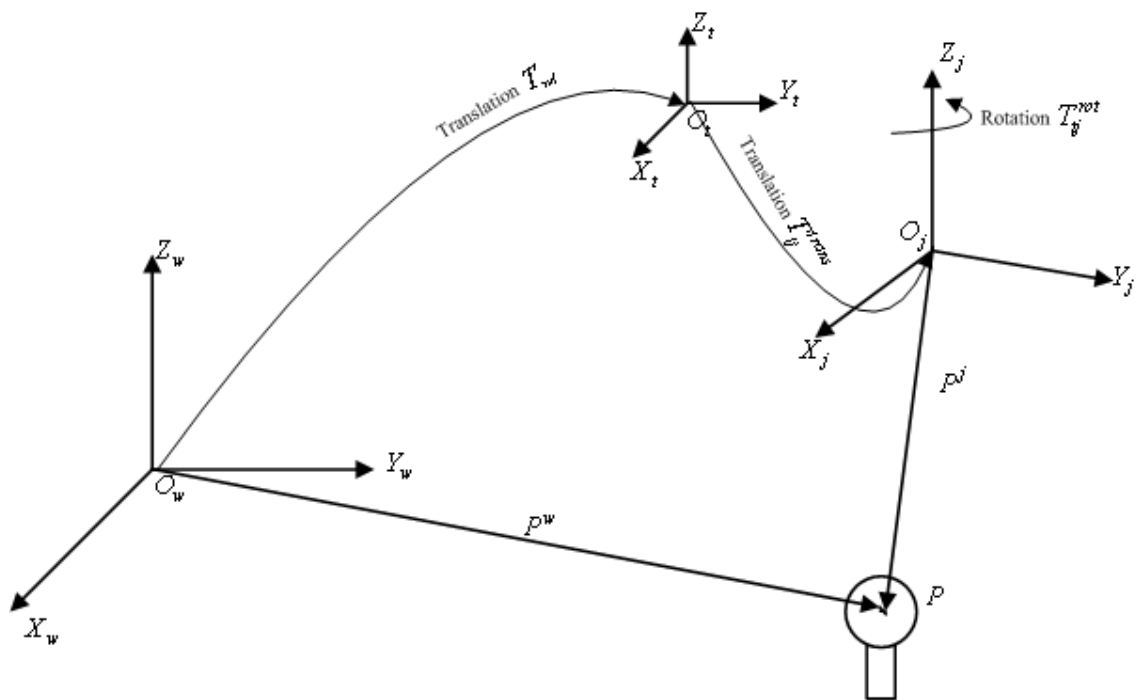


Figure 2.14: Transformation Process in Robot System

$$T_{wt} = \begin{pmatrix} 1 & 0 & 0 & x_{TCP}^w \\ 0 & 1 & 0 & y_{TCP}^w \\ 0 & 0 & 1 & z_{TCP}^w \\ 0 & 0 & 0 & 1 \end{pmatrix} \quad (2.8)$$

From $X_t - Y_t - Z_t$ to $X_j - Y_j - Z_j$, there is a translation followed by a rotation about the axis Z_j , which are described by transformation matrixes in Equation 2.9.

$$T_{tj} = T_{tj}^{trans} T_{tj}^{rot} = \begin{pmatrix} 1 & 0 & 0 & \Delta x \\ 0 & 1 & 0 & \Delta y \\ 0 & 0 & 1 & \Delta z \\ 0 & 0 & 0 & 1 \end{pmatrix} \begin{pmatrix} \cos \delta\theta & -\sin \delta\theta & 0 & 0 \\ \sin \delta\theta & \cos \delta\theta & 0 & 0 \\ 0 & 0 & 1 & 0 \\ 0 & 0 & 0 & 1 \end{pmatrix} \quad (2.9)$$

Describes the position of a tooling ball's spherical center in the world coordinate system by $P^w = \begin{pmatrix} x_P^w & y_P^w & z_P^w & 1 \end{pmatrix}^T$. Describes position of a tooling ball's spherical center in the joystick coordinate system by $P^j = \begin{pmatrix} x_P^j & y_P^j & z_P^j & 1 \end{pmatrix}^T$. They can be converted to each other in accordance with the relationship set forth in Equation 2.10.

$$\begin{aligned} P^w &= T_{wt} T_{tj} P^j \\ &= \begin{pmatrix} 1 & 0 & 0 & x_{TCP}^w \\ 0 & 1 & 0 & y_{TCP}^w \\ 0 & 0 & 1 & z_{TCP}^w \\ 0 & 0 & 0 & 1 \end{pmatrix} \begin{pmatrix} 1 & 0 & 0 & \Delta x \\ 0 & 1 & 0 & \Delta y \\ 0 & 0 & 1 & \Delta z \\ 0 & 0 & 0 & 1 \end{pmatrix} \begin{pmatrix} \cos \delta\theta & -\sin \delta\theta & 0 & 0 \\ \sin \delta\theta & \cos \delta\theta & 0 & 0 \\ 0 & 0 & 1 & 0 \\ 0 & 0 & 0 & 1 \end{pmatrix} \begin{pmatrix} L \cos(-\theta_x) \sin \theta_y \\ L \cos \theta_y \sin(-\theta_x) \\ L \cos(-\theta_x) \cos \theta_y \\ 1 \end{pmatrix} \end{aligned} \quad (2.10)$$

After computing the right side of Equation 2.10, the position of the tooling ball in the world coordinate system can be figured out. Equation 2.11 is derived from Equation 2.10 and applied in the program of computational component.

$$P^w = \begin{pmatrix} x_P^w \\ y_P^w \\ z_P^w \\ 1 \end{pmatrix} = \begin{pmatrix} L(\cos \delta\theta \cos \theta_x \sin \theta_y + \sin \delta\theta \cos \theta_y \sin \theta_x) + x_{TCP}^w + \Delta x \\ L(\sin \delta\theta \cos \theta_x \sin \theta_y - \cos \delta\theta \cos \theta_y \sin \theta_x) + y_{TCP}^w + \Delta y \\ L \cos \theta_x \cos \theta_y + z_{TCP}^w + \Delta z \\ 1 \end{pmatrix} \quad (2.11)$$

2.6.4 Coefficients for Computation

There are ten coefficients in Equation 2.11 for position computation:

1. Deflection angles θ_x and θ_y
2. Distance from the deflection center of the joystick to the spherical center of the tooling ball L
3. The rotation angle of rotation transformation process $\delta\theta$
4. The position of the TCP in the world coordinate system x_{TCP}^w , y_{TCP}^w and z_{TCP}^w
5. The position of the joystick deflection center in the tool coordinate system Δx , Δy and Δz

θ_x and θ_y can be computed from the output signals of the joystick using Equations 2.4 to 2.7. x_{TCP}^w , y_{TCP}^w and z_{TCP}^w can be directly obtained by a robot controller. However, L , $\delta\theta$, Δx , Δy and Δz are not previously known and therefore need to be figured out through detector calibration which will be introduced in Chapter 3.

2.7 Cell System Integration

As a requirement mentioned in Chapter 1, the cell system designed should be able to be integrated by the automatic TIG welding system. Though the integration work has not

been started, some points will be introduced here. Integration contains the following three tasks:

1. Connection between the detector and the sixth axis of the robot arm

The detector is mounted on the sixth axis of the robot arm and the mechanism for the connection needs to be designed. There are two requirements in the design process:

- The torch for welding task should not be removed when detecting the tooling ball because of the complicated assembly work of the torch. In the other hand, the detecting process should not be affected by the torch.
- The detector should be able to be connected with the robot arm quickly and conveniently in order to increase work efficiency. Tooling ball detection is just a small part of the entire welding task, so it is not necessary to spend a lot of time on this.

2. Cables among components for signal transmission and power supply

Both joystick and electrical components require a 5V DC power supply. This is provided by the USB port of the robot controller and cables are required to be assigned. The joystick moves with the robot arm, so the cable that provides power should be securely attached to the robot arm for the convenience of the detecting operation. Lots of signals are to be transmitted among components. The selection of cables for signal transmission and connecting method between cables and ports are important for securing the transmission quality and operation durability.

3. Software integration

The softwares engineer at Tool-Tec Welding Inc developed an application for automatic TIG welding tasks. It is installed in the FlexPendant for the operator to carry

out. All of procedures of the automatic TIG welding task can be achieved by running the application. Tooling ball detection is one of the steps in the task of mould calibration. The program programmed for a computational component should be integrated by the application and this is the software integration of cell detecting system.

2.8 Chapter Summary

Other than for the integration process, the new tooling ball detecting method is designed and implemented and it is theoretically described in this chapter. As mentioned in 2.6.1, four slopes of joystick output signals are to be obtained by the joystick calibration process and five coefficients need to be calibrated by the detector calibration process. Experiments for joystick calibration and detector calibration are designed and will be described in the next chapter. In addition, the next chapter also describes the simulation of the tooling ball detecting process and evaluates the detecting method designed.

Chapter 3

Calibration and Detecting Test

The joystick needs to be calibrated in order to obtain the slopes of the input-output curves for deflection angle computation. The detector also needs to be calibrated to obtain unknown coefficients. Calibration experiments are designed to achieve these targets. They are described in this chapter and include the calibration mechanism, experimental procedure, mathematical modeling, results and analysis.

The mechanical component is first tested on the NC milling machine. The testing process is combined with the detector calibration experiment. Base on the results of the experiment, the mechanical component is also evaluated in this chapter.

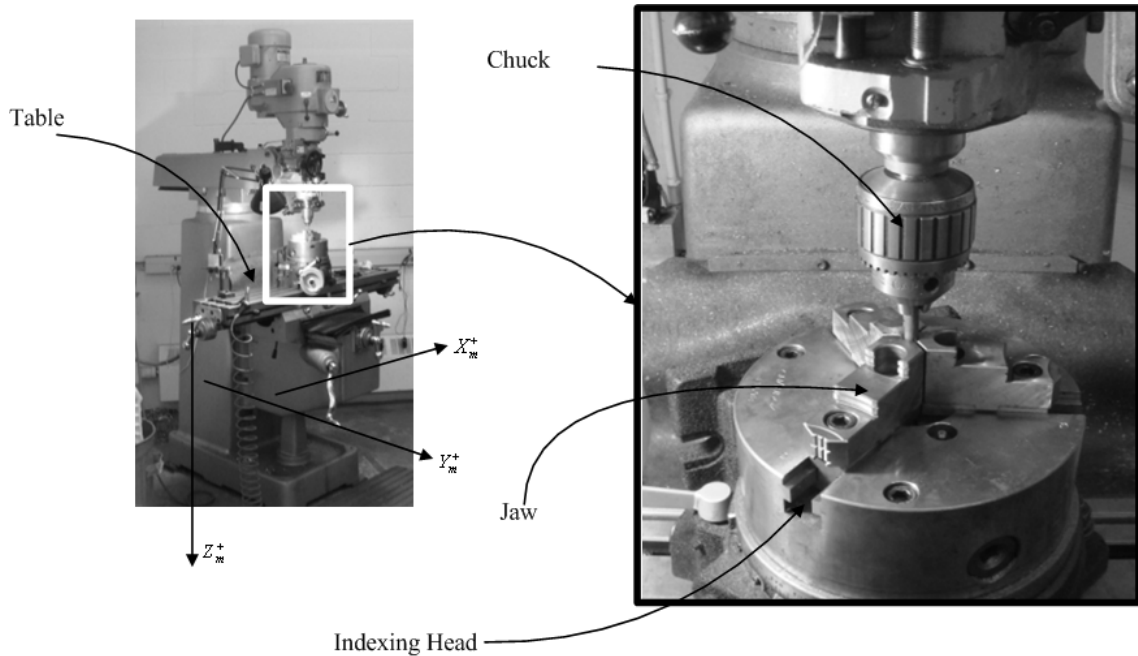


Figure 3.1: Milling Machine

3.1 NC Milling Machine with Indexing Head & Tooling Ball

3.1.1 NC Milling Machine with Indexing Head

The NC milling used in the experiments is described. The axes of the milling machine coordinate system are illustrated in Figure 3.1. The origin is defined by the operator which is not fixed. To decide the position of the origin, select any point on the center axis of the tool holder that is convenient for operation as the Tool Center Point (TCP), detect another selected position in space as the origin of the milling machine coordinate system and set the position of the TCP to zero. The position of the TCP is displayed on the screen of the milling machine.

There is an indexing head mounted on the table of the milling machine, and the center



Figure 3.2: Tooling Ball

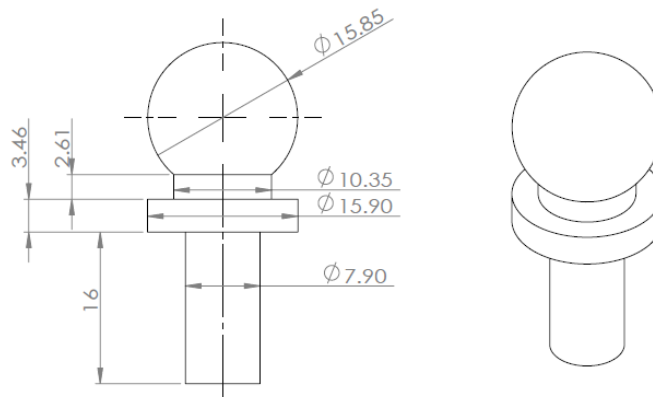


Figure 3.3: Dimension of the Tooling Ball

axis of both the chuck of milling machine and the indexing head are parallel to the vertical axis of the milling machine. The indexing head can be rotated by the operator.

3.1.2 Tooling Ball

The tooling ball used for detection simulation is made of stainless steel and has a diameter of 15.85mm (Figure3.2). The dimension of the tooling ball is provided in Figure3.3.

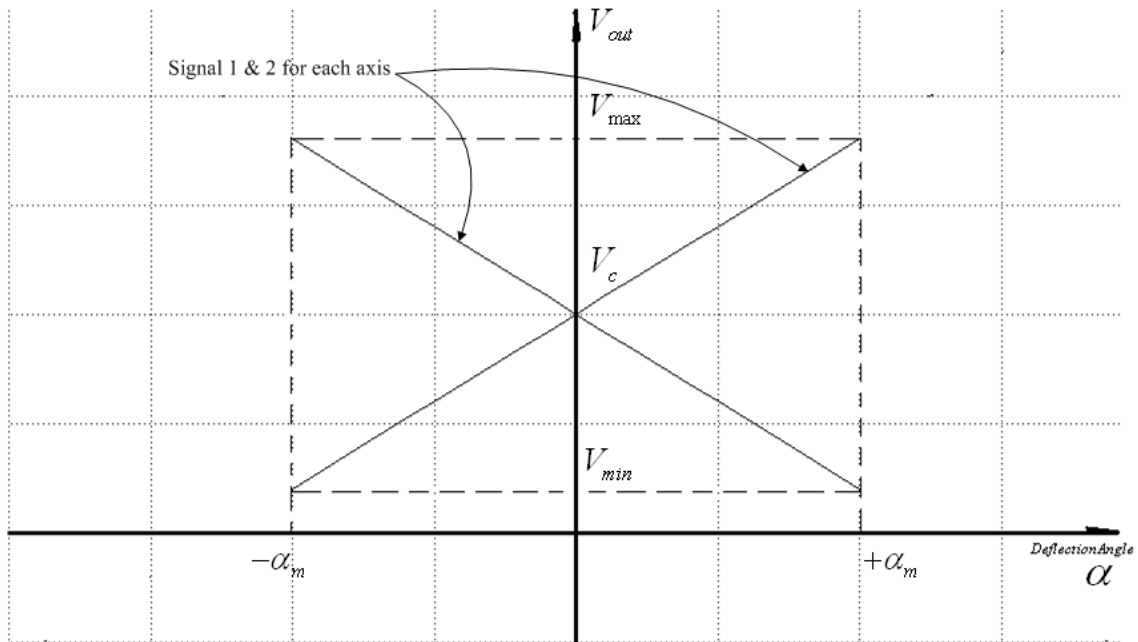


Figure 3.4: The output voltage of joystick is proportional to the deflection angle.

3.2 Joystick Calibration

The joystick used in the mechanical design, J6 series joystick, is a redundant biaxial joystick from Elobau Sensor Technology. The outputs are two pairs of analog voltage signals and each pair represents the deflection angle of one axis. One deflection angle is represented by two output signals and this is why the joystick is called redundant. In each pair, there are two voltage signals of which the values are opposite to each other. The most important property of the output signals is that the output voltage is proportional to the deflection angle as shown in Figure3.4.

In Figure3.4, V_{min} and V_{max} are the minimum and maximum values of the output voltage signals for an operating voltage V_{in} . α_{max} is the max deflection angle and V_c is the value of the output voltage signal when the shaft of the joystick is spring returned to the center position.

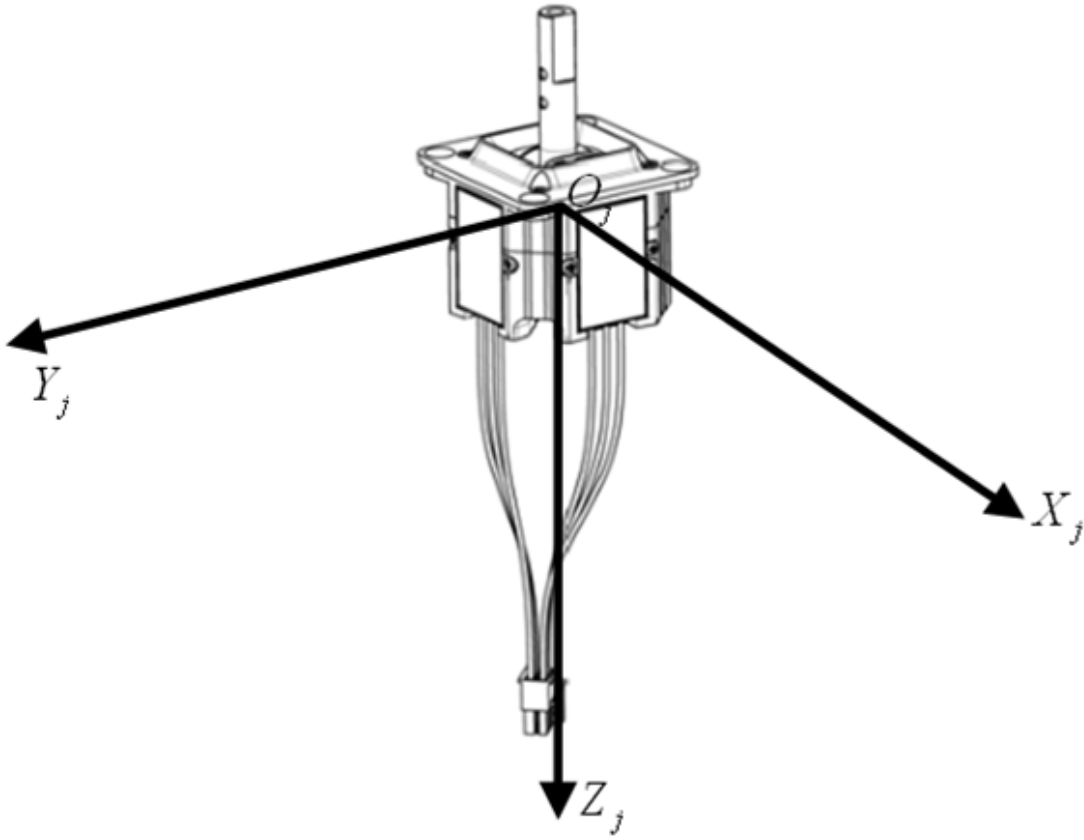


Figure 3.5: Configuration Example of Joystick Coordinate System

The joystick coordinate system is set as shown in Figure 3.5. The deflection angle about the axis X_j , θ_x , outputs voltage signals V_{out}^{x1} and V_{out}^{x2} . The deflection angle about the axis Y_j , θ_y , outputs voltage signals V_{out}^{y1} and V_{out}^{y2} . The slopes of V_{out}^{x1} and V_{out}^{x2} are k_{x1} and k_{x2} respectively. The slopes of V_{out}^{y1} and V_{out}^{y2} are k_{y1} and k_{y2} respectively. The output voltages at the center position with no deflection are V_c^{x1} , V_c^{x2} , V_c^{y1} and V_c^{y2} for the axes X_j and Y_j , respectively. There are thus four input-output relationships as represented by Equation 3.1 to 3.4 respectively.

$$V_{out}^{x1} = k_{x1}\theta_x + V_c^{x1} \quad (3.1)$$

$$V_{out}^{x2} = k_{x2}\theta_x + V_c^{x2} \quad (3.2)$$

$$V_{out}^{y1} = k_{y1}\theta_y + V_c^{y1} \quad (3.3)$$

$$V_{out}^{y2} = k_{y2}\theta_y + V_c^{y2} \quad (3.4)$$

3.2.1 Method for Joystick Calibration

First, a mechanism for joystick calibration is designed. Second, operation instructions about applying the mechanism for calibration is described. Third, a mathematical model is introduced describing the operation process for position computation. Finally, the method for processing the data obtained is given.

Mechanism for Joystick Calibration

The mechanism designed for calibrating the joystick is illustrated in Figure3.6.

Parts within Figure3.6 are listed below:

Part 1: Joystick Mounting Base

Part 2: Joystick Mounting Post

Part 3: Joystick (3-1: body, 3-2: shaft)

Part 4: Shaft Extension

Part 5: Centering Shaft

Part 6: Linear Motion Bearing

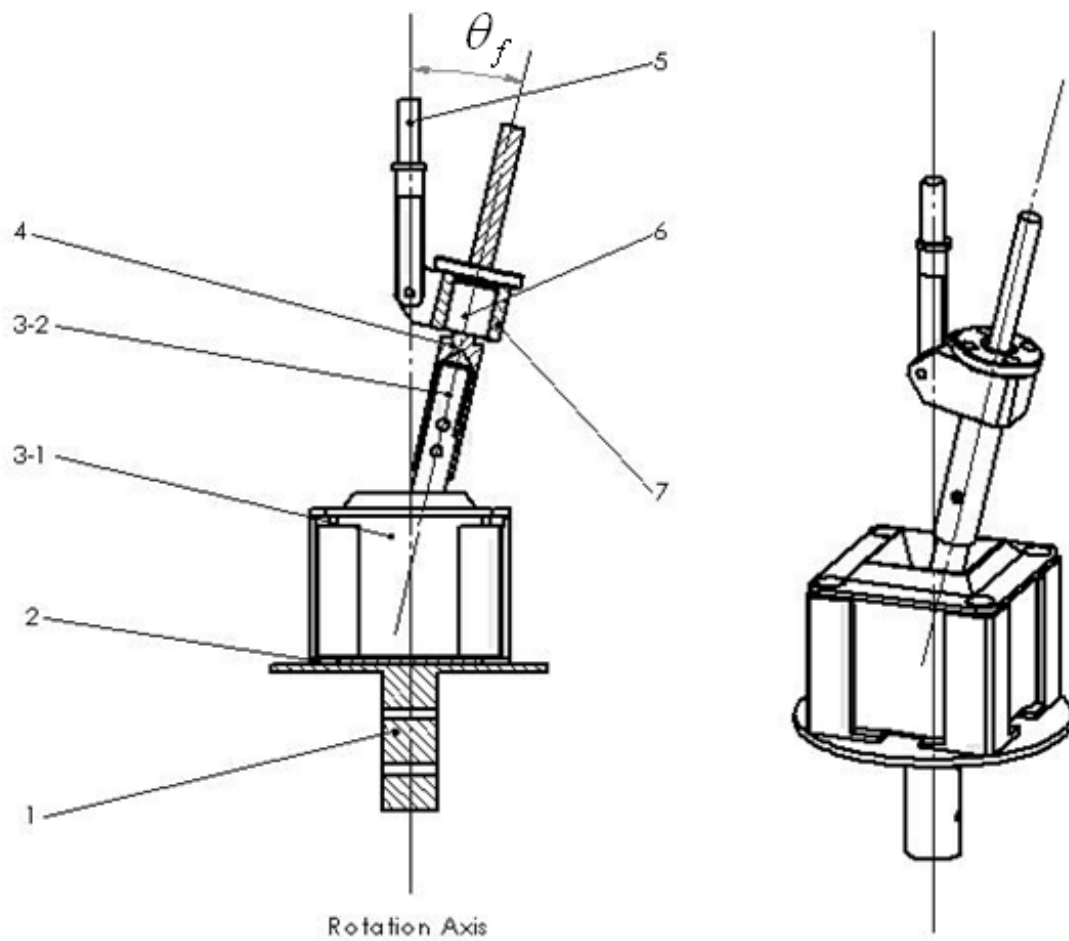


Figure 3.6: Mechanism for Joystick Calibration

Part 7: Bearing Housing

The joystick mounting base is fixed by the jaw of the indexing head. The body of the joystick is secured to the mounting base by means of the mounting post. The shaft extension both extends the length of the joystick shaft and provides a smooth surface for the linear motion bearing to slide along. The linear bearing is mounted in the bearing housing which also provides a pivot by which the linear bearing is attached to the centering shaft. The indexing head on the milling machine table is centered under the chuck and the centering shaft is secured in the tool holder. The rotation axis is vertical during the whole joystick calibration process. The deflection angles around each axis of the joystick change as the indexing head is rotated. However, the combined deflection angle is not changed. The combined deflection angle of the shaft, as is indicated in θ_f , is the angle between the center axis of the shaft and the axis of joystick coordinate system. θ_f is a combination of θ_x and θ_y .

Joystick Calibration Procedure

Step 1: Preset and fasten the indexing head and milling machine.

Locate the indexing head on the table of the milling machine.

Step 2: Align the rotation axes.

Fix a steel rod in the jaws of the indexing head. Adjust the position of the milling machine table until the chuck is centered on the steel rod (Figure3.7). Reset coordinate values x and y displayed on the LCD screen to zero.

Step 3: Obtain V_c^{x1} , V_c^{x2} , V_c^{y1} and V_c^{y2} of joystick at the center position.

Attach the joystick onto the mounting base with the mounting post by M5 counter sunk screws. Locate the mounting base stay in the indexing head jaws and close the



Figure 3.7: Center the tool holder on the steel rod.

jaws securely. With the chuck fully opened, raise the joystick with the mounting base and post to get close to the chuck by operating the table of the milling machine on its vertical axis until the joystick shaft is about 2cm into the chuck. Close the chuck gently until it just makes contact with the joystick shaft (the joystick shaft should still be able to rotate in the chuck). Rotate the indexing head while monitoring the joystick output voltages. If the joystick is properly centered below the chuck, the output voltages will not change significantly as the indexing head is rotated. If the output voltages do change, adjust the position of the table along the axes X_m and Y_m of the milling machine until this voltage change is minimized over one rotation of the indexing head. This is then the properly centered position with center voltage outputs V_c^{x1} , V_c^{x2} , V_c^{y1} and V_c^{y2} .

Step 4: Mount all the parts in Figure3.6.

Open the chuck and lower the joystick with the mounting base and the post by operating the table of the milling machine on its vertical axis. Attach the other parts (4,5,6,7) to the joystick and then raise the whole mechanism so that the centering shaft enters the chuck. Close the chuck on the centering shaft.

Step 5: Rotate the indexing head four degrees for each increment from 0° to 364° . Record output voltage values at the position of each increment.

Step 6: Record z value of milling machine as Z_1 .

Step 7: Change the position of the working table in Z direction of the milling machine. Repeat Step 4 and Step 6 to obtain a second group of output voltage values and another value of milling machine as Z_2 .

Step 8: Process two groups of data obtained and figure out k_{x1} , k_{x2} , k_{y1} and k_{y2} .

Transformations in Calibration Process

There are three coordinate systems in calibration process, as illustrated in Figure3.8:

- Milling Machine Coordinate System F_m :

Axis Z_m is vertical to the ground, pointing down. Axis Y_m points toward the operator and axis X_m follows the right-hand rule.

- Joystick Coordinate System F_j :

The setting of F_j is the same as that described in Figure3.5.

- Indexing Head Coordinate System F_c :

Axis Z_c is vertical to the ground pointing down. Axis X_c maintains the same direction as X_j rotating around axis Z_c and axis Y_c follows the right-hand rule. Plane $X_c - O_c - Y_c$ coincides with plane $X_j - O_j - Y_j$.

From F_m to F_c , the transformation process is a translation followed by a rotation. The corresponding transformation matrix T_{mc} is given in Equation 3.5. T_{mc} describes the pose of F_c in F_m .

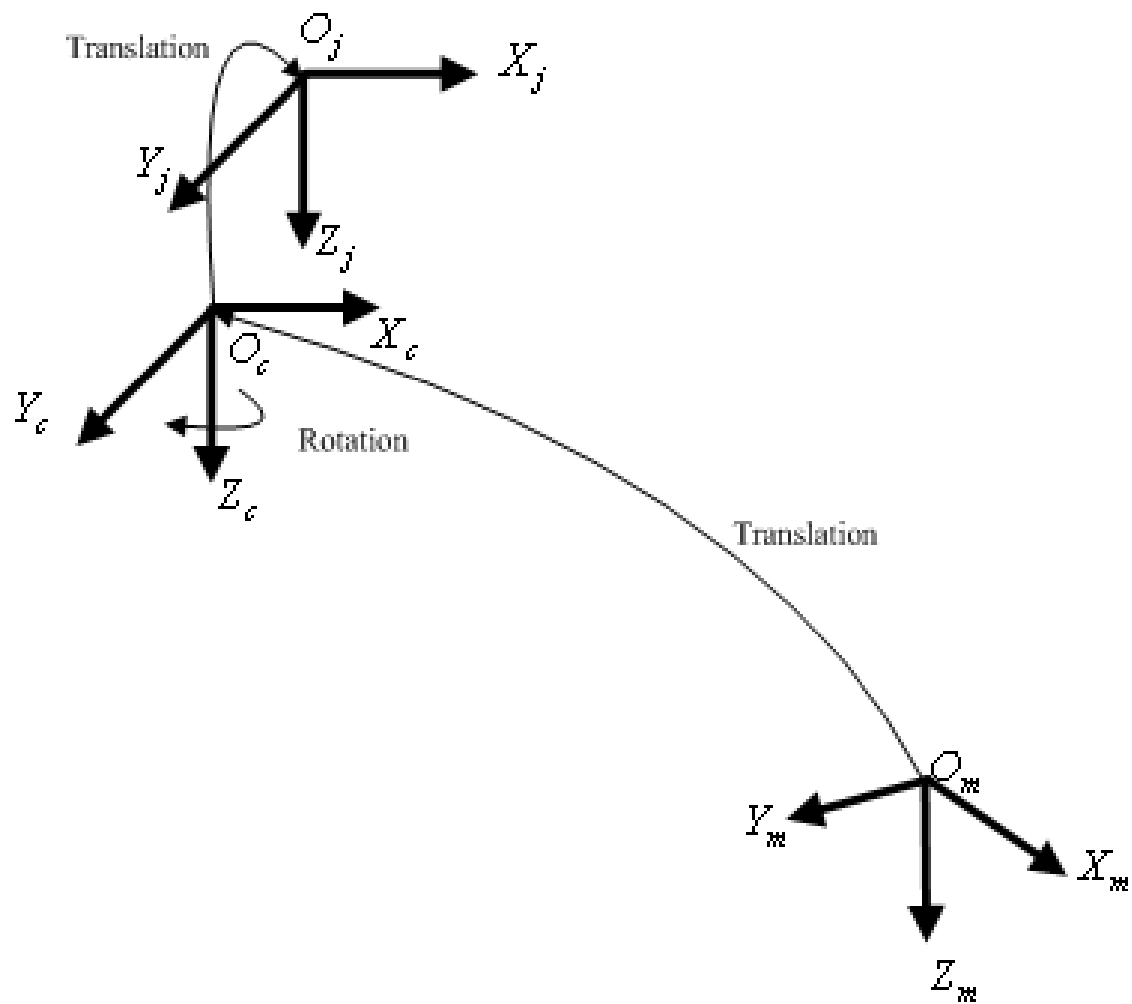


Figure 3.8: Three Coordinate Systems in Joystick Calibration Process

$$T_{mc} = \begin{pmatrix} 1 & 0 & 0 & x_c^m \\ 0 & 1 & 0 & y_c^m \\ 0 & 0 & 1 & z_c^m \\ 0 & 0 & 0 & 1 \end{pmatrix} \begin{pmatrix} \cos \varphi_t & -\sin \varphi_t & 0 & 0 \\ \sin \varphi_t & \cos \varphi_t & 0 & 0 \\ 0 & 0 & 0 & 0 \\ 0 & 0 & 0 & 1 \end{pmatrix} \quad (3.5)$$

φ_t is the angle from X_m to X_c about Z_c . We have $\varphi_t = \varphi_0 + \varphi_i$. φ_0 is the original rotation angle of the indexing head and φ_i is the rotation angle of the indexing head which is accumulated from the original situation. It's 4° for each increment of rotating of the indexing head. If the indexing head has been rotated for i increments, we have $\varphi_t = \varphi_0 + 4 \times i$.

From F_c to F_j , the transformation process is a translation and there are transformation matrix T_{jc} and its inverse matrix T_{cj} are shown in Equation 3.6. T_{jc} describes the pose of F_c in F_j and T_{cj} describes the pose of F_j in F_c .

$$T_{jc} = \begin{pmatrix} 1 & 0 & 0 & x_c^j \\ 0 & 1 & 0 & y_c^j \\ 0 & 0 & 1 & 0 \\ 0 & 0 & 0 & 1 \end{pmatrix} \Rightarrow T_{cj} = T_{jc}^{-1} = \begin{pmatrix} 1 & 0 & 0 & -x_c^j \\ 0 & 1 & 0 & -y_c^j \\ 0 & 0 & 1 & 0 \\ 0 & 0 & 0 & 1 \end{pmatrix} \quad (3.6)$$

As a result, from F_m to F_j , there is a transformation matrix T_{mj} shown in Equation 3.7. It can be simplified into Equation 3.8. T_{mj} describes the pose of F_j in F_m .

$$T_{mj} = T_{mc}T_{cj} = \begin{pmatrix} 1 & 0 & 0 & x_c^m \\ 0 & 1 & 0 & y_c^m \\ 0 & 0 & 1 & z_c^m \\ 0 & 0 & 0 & 1 \end{pmatrix} \begin{pmatrix} \cos \varphi_t & -\sin \varphi_t & 0 & 0 \\ \sin \varphi_t & \cos \varphi_t & 0 & 0 \\ 0 & 0 & 0 & 0 \\ 0 & 0 & 0 & 1 \end{pmatrix} \begin{pmatrix} 1 & 0 & 0 & -x_c^j \\ 0 & 1 & 0 & -y_c^j \\ 0 & 0 & 1 & 0 \\ 0 & 0 & 0 & 1 \end{pmatrix} \quad (3.7)$$

$$T_{mj} = \begin{pmatrix} \cos \varphi_t & -\sin \varphi_t & 0 & x_c^m - x_c^j \cos \varphi_t + y_c^j \sin \varphi_t \\ \sin \varphi_t & \cos \varphi_t & 0 & y_c^m - y_c^j \cos \varphi_t - x_c^j \sin \varphi_t \\ 0 & 0 & 1 & z_c^m \\ 0 & 0 & 0 & 1 \end{pmatrix} \quad (3.8)$$

Also since $T_{jm} = T_{mj}^{-1}$ describing the pose of F_m in F_j , we have transformation matrix T_{jm} for the transformation from F_j to F_m , as is shown in Equation 3.9.

$$T_{jm} = \begin{pmatrix} \cos \varphi_t & \sin \varphi_t & 0 & x_c^j - x_c^m \cos \varphi_t - y_c^m \sin \varphi_t \\ -\sin \varphi_t & \cos \varphi_t & 0 & y_c^j - y_c^m \cos \varphi_t + x_c^m \sin \varphi_t \\ 0 & 0 & 1 & -z_c^m \\ 0 & 0 & 0 & 1 \end{pmatrix} \quad (3.9)$$

Deflection Angles of Joystick in Calibration Process

Figure 3.9 illustrates the geometrical relationship of the mechanism for the deflection angle computing in the joystick calibration process. The pivot point P (the point at which the linear bearing housing is attached to the centering shaft) is located on a virtual plane V to which the axis of the shaft extension is normal. This means that the distance between the pivot point and the shaft extension axis is fixed and in the present design measures 22.5mm, as shown in Figure 3.9. The angle that the joystick axis is deflected can therefore be set by adjusting the distance between the chuck of the milling machine and the indexing head. This angle, indicated as θ_f in Figure 3.9 is what we refer to as the combined deflection angle, in that it is a combination of θ_x and θ_y .

According to Equation 2.3 in Chapter 2, the position of point P in the joystick coordinate system is known by Equation 3.10:

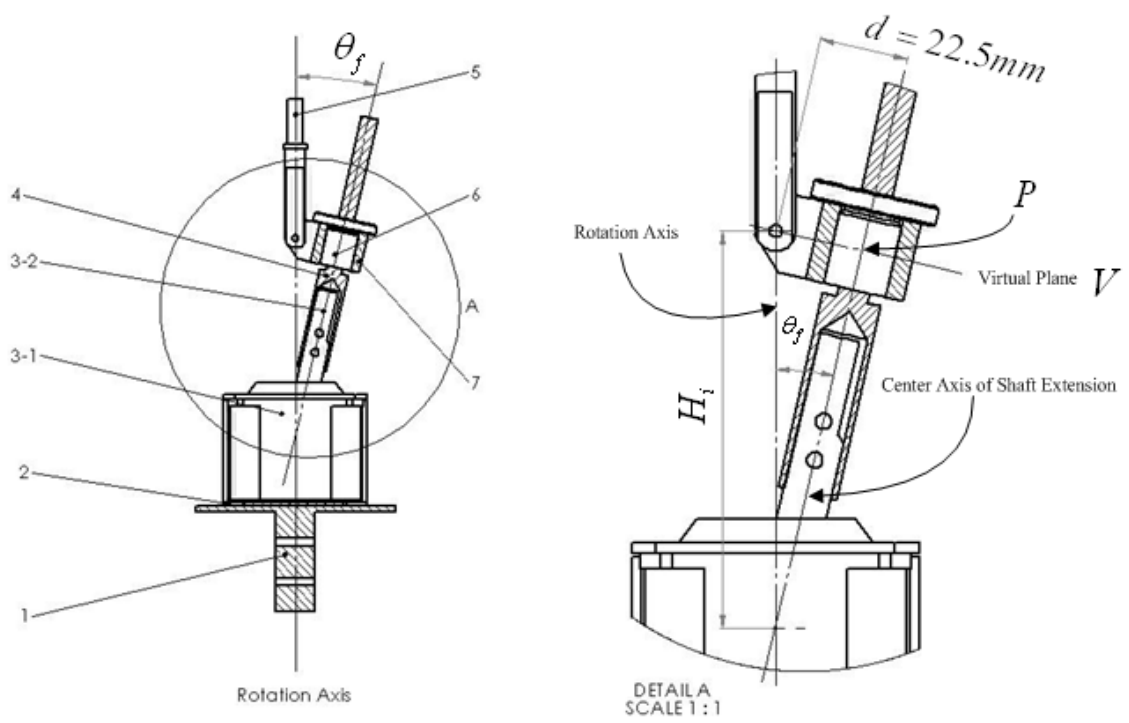


Figure 3.9: Deflection Angles of Joystick in Calibration Process

$$P^j = \begin{pmatrix} x_P^j \\ y_P^j \\ z_P^j \\ 1 \end{pmatrix} = \begin{pmatrix} L \cos(-\theta_x) \sin \theta_y \\ L \cos \theta_y \sin(-\theta_x) \\ L \cos(-\theta_x) \cos \theta_y \\ 1 \end{pmatrix} \quad (3.10)$$

The position of point P in milling machine coordinate system F_m is $P^m = \begin{pmatrix} x_P^m & y_P^m & z_P^m & 1 \end{pmatrix}^T$ and since the transformation matrix T_{jm} defines coordinate system F_m in the coordinate system F_j , the position of point P in the joystick coordinate system is computed by Equation 3.11.

$$\begin{aligned} P^j &= \begin{pmatrix} x_P^j \\ y_P^j \\ z_P^j \\ 1 \end{pmatrix} = \begin{pmatrix} L \cos(-\theta_x) \sin \theta_y \\ L \cos \theta_y \sin(-\theta_x) \\ L \cos(-\theta_x) \cos \theta_y \\ 1 \end{pmatrix} = T_{jm} P^m \\ &= \begin{pmatrix} \cos \varphi_t & \sin \varphi_t & 0 & x_c^j - x_c^m \cos \varphi_t - y_c^m \sin \varphi_t \\ -\sin \varphi_t & \cos \varphi_t & 0 & y_c^j - y_c^m \cos \varphi_t + x_c^m \sin \varphi_t \\ 0 & 0 & 1 & -z_c^m \\ 0 & 0 & 0 & 1 \end{pmatrix} \begin{pmatrix} x_P^m \\ y_P^m \\ z_P^m \\ 1 \end{pmatrix} \end{aligned} \quad (3.11)$$

and so, we have Equation 3.12.

$$P^j = \begin{pmatrix} x_c^j + (x_P^m - x_c^m) \cos \varphi_t + (y_P^m - y_c^m) \sin \varphi_t \\ y_c^j + (y_P^m - y_c^m) \cos \varphi_t + (x_P^m - x_c^m) \sin \varphi_t \\ z_P^m - z_c^m \\ 1 \end{pmatrix} \quad (3.12)$$

Then we can equate the two equations for P^j as shown in Equation 3.13.

$$P^j = \begin{pmatrix} L \cos(-\theta_x) \sin \theta_y \\ L \cos \theta_y \sin(-\theta_x) \\ L \cos(-\theta_x) \cos \theta_y \\ 1 \end{pmatrix} = \begin{pmatrix} x_c^j + (x_P^m - x_c^m) \cos \varphi_t + (y_P^m - y_c^m) \sin \varphi_t \\ y_c^j + (y_P^m - y_c^m) \cos \varphi_t + (x_P^m - x_c^m) \sin \varphi_t \\ z_p^m - z_c^m \\ 1 \end{pmatrix} \quad (3.13)$$

Solve Equation 3.13 and the deflection angles of the joystick can then be obtained by Equations 3.14 and 3.15, respectively.

$$\begin{aligned} \theta_x = -\arctan\left(\frac{y_P^j}{z_P^j}\right) &= -\arctan\left[\frac{y_c^j + (y_P^m - y_c^m) \cos \varphi_t + (x_P^m - x_c^m) \sin \varphi_t}{z_p^m - z_c^m}\right] \\ \text{where : } \operatorname{sgn}(\theta_x) &= -\operatorname{sgn}(y_P^j) \\ &= -\operatorname{sgn}[y_c^j + (y_P^m - y_c^m) \cos \varphi_t + (x_P^m - x_c^m) \sin \varphi_t] \end{aligned} \quad (3.14)$$

$$\begin{aligned} \theta_y = \arctan\left(\frac{x_P^j}{z_P^j}\right) &= \arctan\left[\frac{x_c^j + (x_P^m - x_c^m) \cos \varphi_t + (y_P^m - y_c^m) \sin \varphi_t}{z_p^m - z_c^m}\right] \\ \text{where : } \operatorname{sgn}(\theta_y) &= \operatorname{sgn}(x_P^j) \\ &= \operatorname{sgn}[x_c^j + (x_P^m - x_c^m) \cos \varphi_t + (y_P^m - y_c^m) \sin \varphi_t] \end{aligned} \quad (3.15)$$

Equations 3.14 and 3.15 can also be simplified into Equations 3.16 and 3.17.

$$\begin{aligned} \theta_x &= -\arctan[A \sin(\alpha - \varphi_t) + B] \\ \text{where : } A &= \frac{\sqrt{(y_P^m - y_c^m)^2 + (x_P^m - x_c^m)^2}}{z_p^m - z_c^m} \\ B &= \frac{y_c^j}{z_p^m - z_c^m} \\ \sin \alpha &= \frac{y_P^m - y_c^m}{\sqrt{(y_P^m - y_c^m)^2 + (x_P^m - x_c^m)^2}} \\ \cos \alpha &= \frac{x_P^m - x_c^m}{\sqrt{(y_P^m - y_c^m)^2 + (x_P^m - x_c^m)^2}} \end{aligned} \quad (3.16)$$

$$\begin{aligned}
\theta_y &= \arctan[A \cos(\alpha - \varphi_t) + D] \\
\text{where : } A &= \frac{\sqrt{(y_P^m - y_c^m)^2 + (x_P^m - x_c^m)^2}}{z_p^m - z_c^m} \\
D &= \frac{x_c^j}{z_p^m - z_c^m} \\
\sin \alpha &= \frac{y_P^m - y_c^m}{\sqrt{(y_P^m - y_c^m)^2 + (x_P^m - x_c^m)^2}} \\
\cos \alpha &= \frac{x_P^m - x_c^m}{\sqrt{(y_P^m - y_c^m)^2 + (x_P^m - x_c^m)^2}} \tag{3.17}
\end{aligned}$$

Parameters x_c^j and y_c^j are distances between the axis Z_j of joystick coordinate system and the axis Z_c of indexing head coordinate system. Ideally, they should both be zero. The mounting base was designed so as to minimize them. However, it is necessary to indicate them in the calibration process, although their values are both less than one-half millimeter.

The value of $z_p^m - z_c^m$ is the distance $d / \tan \theta_f$ in which $d = 22.5mm$, $\theta_f \in (0^\circ, 25^\circ)$ and corresponds to the distance between the pivot on the centering shaft and the pivot axes of the joystick (which is not acceptable). This distance can be varied between $48.25mm$ and $53.24mm$. Consequently, B and D in Equation 3.16 and 3.17 will be very small (< 0.01) and can be safely ignored in the computations. (Equation 3.18 and 3.19)

$$\theta_x = -\arctan[A \sin(\alpha - \varphi_t)] \tag{3.18}$$

$$\theta_y = \arctan[A \cos(\alpha - \varphi_t)] \tag{3.19}$$

$$\text{where : } A = \frac{\sqrt{(y_P^m - y_c^m)^2 + (x_P^m - x_c^m)^2}}{z_p^m - z_c^m} \tag{3.20}$$

$$\sin \alpha = \frac{y_P^m - y_c^m}{\sqrt{(y_P^m - y_c^m)^2 + (x_P^m - x_c^m)^2}} \tag{3.21}$$

$$\cos \alpha = \frac{x_P^m - x_c^m}{\sqrt{(y_P^m - y_c^m)^2 + (x_P^m - x_c^m)^2}} \tag{3.22}$$

Output Voltage Values for Result Estimating of Calibration Experimental Result

Equation 3.23 to 3.26 is derived from Equation 3.1 to 3.4.

$$\theta_x = (V_{out}^{x1} - V_c^{x1})/k_{x1} = \Delta V_{x1}/k_{x1} \quad (3.23)$$

$$\theta_x = (V_{out}^{x2} - V_c^{x2})/k_{x2} = \Delta V_{x2}/k_{x2} \quad (3.24)$$

$$\theta_y = (V_{out}^{y1} - V_c^{y1})/k_{y1} = \Delta V_{y1}/k_{y1} \quad (3.25)$$

$$\theta_y = (V_{out}^{y2} - V_c^{y2})/k_{y2} = \Delta V_{y2}/k_{y2} \quad (3.26)$$

Considering Equations 3.18 and 3.19 and Equations 3.23 to 3.26, the voltage values of the output signals can be written as Equations 3.27 to 3.30.

$$V_{out}^{x1} = \{-\arctan[A_{x1} \sin(\alpha_{x1} - \varphi_t)]\}k_{x1} + V_c^{x1} \quad (3.27)$$

$$V_{out}^{x2} = \{-\arctan[A_{x2} \sin(\alpha_{x2} - \varphi_t)]\}k_{x2} + V_c^{x2} \quad (3.28)$$

$$V_{out}^{y1} = \{\arctan[A_{y1} \cos(\alpha_{y1} - \varphi_t)]\}k_{y1} + V_c^{y1} \quad (3.29)$$

$$V_{out}^{y2} = \{\arctan[A_{y2} \cos(\alpha_{y2} - \varphi_t)]\}k_{y2} + V_c^{y2} \quad (3.30)$$

Method for Data Processing

Parameters H_i , d and the corresponding parameter $\theta_{f,i}$ in Figure 3.9 are related as relationship:

$$\sin \theta_{f,i} = d/H_i \quad (3.31)$$

where subscript i refers to group number. This can be used for processing data from the calibration experiments in order to obtain values for k_{x1} , k_{x2} , k_{y1} and k_{y2} . Two groups of

outputs are measured at two different heights of the working table, following the calibration procedure previously described.

For the i^{th} group of data, $\theta_{x,i} = \theta_{f,i}$ when $\theta_{y,i} = 0$ and $\theta_{y,i} = \theta_{f,i}$ when $\theta_{x,i} = 0$. This means that the maximum and the minimum output voltage values of signals represent the same deflection angle $\theta_{f,i}$. As a result, we have Equation 3.32 to 3.35 for computing $\theta_{f,i}$ from the two groups of data.

$$\theta_{f,i} = \{[max(V_{out,i}^{x1}) - min(V_{out,i}^{x1})]/2 - V_c^{x1}\}/k_{x1} = \arcsin(d/H_i) \quad (3.32)$$

$$\theta_{f,i} = \{[max(V_{out,i}^{x2}) - min(V_{out,i}^{x2})]/2 - V_c^{x2}\}/k_{x2} = \arcsin(d/H_i) \quad (3.33)$$

$$\theta_{f,i} = \{[max(V_{out,i}^{y1}) - min(V_{out,i}^{y1})]/2 - V_c^{y1}\}/k_{y1} = \arcsin(d/H_i) \quad (3.34)$$

$$\theta_{f,i} = \{[max(V_{out,i}^{y2}) - min(V_{out,i}^{y2})]/2 - V_c^{y2}\}/k_{y2} = \arcsin(d/H_i) \quad (3.35)$$

Because the z values of the milling machine at each measuring position of the working table are recorded as Z_1 and Z_2 at Step 6 and Step 7, the difference between H_1 and H_2 can be computed as $\Delta H = \Delta H_2 - \Delta H_1 = Z_2 - Z_1$. Thus we have Equation 3.36 to 3.39.

$$\begin{aligned} \{[max(V_{out,1}^{x1}) - min(V_{out,1}^{x1})]/2 - V_c^{x1}\}/k_{x1} &= \arcsin(d/H_1) \\ \{[max(V_{out,2}^{x1}) - min(V_{out,2}^{x1})]/2 - V_c^{x1}\}/k_{x1} &= \arcsin[d/(H_1 + \Delta H)] \end{aligned} \quad (3.36)$$

$$\begin{aligned} \{[max(V_{out,1}^{x2}) - min(V_{out,1}^{x2})]/2 - V_c^{x2}\}/k_{x2} &= \arcsin(d/H_1) \\ \{[max(V_{out,2}^{x2}) - min(V_{out,2}^{x2})]/2 - V_c^{x2}\}/k_{x2} &= \arcsin[d/(H_1 + \Delta H)] \end{aligned} \quad (3.37)$$

$$\begin{aligned} \{[max(V_{out,1}^{y1}) - min(V_{out,1}^{y1})]/2 - V_c^{y1}\}/k_{y1} &= \arcsin(d/H_1) \\ \{[max(V_{out,2}^{y1}) - min(V_{out,2}^{y1})]/2 - V_c^{y1}\}/k_{y1} &= \arcsin[d/(H_1 + \Delta H)] \end{aligned} \quad (3.38)$$

$$\begin{aligned} \{[max(V_{out,1}^{y2}) - min(V_{out,1}^{y2})]/2 - V_c^{y2}\}/k_{y2} &= \arcsin(d/H_1) \\ \{[max(V_{out,2}^{y2}) - min(V_{out,2}^{y2})]/2 - V_c^{y2}\}/k_{y2} &= \arcsin[d/(H_1 + \Delta H)] \end{aligned} \quad (3.39)$$

Table 3.1: Results of Joystick Calibration Experiment

V_c^{x1}	V_c^{x2}	V_c^{y1}	V_c^{y2}
2.55V	2.56V	2.55V	2.53V
k_{x1}	k_{x2}	k_{y1}	k_{y2}
-0.0836	+0.0828	+0.0828	-0.0812

There are only two unknown values $k_{x1}/k_{x2}/k_{y1}/k_{y2}$ and H_1 in each group with only two equations. Thus, k_{x1} , k_{x2} , k_{y1} , k_{y2} and H_1 can be solved.

3.2.2 Result of Joystick Calibration Experiment

The recorded data for the two heights are plotted in Figure3.10. The horizontal axis is the values of φ_i ranging from 0° to 364° and the vertical axis is the output voltage values of joystick V^{out} . According to Equation 3.27 to 3.30, it is known that phases and periods of output voltage values V_{x1}^{out} and V_{x2}^{out} are the same with opposite values to the center output voltage values. Output voltage values V_{y1}^{out} and V_{y2}^{out} have the same condition as V_{x1}^{out} and V_{x2}^{out} with $\frac{\pi}{2}$ phase difference. Therefore, Figure3.10 shows that data obtained from the calibration experiment are reasonable. Table3.1 shows the center position voltage outputs and the slopes of each signal computed from the data obtained from the experiment, as described in 3.2.1.

Two groups of data obtained from the calibration experiment follow Equations 3.27 to 3.30. Knowing the slopes of each signal, output voltages and angle of rotation, the other four parameters, A_{xi} , A_{yi} and α_{xi} , α_{yi} can be obtained using the nonlinear fitting tool box in Matlab by the following steps. The results are given in Tables3.2 and 3.3. The fitting curves are illustrated in Figure3.11.

Step 1: Create data set for two groups of data in the form of V^{out} vs φ_i .

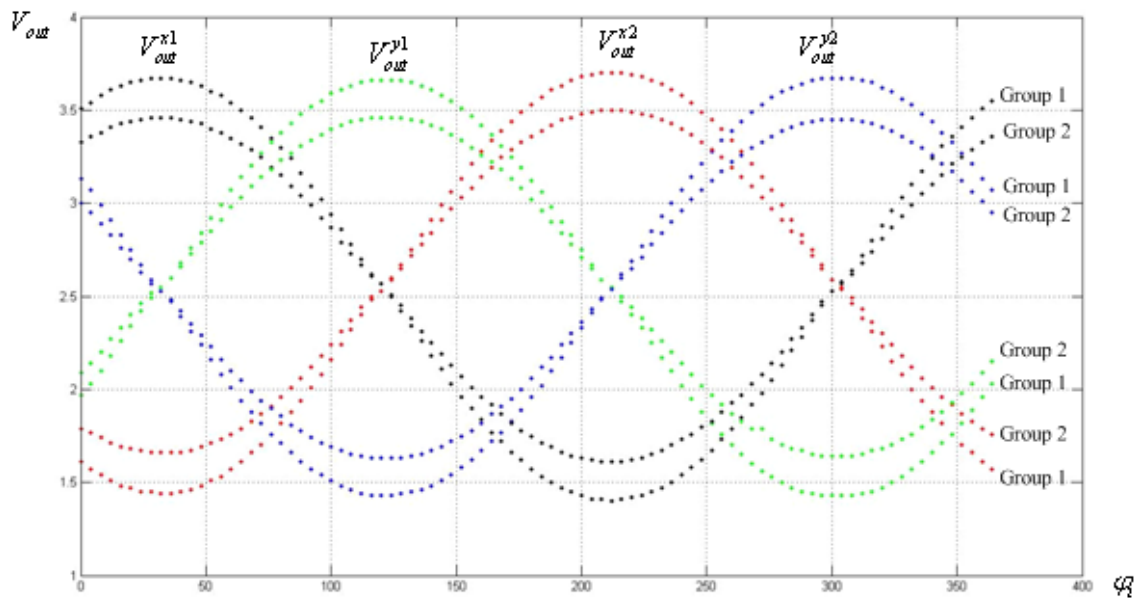


Figure 3.10: Output Voltage Values of Joystick at Two Heights in Joystick Calibration Process

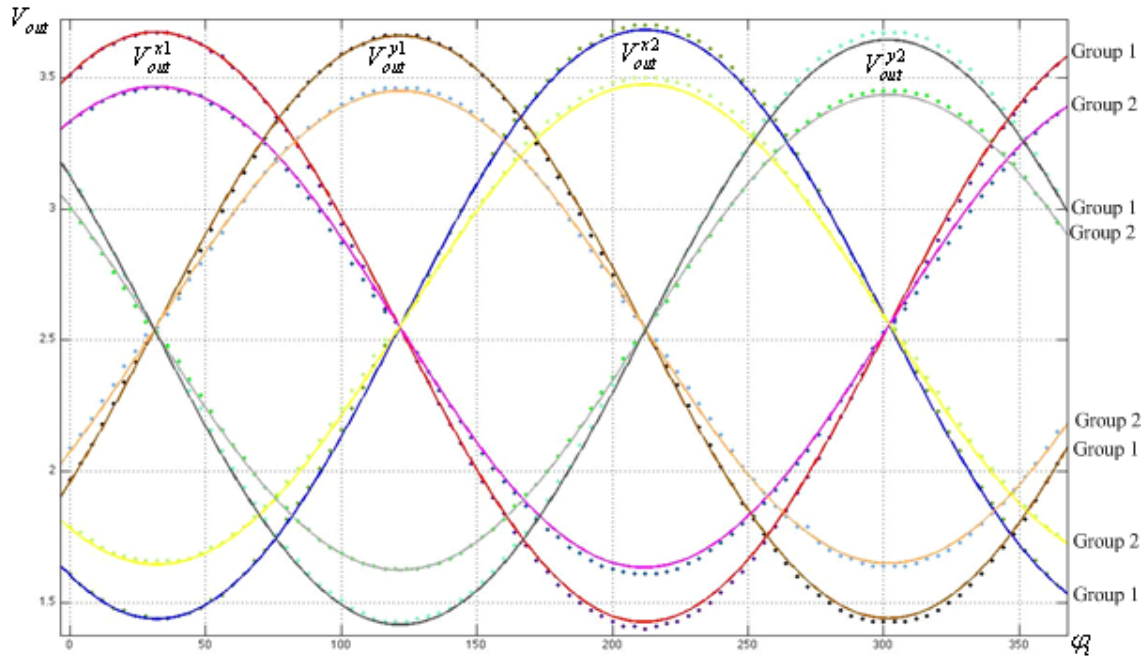


Figure 3.11: Fit to the Data of Joystick Calibration Experiment

Step 2: Type 'cftool' in Matlab to open the curve fitting tool box.

Step 3: Smooth data sets created previously in Step 1.

Step 4: Select 'Custom Equations' as the fitting type and input Equation 3.27 to 3.30 for fitting.

Step 5: For each smoothed data set of output voltage value, fit data with curves by Levenberg-Marquardt fitting method which is a kind of least square fitting method and output result. [15] The result of fitting contains amplitudes A_{xi} , A_{yi} and phases α_{xi} , α_{yi} for each data set.

According to Equation 3.20, $|A|$ represents the value of $\tan \theta_f$. Since θ_f does not change during the rotation of indexing head, ideally speaking, values of A that are computed from four signals in each group should be the same and the eight values of α should also be

Table 3.2: Amplitudes and Phases Offsets of Data in Group 1

A_{xi}, A_{yi}	α_{xi}, α_{yi}	Goodness of Fitting $RMSE$
$A_{x1} = -0.2387(\theta_f = 13.4253)$	$\alpha_{x1} = -58.47$	0.01580
$A_{x2} = -0.2408(\theta_f = 13.5391)$	$\alpha_{x2} = -58.03$	0.01535
$A_{y1} = -0.2381(\theta_f = 13.3928)$	$\alpha_{y1} = -58.34$	0.01409
$A_{y2} = -0.2440(\theta_f = 13.7122)$	$\alpha_{y2} = -58.35$	0.01983

Table 3.3: Amplitudes and Phases Offsets of Data in Group 2

A_{xi}, A_{yi}	α_{xi}, α_{yi}	Goodness of Fitting $RMSE$
$A_{x1} = -0.1934(\theta_f = 10.9459)$	$\alpha_{x1} = -58.43$	0.01727
$A_{x2} = -0.1950(\theta_f = 11.0342)$	$\alpha_{x2} = -57.94$	0.01876
$A_{y1} = -0.1918(\theta_f = 10.8575)$	$\alpha_{y1} = -58.39$	0.01268
$A_{y2} = -0.1969(\theta_f = 11.1390)$	$\alpha_{y2} = -58.39$	0.01049

the same in the two groups of data. Therefore, considering the data in Table3.2 and 3.3, the values of A and α are reasonable. The average value of θ_f is 13.5175° in group 1 and 10.9942° in group 2. The average value of α is -58.29° which is computed from eight values of two groups.

Deflection angle computation

After obtaining voltage outputs for joystick ($V_{out}^{x1}, V_{out}^{x2}, V_{out}^{y1}$ and V_{out}^{y2}), the deflection angles θ_x and θ_y can be computed using Equation 3.40 and 3.41. Values of $k_{x1}, k_{x2}, k_{y1}, k_{y2}$, and $V_c^{x1}, V_c^{x2}, V_c^{y1}, V_c^{y2}$ are listed in Table3.1.

$$\theta_x = (\theta_{x1} + \theta_{x2})/2 \quad (3.40)$$

$$\text{where : } \theta_{x1} = (V_{out}^{x1} - V_c^{x1})/k_{x1}$$

$$\theta_{x2} = (V_{out}^{x2} - V_c^{x2})/k_{x2}$$

$$\theta_y = (\theta_{y1} + \theta_{y2})/2 \quad (3.41)$$

$$\text{where : } \theta_{y1} = (V_{out}^{y1} - V_c^{y1})/k_{y1}$$

$$\theta_{y2} = (V_{out}^{y2} - V_c^{y2})/k_{y2}$$

3.3 Detector Calibration and Testing

3.3.1 Objectives of Detector Calibration Experiment

The objectives of the detector calibration experiment are to determine unknown coefficients for position computation. As mentioned in Chapter 2, there are ten coefficients in Equation 2.11 for tooling ball position computation. These coefficients are described below:

1. Deflection angles θ_x and θ_y

Two coefficients depend on deflection angles of the joystick. They can be computed according to the output voltage values, center voltage outputs and slopes obtained from the joystick calibration experiment. Therefore, they are known values in Equation 2.11 after the joystick calibration experiment.

2. Distance from the deflection center of the joystick to the spherical center of the tooling ball L

Once the parts of the detector have been machined, measured and assembled, this parameter only depends on the diameter of the tooling ball to be detected. Before

locating the tooling ball on the mould, the diameter of the tooling ball is to be measured and recorded for computing L .

Tooling balls with different diameters to be detected cause different L . As shown in Figure3.12, the diameter of the tooling ball measured is d with corresponding distance L . L' is the distance from the deflection center of joystick to the peak of cone surface. β is the angle between the center axis of the detecting part and the cone surface. w is the width of the cone surface. Thus we have the relationship:

$$L = L' + (d/2)/\sin \beta \quad (3.42)$$

For different sizes of tooling ball, L' does not change and L can be computed by L' and β . However, because of machining tolerance and the activation distance of the tactile switch, L may not be exactly as designed. As a result, obtaining the value of L corresponding to the different values of the tooling ball diameter is the first target of the detector calibration experiment. There is only one tooling ball to be detected, so only L is computed in the detector calibration process without computing L' .

3. Rotation angle of rotation transformation process $\delta\theta$

The detector is mounted on the sixth axis of a robot arm or other type of machine. Different mechanism designs for attaching the detector to the machine or robot are required. After mounting the detector, the x axis of the joystick coordinate system X_j usually does not coincide with the x axis of the tool coordinate system X_t . This is the rotation angle $\delta\theta$ as the second compact of detector calibration.

4. Position of TCP in world coordinate system x_{TCP}^w, y_{TCP}^w and z_{TCP}^w

These are obviously known values in the ABB welding system and are also known in most of the systems of NC machines as the NC milling machine to be used for detector calibration, for instance.

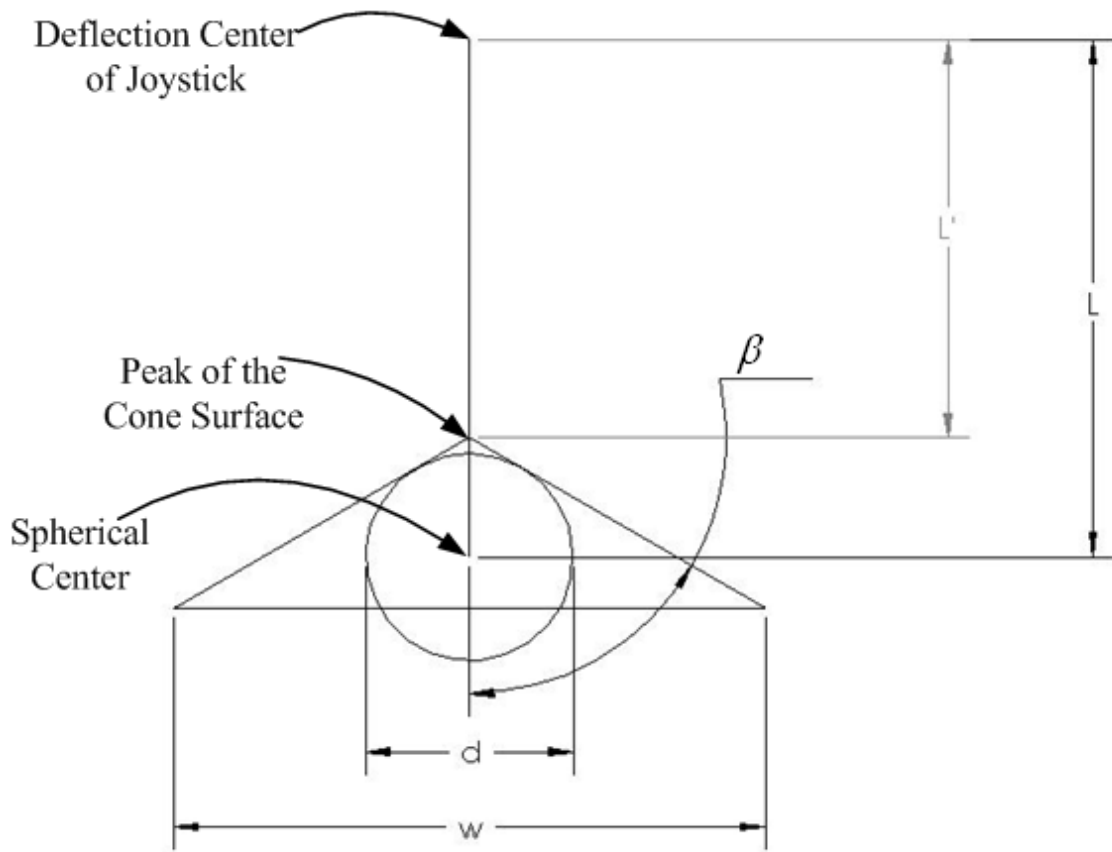


Figure 3.12: The relationship between L and d

5. The position of joystick deflection center in tool coordinate system Δx , Δy and Δz .

Determining the values of these three coefficients is the last target of detector calibration. They designate the position of the joystick's deflection center in the tool coordinate system so that different settings of tool coordinate system cause different values of these three values.

In order to achieve the targets, the calibration method is designed based on the process of solving Equation 2.11. Suppose the position of the tooling ball is known and simulate the detecting process designed in Chapter 2, Equation 2.11 becomes an equation set with three equations and five unknown coefficients. Once two of the unknown coefficients are fixed, the other three can be determined. The NC milling machine with indexing head is utilized for the detector calibration.

3.3.2 Detector Calibration Procedure

Step 1: Obtain x and y value of the tooling ball in the milling machine coordinate system.

In the later processes of tooling ball detection, the tooling ball is fixed in the jaws of the indexing head. As a result, the x and y values of the tooling ball center are positioned at the center axis of the indexing head in the milling machine coordinate system. By repeating the first two steps of the joystick calibration experiment, the x and y values of the tooling ball center can be obtained. For convenience in computing, set the x and y values displayed on the screen of the milling machine to zero.

Step 2: Obtain z value of tooling ball center in milling machine coordinate system.

Remove the steel rod and fix the tooling ball with the jaws of the indexing head. Close the chuck and let the bottom surface of the chuck tangent contact the surface of the tooling ball, as shown in Figure 3.13. Set the z value of the milling machine to

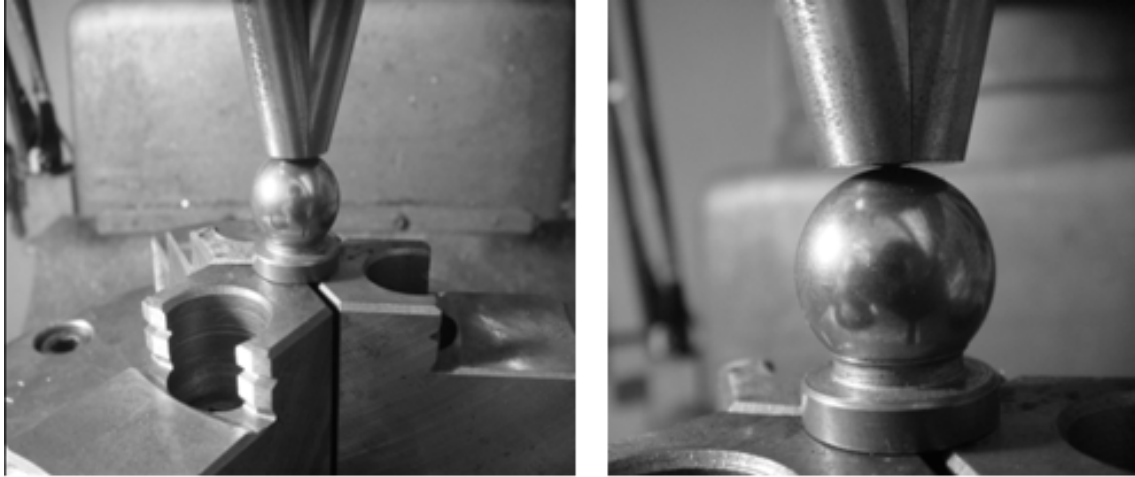


Figure 3.13: Obtain z value of the tooling ball center by the chuck.

zero. The origin of the milling machine coordinate system is then set at the highest point of the tooling ball surface. With the radius of the tooling ball $R(7.925mm)$ measured previously, the position of the center of the tooling ball in milling machine coordinate system is:

$$P^m = \begin{pmatrix} x_p^m & y_p^m & z_p^m & 1 \end{pmatrix}^T = \begin{pmatrix} 0 & 0 & R & 1 \end{pmatrix}^T = \begin{pmatrix} 0 & 0 & 7.925 & 1 \end{pmatrix}^T.$$

Step 3: Set up the detector.

Mount the detector to the milling machine by the tool holder. Figure3.14 illustrates the coordinate systems in the detector calibration process.

Step 4: Detect the tooling ball from different positions.

Change the position of the TCP and detect the tooling ball to obtain voltage signal outputs. Record voltage values at each detecting position and position the TCP when the digital signal is activated. (Use the multi-meter to measure the resistor of the tactile switch; once the resistor changes from infinite to a very small value, the digital signal is considered as being activated.) The position of the measured locations should follow the x and y values of the TCP as shown in Table3.4 and as

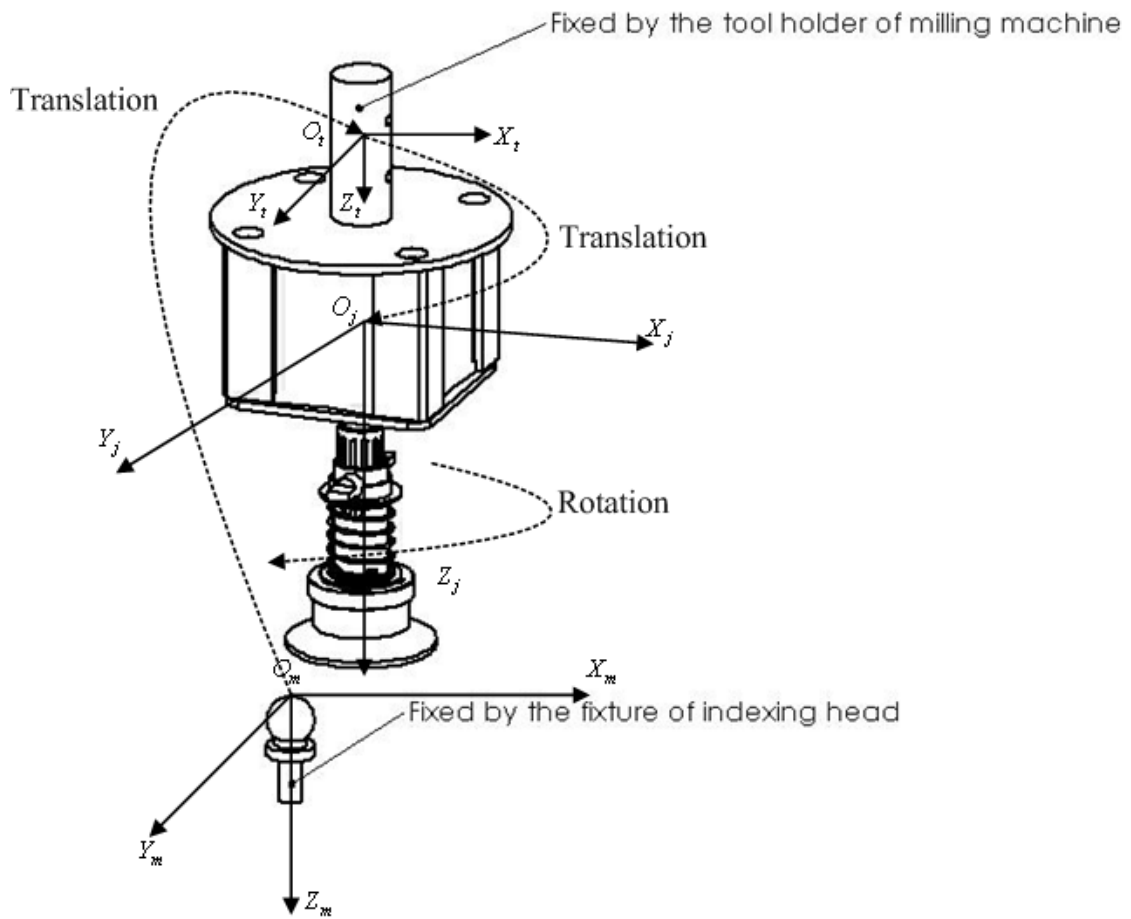


Figure 3.14: Coordinate Systems in Detector Calibration Process

Table 3.4: Ideal Detecting positions of TCP (mm)

index	x_{TCP}^m	y_{TCP}^m	index	x_{TCP}^m	y_{TCP}^m
1	25	0	11	-25	0
2	23.776	7.725	12	-23.776	-7.725
3	20.225	14.695	13	-20.225	-14.695
4	14.695	20.225	14	-14.695	-20.225
5	7.725	23.776	15	-7.725	-23.776
6	0	25	16	0	-25
7	-7.725	23.776	17	7.725	-23.776
8	-14.695	20.225	18	14.695	-20.225
9	-20.225	14.695	19	20.225	-14.695
10	-23.776	7.725	20	23.776	-7.725

illustrated in Figure3.15. The positions do not need to be exactly the same as the data in Table3.4.

3.3.3 Transformation Process

The transformation process is similar to the process in the ABB robot system. Firstly, there is a translation from the milling machine coordinate system to the tool coordinate system. Secondly, there is a translation from the tooling coordinate system to the joystick coordinate system followed by a rotation about the axis Z_j . Then, according to Equation 2.11, the position of the tooling ball in the milling machine coordinate system can be computed by Equation 3.43. The milling machine coordinate system is simply the world coordinate system discussed in Chapter 2. The position of the TCP in the world coordinate system is then represented by $TCP^m = \begin{pmatrix} x_{TCP}^m & y_{TCP}^m & z_{TCP}^m & 1 \end{pmatrix}^T$ instead of $TCP^w = \begin{pmatrix} x_{TCP}^w & y_{TCP}^w & z_{TCP}^w & 1 \end{pmatrix}^T$.

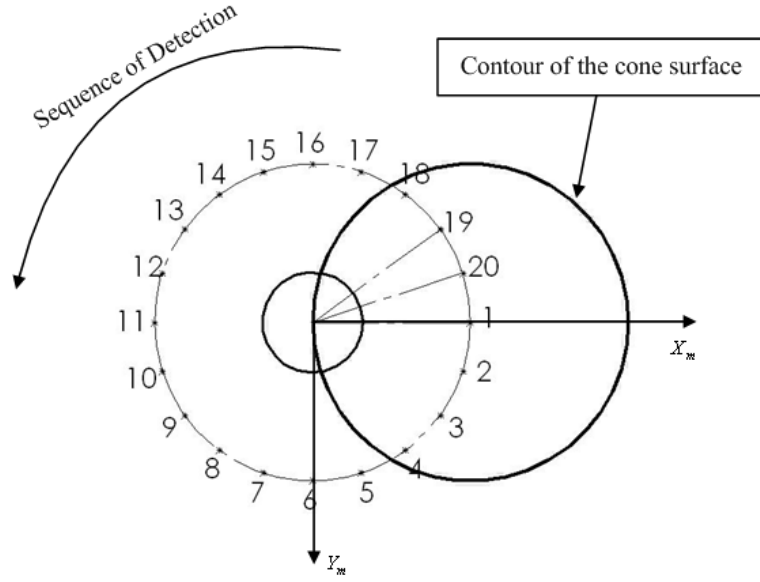


Figure 3.15: Positions of TCP for Tooling Ball Detection

$$P^m = \begin{pmatrix} x_P^m \\ y_P^m \\ z_P^m \\ 1 \end{pmatrix} = \begin{pmatrix} L(\cos \delta\theta \cos \theta_x \sin \theta_y + \sin \delta\theta \cos \theta_y \sin \theta_x) + x_{TCP}^m + \Delta x \\ L(\sin \delta\theta \cos \theta_x \sin \theta_y - \cos \delta\theta \cos \theta_y \sin \theta_x) + y_{TCP}^m + \Delta y \\ L \cos \theta_x \cos \theta_y + z_{TCP}^m + \Delta z \\ 1 \end{pmatrix} \quad (3.43)$$

Equation 3.43 is simplified into Equation 3.44.

$$P^m = \begin{pmatrix} x_P^m \\ y_P^m \\ z_P^m \\ 1 \end{pmatrix} = \begin{pmatrix} L\sqrt{a^2 + b^2} \sin(\delta\theta + \alpha) + x_{TCP}^m + \Delta x \\ -L\sqrt{a^2 + b^2} \cos(\delta\theta + \alpha) + y_{TCP}^m + \Delta y \\ cL + z_{TCP}^m + \Delta z \\ 1 \end{pmatrix} \quad (3.44)$$

$$\text{where : } a = \cos \theta_x \sin \theta_y$$

$$b = \cos \theta_y \sin \theta_x$$

$$c = \cos \theta_x \cos \theta_y$$

$$\sin \alpha = a/\sqrt{a^2 + b^2}$$

$$\cos \alpha = b/\sqrt{a^2 + b^2}$$

3.3.4 Method for Data Processing

After the detector calibration procedure, we have the following data and equations.

1. Positions of TCP at 20 detecting positions at which the digital signal is activated (see Table3.5). Twenty detecting positions are predetermined in 3.3.2 according to positions in Table3.4. Operate the position of table on axes X_m and Y_m of the milling machine until values of x_{TCP}^m and y_{TCP}^m become almost the same as the data in Table3.4 within the range of $\pm 0.1mm$. Coordinate values of TCP of the milling machine are displayed on the LCD screen with three significant digits which can be read directly and be recorded manually.
2. Twenty groups of voltage outputs of the joystick at which the digital signal is activated (see Table3.6). After recording the position of TCP at each detecting position, multimeter is used for measuring output voltage values of the joystick. The voltage values are measured by the multi-meter with three significant digits.

Table 3.5: Actual Detecting positions of TCP (mm)

index	x_{TCP}^m	y_{TCP}^m	z_{TCP}^m	index	x_{TCP}^m	y_{TCP}^m	z_{TCP}^m
1	24.990	-0.005	-20.100	11	-24.965	-0.010	-20.085
2	23.770	6.715	-20.170	12	-23.770	-7.705	-20.000
3	20.230	14.695	-20.145	13	-20.200	-14.670	-20.010
4	14.690	20.225	-20.175	14	-14.690	-20.160	-20.070
5	7.745	23.770	-20.060	15	-7.730	-23.770	-20.040
6	0.005	24.990	-20.120	16	0.005	-24.990	-20.160
7	-7.730	23.775	-20.115	17	7.735	-23.745	-20.090
8	-14.700	20.230	-20.115	18	14.685	-20.235	-20.085
9	-20.210	14.685	-20.125	19	20.195	-14.700	-20.055
10	-23.8050	7.710	-20.110	20	23.775	-7.730	-20.025

Table 3.6: Voltage Signal Outputs

index	V_{out}^{x1}/V	V_{out}^{x2}/V	V_{out}^{y1}/V	V_{out}^{y2}/V	index	V_{out}^{x1}/V	V_{out}^{x2}/V	V_{out}^{y1}/V	V_{out}^{y2}/V
1	3.694	1.364	2.268	2.796	11	1.338	3.756	2.757	2.288
2	3.713	1.352	2.556	2.495	12	1.317	3.786	2.438	2.624
3	3.642	1.432	2.982	2.070	13	1.409	3.699	2.058	3.008
4	3.445	1.640	3.310	1.749	14	1.610	3.499	1.724	3.340
5	3.149	1.936	3.556	1.508	15	1.909	3.206	1.476	3.588
6	2.780	2.309	3.694	1.373	16	2.265	2.835	1.343	3.725
7	2.427	2.644	3.714	1.351	17	2.604	2.470	1.318	3.749
8	2.049	3.025	3.622	1.442	18	2.982	2.089	1.403	3.663
9	1.719	3.363	3.421	1.638	19	3.316	1.759	1.602	3.462
10	1.472	3.621	3.125	1.925	20	3.561	1.507	1.904	3.162

3. Position of the tooling ball center in the milling machine coordinate system (Equation 3.45). This is obtained from the second step of the detector calibration procedure described in 3.3.2.

$$P^m = \begin{pmatrix} x_p^m \\ y_p^m \\ z_p^m \\ 1 \end{pmatrix} = \begin{pmatrix} 0 \\ 0 \\ R \\ 1 \end{pmatrix} = \begin{pmatrix} 0 \\ 0 \\ 7.925 \\ 1 \end{pmatrix} \quad (3.45)$$

4. Equation 3.44 for position computation.

The data are processed by the following steps:

Step 1: Compute the deflection angles according to the voltage outputs and results obtained from the joystick calibration procedure for Equations 3.40 and 3.41.

Step 2: Compute a , b , c and α according to Equation 3.44.

Step 3: For $\Delta x = 0$ and $\Delta y = 0$, we have Equation 3.46.

$$P^m = \begin{pmatrix} x_P^m \\ y_P^m \\ z_P^m \\ 1 \end{pmatrix} = \begin{pmatrix} L\sqrt{a^2 + b^2} \sin(\delta\theta + \alpha) + x_{TCP}^m \\ -L\sqrt{a^2 + b^2} \cos(\delta\theta + \alpha) + y_{TCP}^m \\ cL + z_{TCP}^m + \Delta z \\ 1 \end{pmatrix} \quad (3.46)$$

Step 4: Solve $\delta\theta$ as Equation 3.47:

$$\delta\theta = \text{atan2}(-x_{TCP}^m, y_{TCP}^m) - \alpha \quad (3.47)$$

where $\text{atan2}()$ is a function in Matlab[16].

Step 5: Solve L as Equation 3.48:

$$L = -x_{TCP}^w / [\sqrt{a^2 + b^2} \sin(\delta\theta + \alpha)] \quad (3.48)$$

Step 6: Solve Δz as Equation 3.49:

$$\Delta z = r - cL - z_{TCP}^m \quad (3.49)$$

Equations 3.47, 3.48 and 3.49 are derived from Equation 3.46. Any detecting position with $x_{TCP}^w = 0$ cannot be selected for calibration because when $x_{TCP}^w = 0$, $\delta\theta$ and L will be zero in Equations 3.47 and 3.48.

3.3.5 Detector Testing

Detector testing is aimed at testing the performance of the detector, including the operating condition of the mechanical components and the accuracy of detection. Firstly, the position of the tooling ball to be detected should be known. Secondly, the coefficients for position computing should be obtained from the detector calibration process. Finally, the position of the tooling ball obtained from the computation process should be compared with the position value that is known.

The procedure for detector calibration and detector testing are the same, so the data obtained in the detector calibration process can be used for detector testing. There are twenty groups of data obtained. Four groups of the data are used for detector calibration and the other 16 groups are used for detector testing.

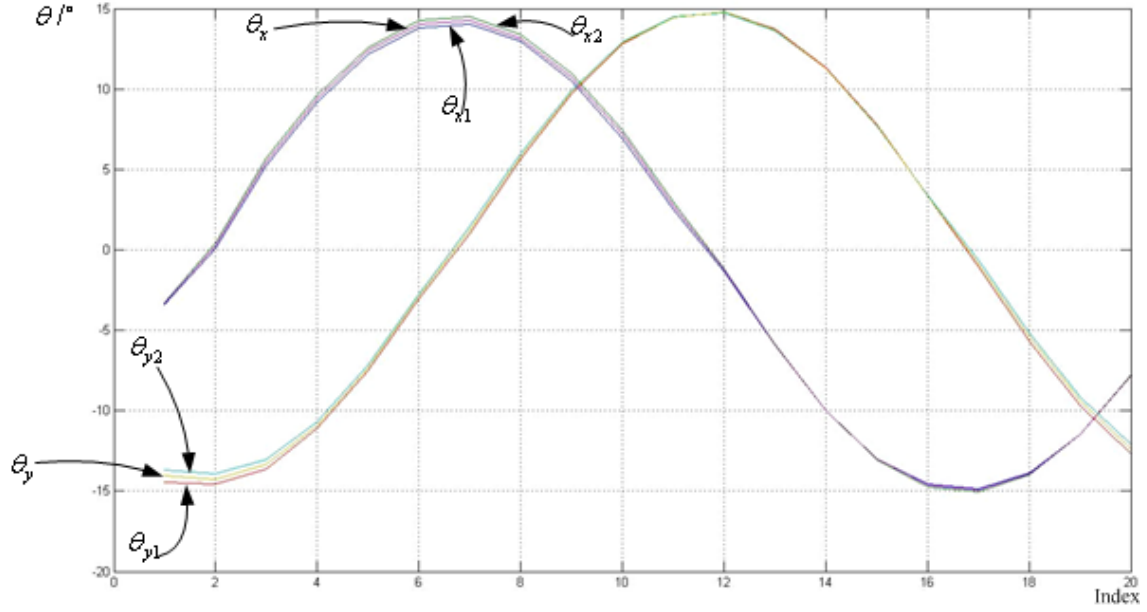


Figure 3.16: Consistency of Angle Computation

3.3.6 Results of Data Processing

Data are processed following the steps described in 3.3.4. Firstly, all voltage signals are converted into deflection angles according to Equations 3.40 and 3.41, as given in Table 3.7.

There are six voltage values obtained in each detecting position. Four values (θ_{x1} , θ_{x2} , θ_{y1} and θ_{y2}) are computed from output voltage values measured from the joystick according to the result of joystick calibration experiment (3.2.2). θ_{x1} and θ_{x2} represent deflection angle of the joystick shaft about axis X_j ; θ_{y1} and θ_{y2} represent deflection angle of the joystick shaft about axis Y_j . Therefore, the smaller the value difference between θ_{x1} and θ_{x2} and the value difference between θ_{y1} and θ_{y2} , the better the results for joystick calibration. Figure 3.16 illustrates the consistency of angle computation.

The maximal difference of θ_x is 0.51° and the maximal difference of θ_y is 0.76° .

Secondly, following Step 2 to Step 6 described in 3.3.4, we have $\delta\theta$, L and Δz computed

Table 3.7: Results of Deflection Angle Computation

index	$\theta_{x1}/^\circ$	$\theta_{x2}/^\circ$	$\theta_x/^\circ$	$\theta_{y1}/^\circ$	$\theta_{y2}/^\circ$	$\theta_y/^\circ$
1	-3.41	-3.28	-3.34	-14.44	-13.68	-14.06
2	0.07	0.43	0.25	-14.59	-13.91	-14.25
3	5.22	5.67	5.44	-13.62	-13.06	-13.34
4	9.18	9.62	9.40	-11.11	-10.71	-10.91
5	12.15	12.59	12.37	-7.54	-7.17	-7.35
6	13.82	14.25	14.03	-3.03	-2.75	-2.89
7	14.06	14.52	14.29	1.01	1.47	1.24
8	12.95	13.40	13.17	5.62	5.99	5.80
9	10.52	10.99	10.75	9.70	9.94	9.82
10	6.94	7.45	7.20	12.81	12.90	12.85
11	2.50	2.98	2.74	14.44	14.50	14.47
12	-1.35	-1.16	-1.26	14.81	14.75	14.78
13	-5.94	-5.89	-5.91	13.76	13.65	13.70
14	-9.98	-9.98	-9.98	11.34	11.24	11.29
15	-12.97	-13.03	-13.00	7.80	7.67	7.73
16	-14.58	-14.72	-14.65	3.32	3.41	3.37
17	-14.88	-15.01	-14.95	-1.08	-0.65	-0.87
18	-13.85	-13.95	-13.90	-5.69	-5.17	-5.43
19	-11.45	-11.48	-11.46	-9.67	-9.16	-9.42
20	-7.80	-7.78	-7.79	-12.72	-12.09	-12.41

Table 3.8: Results of Detector Calibration Experiment

index	$\delta\theta/^\circ$	L/mm	$\Delta z/mm$	index	$\delta\theta/^\circ$	L/mm	$\Delta z/mm$
1	13.105	100.32	-69.125	11	10.529	98.341	-67.103
2	14.784	100.33	-69.145	12	13.212	97.651	-66.473
3	14.113	101.00	-69.758	13	12.969	97.519	-66.305
4	13.350	101.57	-70.295	14	12.545	97.059	-65.746
5	12.421	101.43	-70.281	15	12.454	96.648	-65.349
6	11.413	101.15	-69.961	16	12.691	96.584	-65.200
7	13.142	100.95	-69.765	17	14.800	96.687	-65.390
8	12.527	101.17	-69.960	18	14.969	97.581	-66.288
9	11.651	100.44	-69.180	19	14.667	98.611	-67.361
10	11.015	99.19	-67.907	20	13.877	99.731	-68.553

Table 3.9: Average Values of $\delta\theta$, L and Δz at Calibration Positions

	$\delta\theta/^\circ$	L/mm	$\Delta z/mm$
Average Value	13.9845	98.9045	-67.6933

for each group of data using values of θ_x and θ_y in Table3.7. Results of computation are shown in Table3.8 and plotted in Figure3.17, 3.18 and 3.19 respectively.

Thirdly, select the 2nd, 7th, 12th and 17th detecting positions as positions for calibration. The other positions are used for testing the detector. Compute average values of $\delta\theta$, L and Δz at calibration positions are the final result of calibration and they are given in Table3.9.

Finally, use results in Table3.9 and the other 16 groups of deflection angles in Table3.8 to compute positions of the tooling ball according to Equation 3.44. We also have positions of tooling ball computations shown in Table3.10.

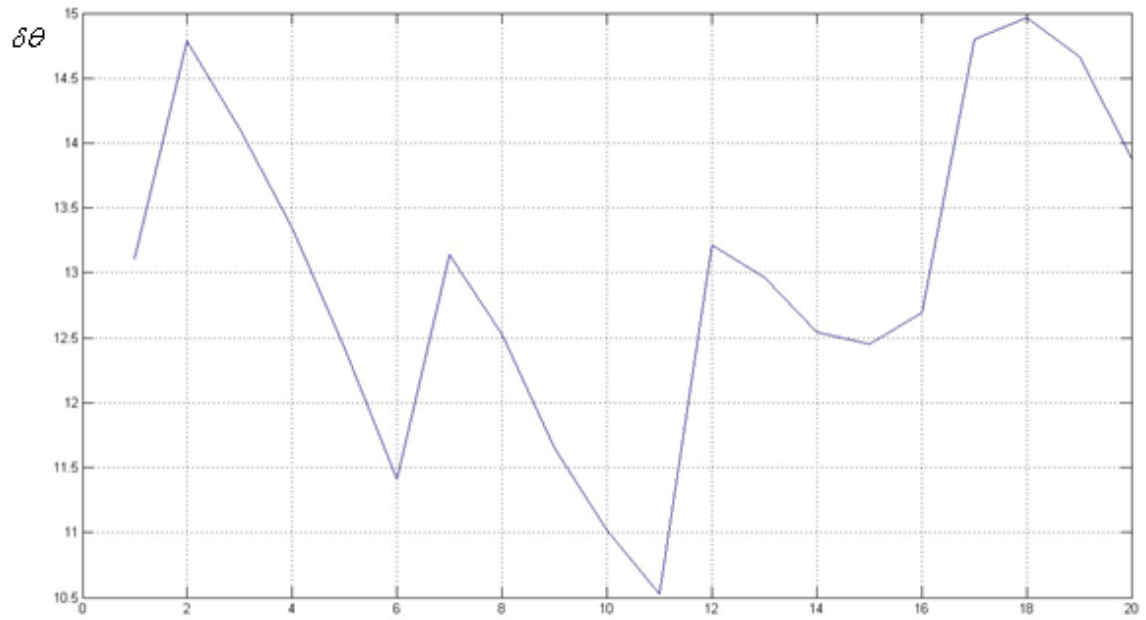


Figure 3.17: $\delta\theta$

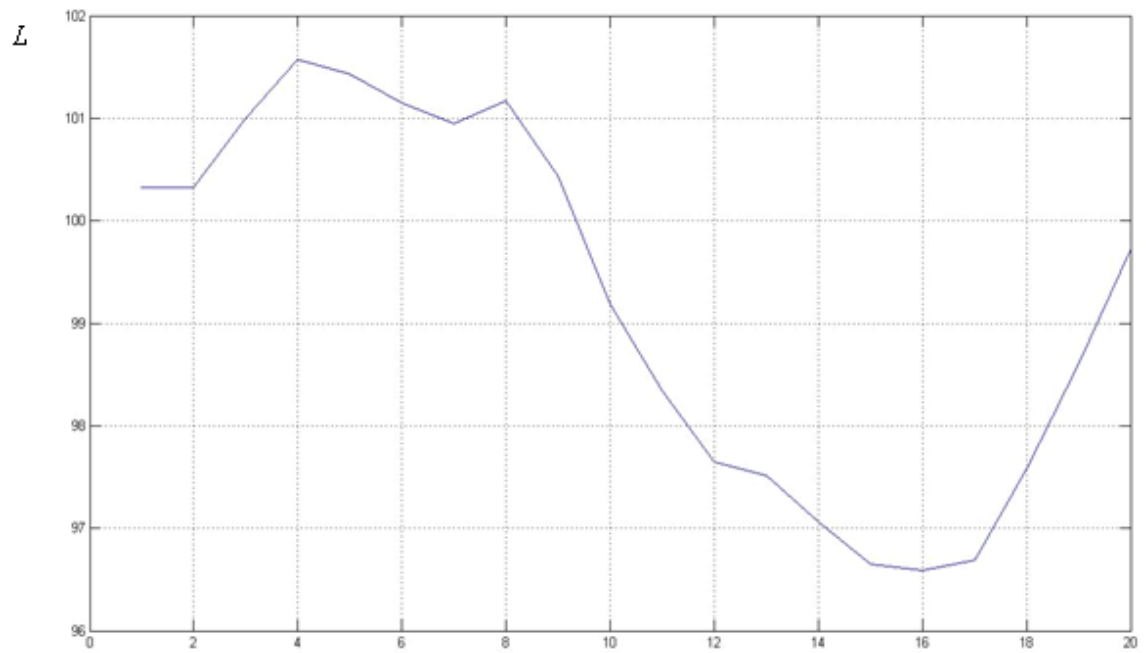


Figure 3.18: L

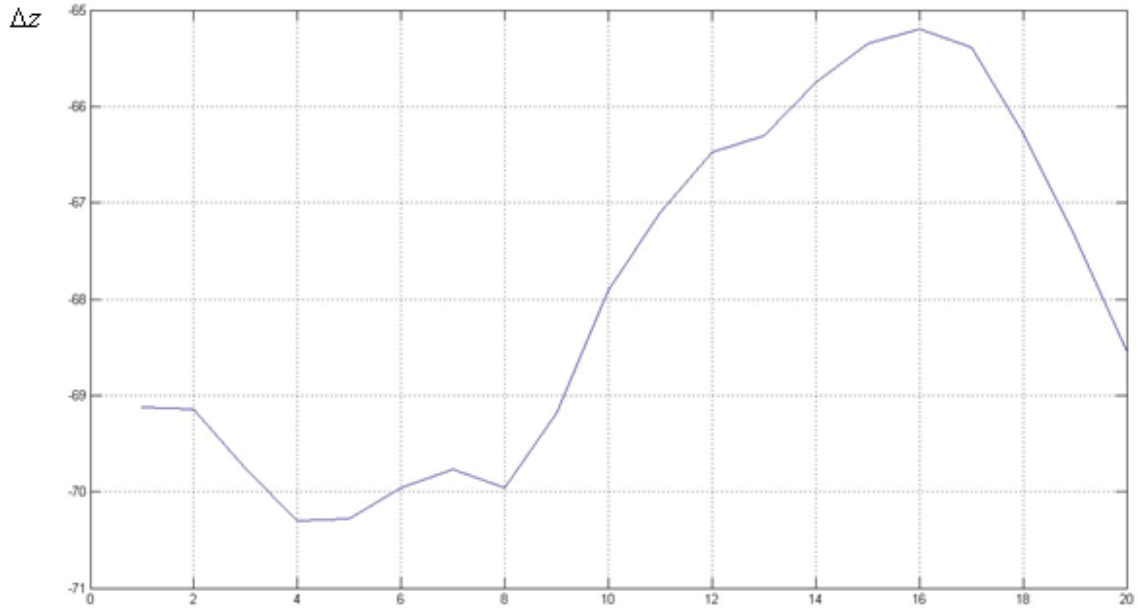


Figure 3.19: Δz

Table 3.10: Results of Detector Calibration Experiment

index	TCP_x	TCP_y	TCP_z	index	TCP_x	TCP_y	TCP_z
1	0.003	-0.384	9.356	11	-0.046	1.505	7.334
3	-0.033	0.046	9.990	13	-0.263	0.356	6.536
4	0.225	-0.161	10.527	14	-0.511	0.363	5.978
5	0.651	-0.202	10.513	15	-0.638	0.198	5.581
6	1.121	0.025	10.193	16	-0.564	-0.006	5.431
8	0.510	0.380	10.192	18	0.350	0.249	6.519
9	0.581	0.835	9.412	19	0.176	0.239	7.593
10	0.367	1.244	8.139	20	-0.014	-0.045	8.785

Table 3.11: Errors of Tooling Ball Position Detection (mm)

index	x-error	y-error	z-error	index	x-error	y-error	z-error
1	0.003	-0.384	1.431	11	-0.046	1.505	-0.591
3	-0.033	0.046	2.065	13	-0.263	0.356	-1.389
4	0.225	-0.161	2.602	14	-0.511	0.363	-1.947
5	0.651	-0.202	2.588	15	-0.638	0.198	-2.344
6	1.121	0.025	2.268	16	-0.564	-0.006	-2.494
8	0.510	0.380	2.267	18	0.350	0.249	-1.406
9	0.581	0.835	1.487	19	0.176	0.239	-0.331
10	0.367	1.244	0.214	20	-0.014	-0.045	0.860

The differences between the position of the tooling ball in computation and the position of the ball in actual space are the error of detection. Errors computed are given in Table3.11 and plotted in Figure3.20. As the accuracy of detection required in 1.1.4, position errors on each axis of milling machine coordinate system should locate within the range of $\pm 1mm$. Two black lines in the Figure3.20 are the boundaries of accuracy requirement. Result points plotted in the figure should locate between two black lines. If not, the detection is not as accurate as is required.

3.4 Evaluation and Analysis

The accuracy of position computation is not satisfied according to Figure3.20. All of position errors on the three axis of the milling machine coordinate system do not fully locate within the range of $\pm 1mm$, especially the value of 'z-error' on axis Z_m .

In order to determine what is causing the low detecting accuracy, a common phenomenon within the distribution of errors and target values (difference between θ_{x1} and

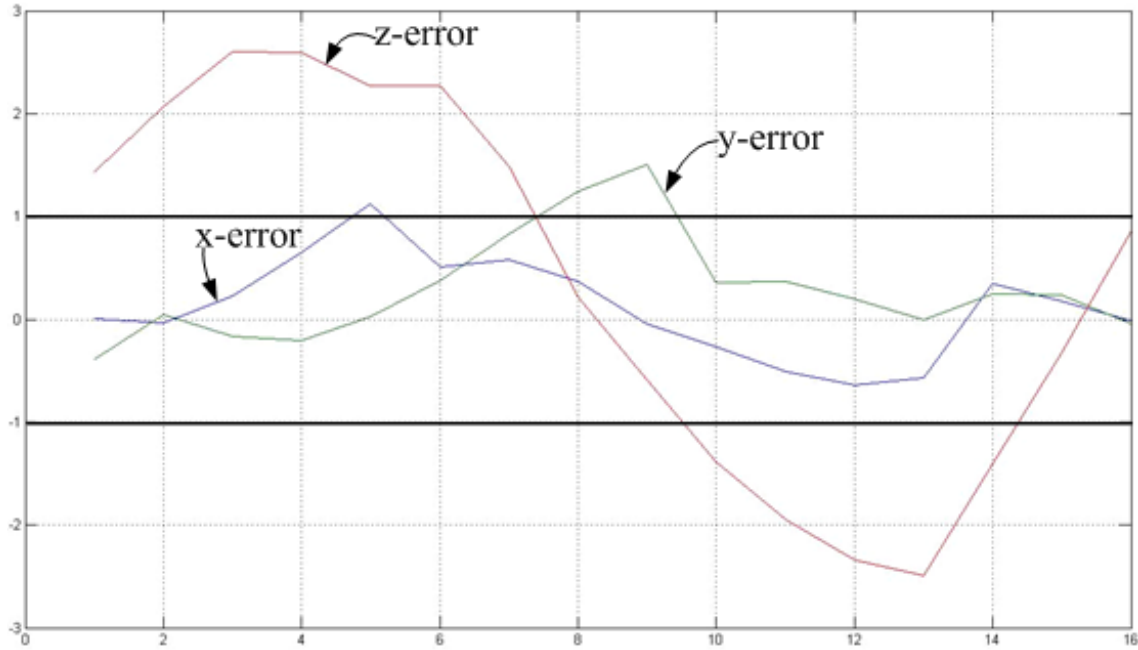


Figure 3.20: Errors of Tooling Ball Position Detection

θ_{x2} , difference between θ_{y1} and θ_{y2} , $\delta\theta$, L and Δz) are found. The trends of errors and target values are similar to the trends of positions of TCP as shown in Figure3.21 to 3.25.

Figure3.21 shows the relationship between curves of $(\theta_{x1} - \theta_{x2})^2$ and $(\theta_{y1} - \theta_{y2})^2$ and correspondent positions of TCP on axis X_m and axis Y_m . Values of $(\theta_{x1} - \theta_{x2})^2$ and $(\theta_{y1} - \theta_{y2})^2$ are used to describe the difference between θ_{x1} and θ_{x2} and the difference between θ_{y1} and θ_{y2} respectively.

Figures3.22 to 3.24 show the relationship between values of $\delta\theta$, L and Δz and correspondent positions of TCP on axis X_m and axis Y_m .

Figure3.25 shows the relationship between errors on axes X_m , Y_m and Z_m and correspondent positions of TCP on axes X_m and Y_m .

This phenomenon shows that the problem of generating unsatisfied results may happen at the process of calibrating the joystick for computing deflection angle. After rethinking

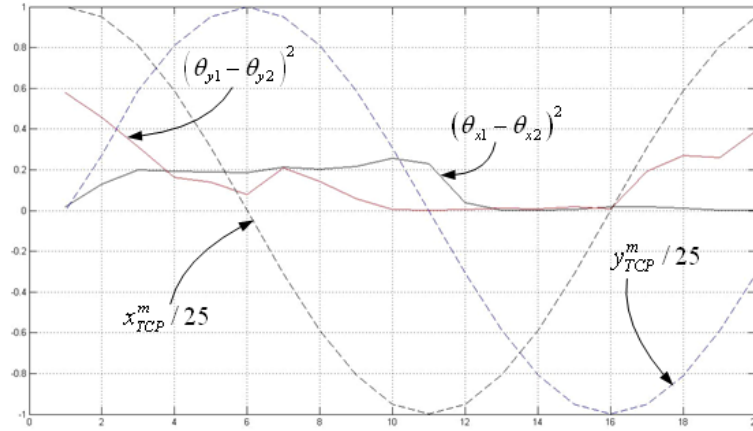


Figure 3.21: Relationship between $(\theta_{x1} - \theta_{x2})^2$ and $(\theta_{y1} - \theta_{y2})^2$ and Correspondent Positions of TCP

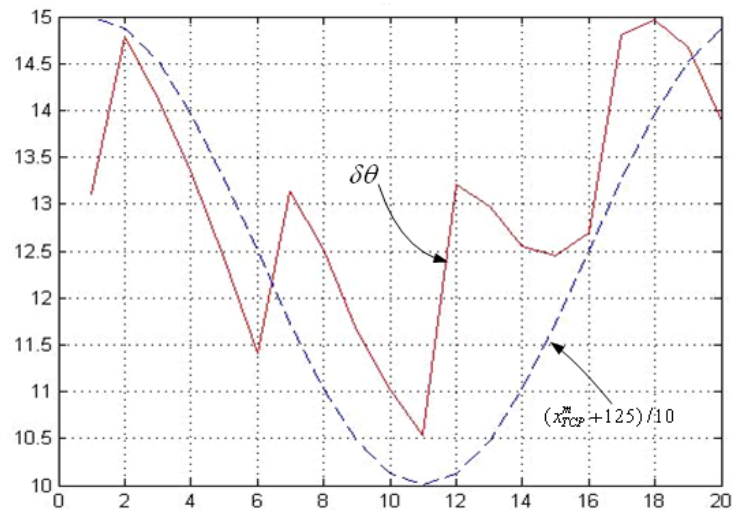


Figure 3.22: Relationship Between $\delta\theta$ and Correspondent Positions of TCP on X_m

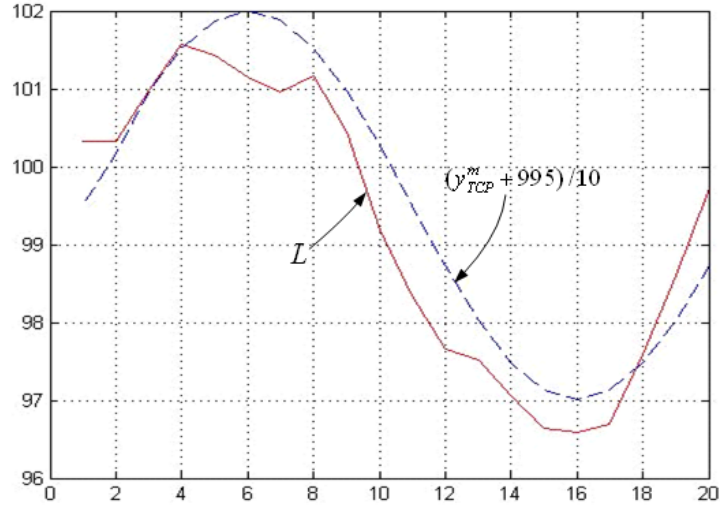


Figure 3.23: Relationship Between L and Correspondent Positions of TCP on Y_m

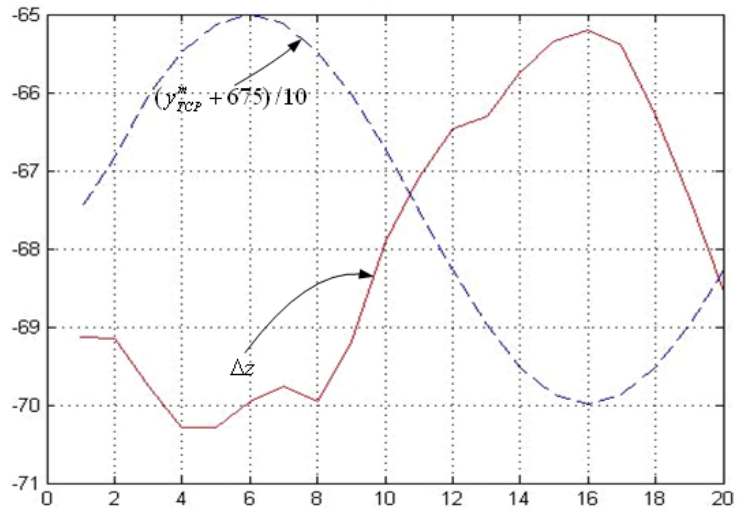


Figure 3.24: Relationship Between Δz and Correspondent Positions of TCP on Y_m

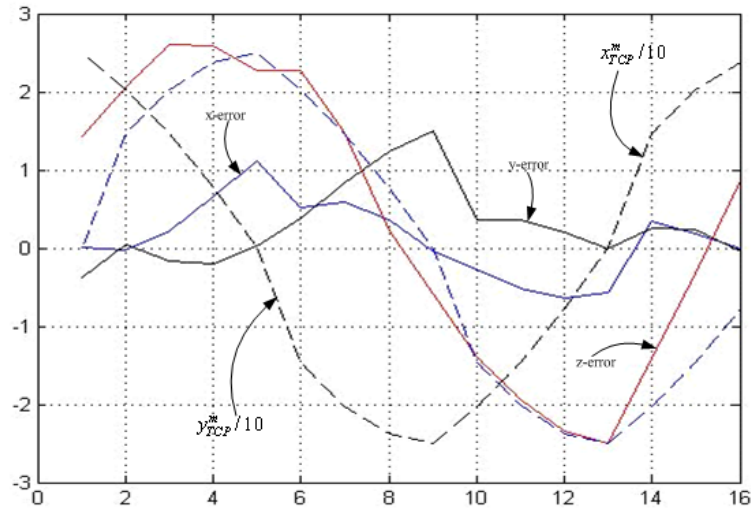


Figure 3.25: Relationship between Errors of Position Detection and Correspondent Positions of TCP

the design of the joystick calibration process, three deficiencies were found.

1. Loose fit caused by using the screw connecting the centering shaft and bearing fixer.

The centering shaft and bearing housing are connected by an M3-40 socket head cap screw with nut. The screw is also utilized as the shaft for the bearing housing to rotate about. The distance between the center axis of this shaft and the center axis of the linear motion bearing (d) is one of the most important distances for slope computation. The screw and the hole are loose fit so that distance d cannot be satisfied as the one designed in 3D modeling software.

2. Scoring of shaft extension caused by the bearing balls.

The shaft extension is inserted into the linear motion bearing. In the process of rotating the indexing head, the shaft extension keeps rotating in the bearing. However, the hardness of stainless steel balls is much higher than the hardness of the shaft extension which is made of 1045 without being heat treated. After rounds of rotation,

the shaft extension is broken by the balls of bearing and the coaxiality between the shaft extension and the linear motion bearing decreases. The combined deflection angle θ_f can not be maintained the same in the whole rotation process.

3. Low accuracy of multi-meter for measuring the output voltage signals.

Finally, the accuracy of multi-meter for measuring the output voltage signals is too low (with two significant digits) to secure the accuracy of the voltage value measurement.

Future works is required to improve these three deficiencies in order to achieve better results from the joystick calibration experiment.

Chapter 4

An Extension: Optical Detecting Method Design

The idea of developing a vision-based detecting method comes from the project requirement of course SYDE 677 'Computer Vision' taught by Professor Tizhoosh. According to the knowledge of image processing and concepts of computer vision obtained from the course, a simplified and specialized vision-based detecting method is designed. The simplification and specialization are achieved by utilizing the geometry properties of reflection image which is formed by a 'C' shape light source onto the spherical surface of a stainless steel tooling ball.

Because the vision-based detecting is a non-touch detection method and the distance in taking photos can be controlled, it may perform better than mechanical touching in a high temperature environment. Therefore, for tooling ball detecting purposes in a mould calibration process in a high-temperature working environment at about $700F^{\circ}$, a vision-based tooling ball detecting method can be applied as an extension for the mechanical touch detection described in Chapters 2 and 3.

Due to lack of time and devices to achieve the entire detecting method based on an



Figure 4.1: Partial Ring Shaped Light Source

ABB robot, the target of the course project is simply to find out the 'C' shape reflection image in photos and compute the position of the tooling ball in a photo coordinate system in order to test the feasibility of the vision-based method. Firstly, the hardware setting for taking photos of the tooling ball is introduced. Secondly, relevant optical characteristics are mentioned. Thirdly, a vision-based tooling ball detecting method is described with the results of the experiment provided. Finally, the chapter summary concludes the vision-based detecting method design and the compensation relationship between the mechanical-touch detection and vision-based detecting methods are discussed.

4.1 Hardware Setting

- Light source:

The light source is a partial ring-shaped light source which is shown in Figure4.1.

- Camera:

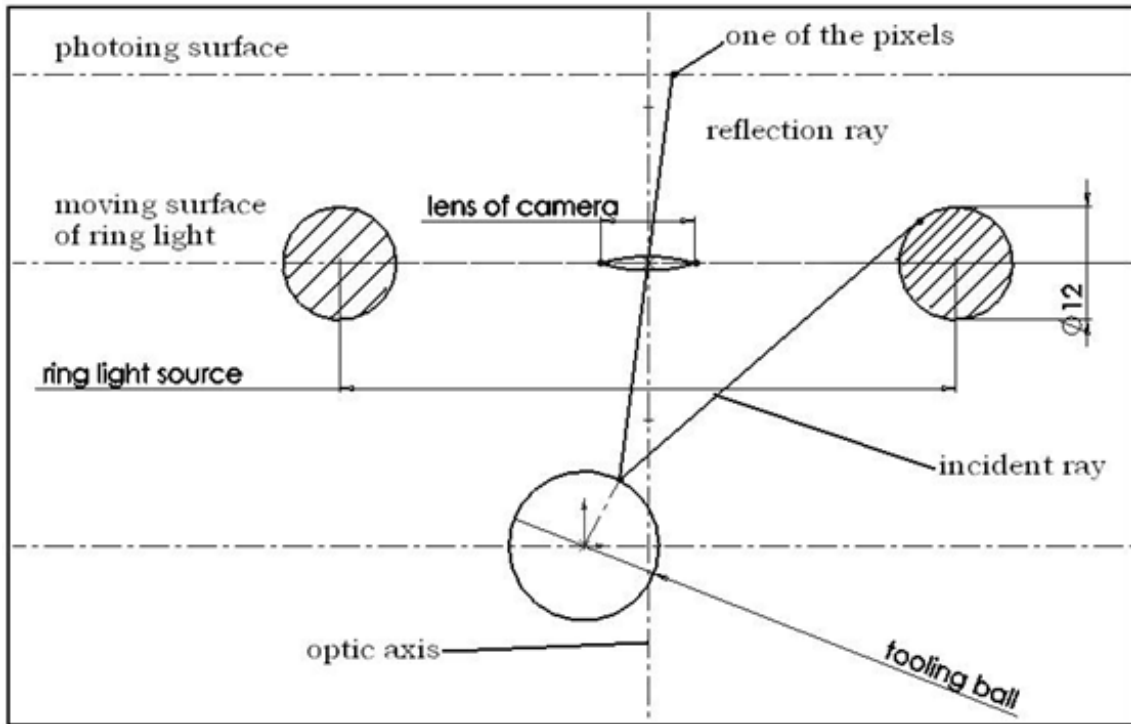


Figure 4.2: Position Relationship among the Camera, Light Source and the Tooling Ball

'SONY T100 Cyber-shot' digital camera is selected to take images of the tooling ball. The resolution of the camera is 1536 by 2048 pixels.

- Position and Operation Configuration:

When the camera is taking images of tooling ball, the optic axis of the camera's lens should always coincide with the center axis of the ring-shaped light source. As well, the optic axis should always be perpendicular to the $X_w - O_w - Y_w$ plane of the world coordinate system. The position relationship amongst the camera, the light source and the tooling ball is briefly displayed in Figure4.2.

4.2 Optical Characteristics of Tooling Ball

The fine polished surface makes the tooling ball appears as a spherical mirror with unique optic characteristics regarding light reflection and reflection image formation, if it is compared with the surface of work pieces like moulds of autos, for instance. Two differences (O Difference) between optic characteristics of the tooling ball and the work piece are described as followings.

O Difference 1: The ratio between the diameter of the tooling ball's effective reflection surface and the radius of the ball is always two. The ratio of the work pieces' surface is smaller than $1/3$ in most cases. Geometrical characteristics of image formation are totally different between the two types of reflection surfaces. A light source with special shape will form different reflection images on two different types of surfaces. [17]

O Difference 2: Since the spherical surface of a tooling ball is fine polished, the surface smoothness of a tooling ball is always higher than the surface of a work piece. As well, the surface of a tooling ball is always closer to the light source than the work piece. As a result, the gray level of the pixels in the image which is formed by reflecting light from the tooling ball is one of the highest areas of pixels within the image. Moreover, dark regions with high contrast to the region where the reflection image is formed will also be formed on the tooling ball's spherical surface around the brightened region.

4.3 The Reflection Phenomenon

According to the mirror reflection principle of light[17], if the stainless steel tooling ball is located within the lighting environment which is described below, a 'C' shape reflection

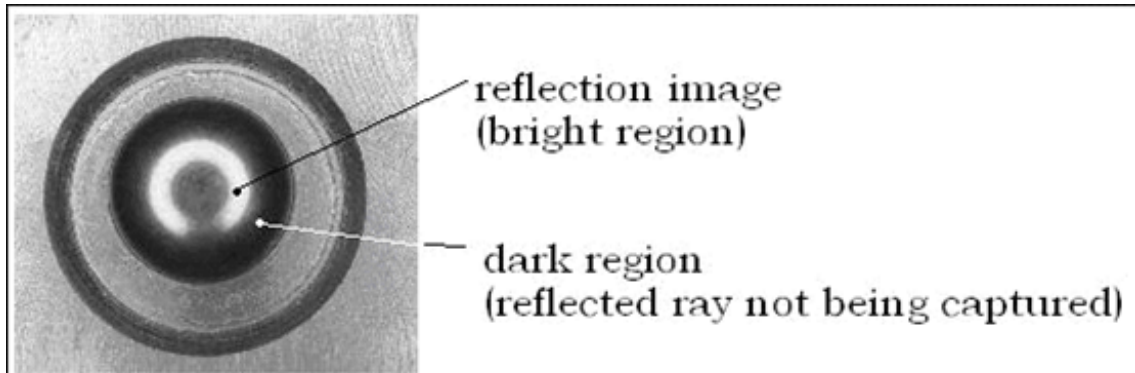


Figure 4.3: Reflection Image

image of the light source will be formed on the tooling ball's spherical surface with the following three properties (R Property):

R Property 1: A group of high gray value pixels (always higher than 128) will always exist within the image, and these pixels will appear as a shape ("C" shape) similar to the shape of the light source. The position of reflection image within the photo can be considered an approximate position of tooling ball.

R Property 2: The gray values of the pixels which are close to the high gray value pixels appear dark (the gray value is always lower than 128) because the reflected ray at these regions cannot be captured by the camera.

R Property 3: The gray values of pixels which are surrounding dark regions of the tooling ball are much higher than the dark regions.

A sample of the reflection image of the light source is shown in Figure4.3.

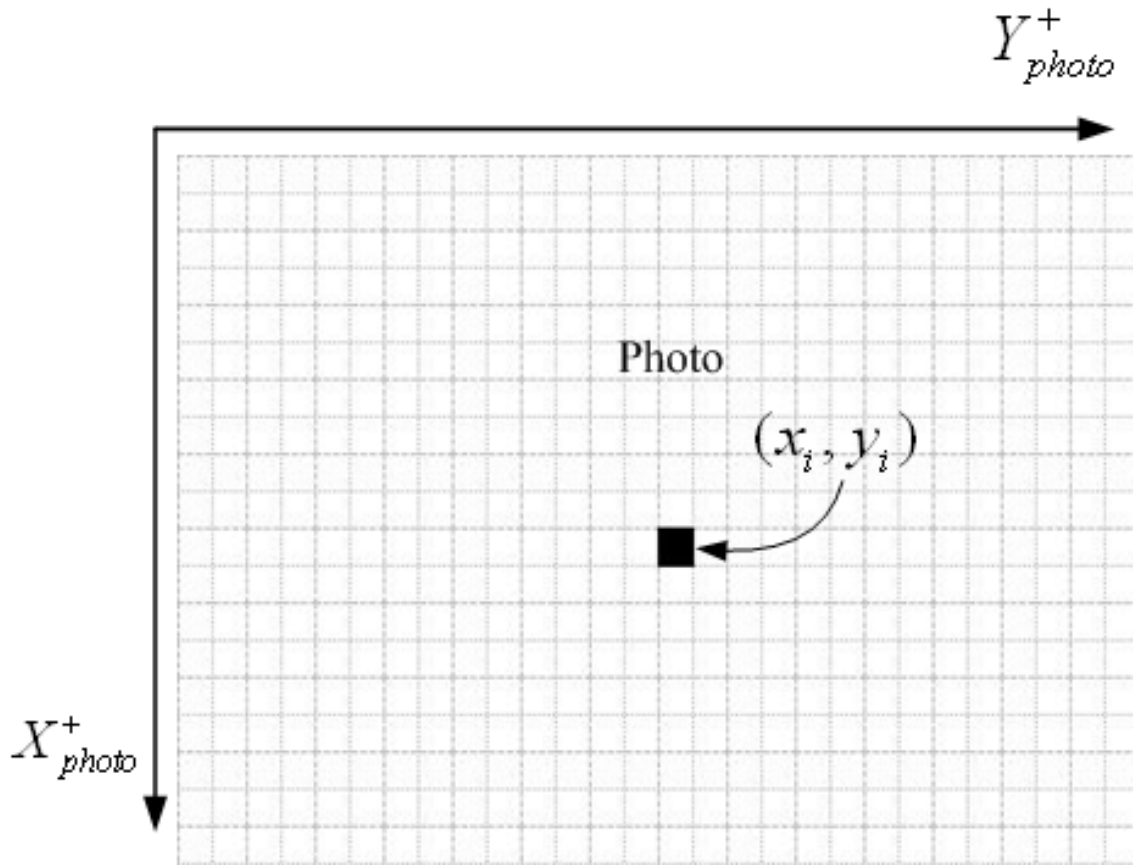


Figure 4.4: Pixel in Photo Coordinate System

4.4 Vision-Based Tooling Ball Detecting Method Design

4.4.1 Pre-described Concepts

- Photo Coordinate System:

Figure 4.4 defines the photo coordinate system of a photo. The position of a pixel within the photo can be defined by a pair of coordinate values.

- Object Pixel and Background Pixel:

All the values of elements in the binary image are binary numbers 1 and 0. Binary number 0 represents a background pixel of the color black and the binary number 1 represents an object pixel of the color white.

- **Objects:**

If a group of object pixels are called one object, they are 8-connected. [16]

- **Fitting Circle:**

Fit pixels of an object into a circle through direct least-squares circle fitting algorithm by V. Pratt. [18] This circle is called the "fitting circle" of this object. The fitting circle is described by three parameters: position of circle center and its radius. In the process of implementing the circle fitting algorithm, the direct circle fitting function is programmed by Nikolai Chernov in Matlab according to V. Pratt's paper.

- **Position of Object:**

The position of the object's fitting circle center is the position of the object.

- **Geometry Properties (G Property) of an Object:**

An object within a photo has six geometric properties: similarity, area, compactness, contour number, fullness, and the radius of fitting circle.

G property 1: Similarity

$$Similarity = \left[\sum_{i=1}^n (D_i - R) \right] / nR \quad (4.1)$$

where : $D_i = |CP_i|$

Equation 4.1 describes the degree of the fitting condition between the object and its fitting circle. Parameter D_i is the distance between object pixels P and

the center C of the object's fitting circle and parameter R is the radius of the fitting circle. There are n pixels in total belonging to the object.

G property 2: Area

Area is the size of the object measured by its number of pixels.

G property 3: Compactness

$$Compactness = Area_{Object} / Area_{FilledCircle} \quad (4.2)$$

Compactness of an object is not able to be affected by the object's scale. Thus, it is useful for distinguishing an object with specific shape. As shown in Equation 4.2, parameter $Area_{Object}$ represents the pixel number of the object and parameter $Area_{FilledCircle}$ represents the area of a fulfilled circle which has the same perimeter as the object.

G property 4: Contour Number

There is only one contour for the fulfilled object, and the number is more than one when the object has holes. [19]

G property 5: Fullness

Fullness describes how many percentages that the contour of the object's fitting circle is covered by object pixels. Project the object to another side of the fitting circle with respect to the circle center. If the total object number becomes two, then the fullness of the object is 2 or else the fullness of the object is 1.

G property 6: Radius

Radius of an object is the radius of the object's Fitting Circle.

- Difference Matrix M_{diff} :

Suppose we have two binary images and there are i and j objects within the images, respectively. Compute all six G Properties and put the G Properties 1, 2, 3 and 6 into two property matrices (Equations 4.3 and 4.4).

$$M_{p1}(m, 1 : 4) = \begin{pmatrix} P_{m1}^1 & P_{m2}^1 & P_{m3}^1 & P_{m6}^1 \end{pmatrix} \quad (4.3)$$

$$\text{where : } m = 1, 2 \dots i$$

$$M_{p2}(n, 1 : 4) = \begin{pmatrix} P_{n1}^2 & P_{n2}^2 & P_{n3}^2 & P_{n6}^2 \end{pmatrix} \quad (4.4)$$

$$\text{where : } n = 1, 2 \dots j$$

Where row vector $\begin{pmatrix} P_{m1}^1 & P_{m2}^1 & P_{m3}^1 & P_{m6}^1 \end{pmatrix}$ represents the G properties of the m^{th} object in the first image and row vector $\begin{pmatrix} P_{n1}^2 & P_{n2}^2 & P_{n3}^2 & P_{n6}^2 \end{pmatrix}$ represents the G properties of the n^{th} object in the second image.

Then we have a $i \times j$ difference matrix M_{diff} through Equation 4.5.

$$M_{diff}(m, n) = \left| \frac{1}{4} \sum_{s=1}^6 \left(\frac{P_{ms}^1}{P_{ns}^2} \right) - 1 \right| \quad (4.5)$$

$$\text{where : } s = 1, 2, 3, 6$$

Finally, M_{diff} needs to be adjusted by G properties 4 and 5 of each $M_{diff}(m, n)$. Once one of the G properties 4 or 5 of either the m^{th} object in the first image or the n^{th} object in the second image is not equal to one, $M_{diff}(m, n)$ is reset to a very large number so that this pair of objects cannot be selected as the target result. G properties 4 or 5 sharply reduce the number of irrelative objects.

- Dark Region:

According to the three R properties of the 'C' shape reflection image, the area of the tooling ball within the photo has two types of region: a bright region and a dark

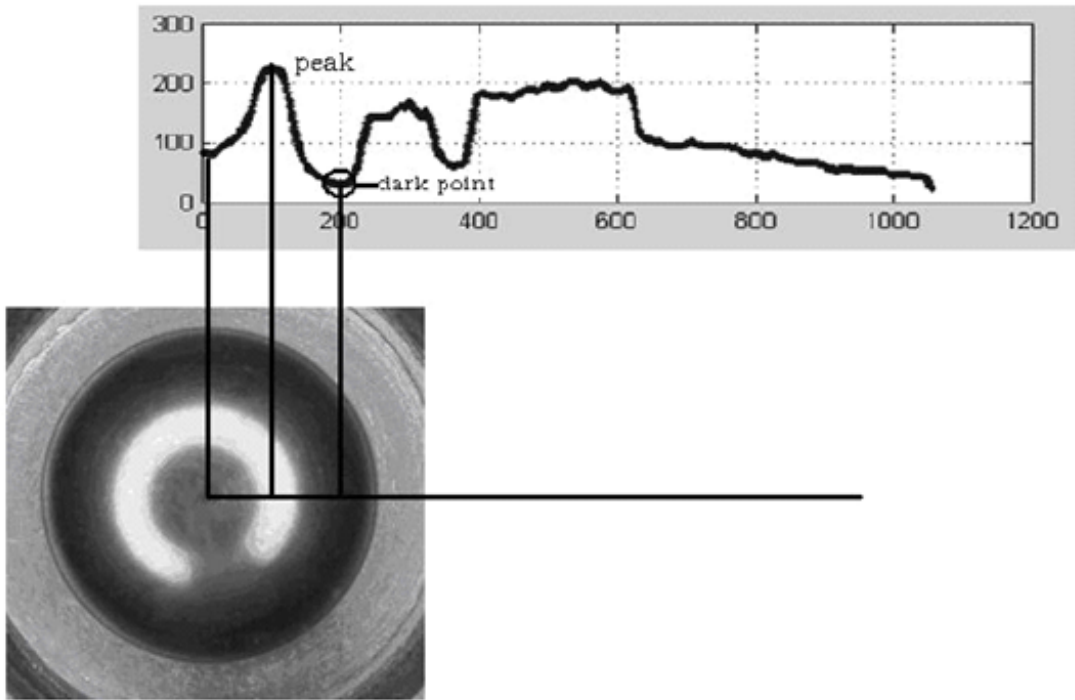


Figure 4.5: Dark Region

region. The dark region is divided into two parts by the bright region. Therefore from the center position of the tooling ball to the outside in any directions the gray value of each pixel has useful characteristics which is shown in Figure4.5. The vertical axis represents the gray value of the pixel and the horizontal axis represents the distance from the tooling ball center to the pixel in that direction. The changing condition of gray values always has a peak first followed by a local minimum. Define the first local minimum as the dark point.

Even if the gray values of the pixels in the direction of where the gap of shape 'C' is, the gray value of the dark point is still the first local minimum after a peak, as is shown in Figure4.6.

- 8 Dark Points:

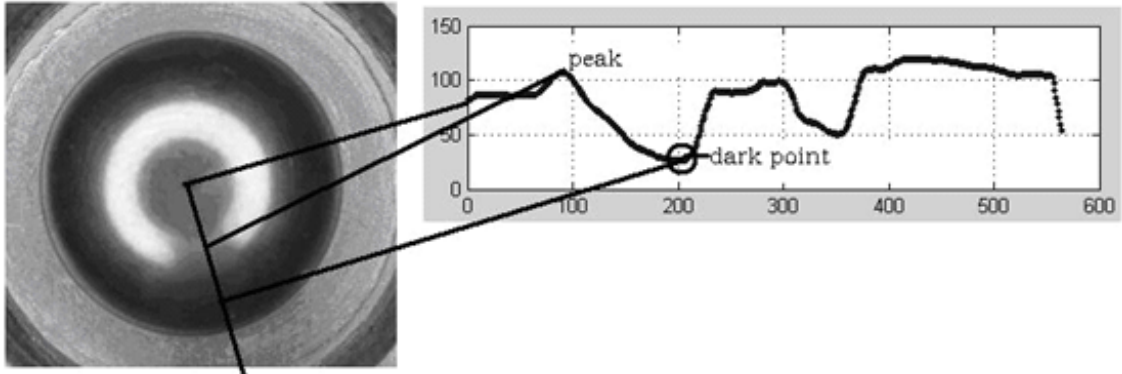


Figure 4.6: Dark Region at the Gap of 'C' Shape

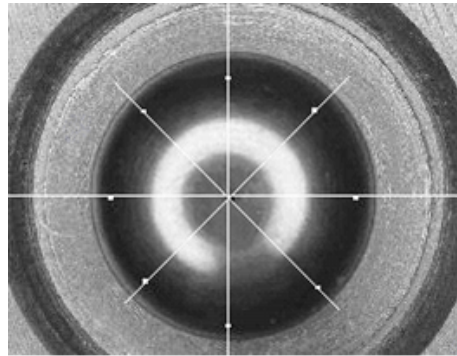


Figure 4.7: 8 Dark Points

Create eight direction vectors from center of tooling ball to the outside. Vectors and Y positive axis of the photo form angles from 0° to 135° with a step increase of 45° . Eight dark points are the dark points along these eight directions. Figure4.7 illustrates one of the examples of these eight dark points.

4.4.2 Procedures for Acquiring Position of Tooling Ball in Photos

A simplified and specialized vision-based tooling ball detecting method is designed as following steps.

Step 1: Set the camera and the light source.

Step 2: Take two photos for the tooling ball from two different positions. Two photos I_1 and I_2 are acquired, and then record two photos taking places in the world coordinate system as $C_1^w = \begin{pmatrix} x_{c1}^w & y_{c1}^w & z_{c1}^w & 1 \end{pmatrix}$ and $C_2^w = \begin{pmatrix} x_{c2}^w & y_{c2}^w & z_{c2}^w & 1 \end{pmatrix}$ respectively.

Step 3: Process and analyze two photos I_1 and I_2 .

Substep 3-1: Apply average filter to get two filtered images I_{a1} and I_{a2} .

Substep 3-2: Threshold I_{a1} and I_{a2} using threshold value of 128 into two binary images I_{t1} and I_{t2} .

Substep 3-3: Segment I_{t1} and I_{t2} into several binary images with only one object inside. Delete objects whose areas are less than 1/1000 of the whole image size. The remaining objects are called the main objects of the two images.

Substep 3-4: Compute the G properties of the main objects.

Substep 3-5: Compute the difference matrix M_{diff} using the G properties of the main objects.

Substep 3-6: Find out the index (i_{tm}, i_{tn}) of the element in M_{diff} with the minimal value. We say the target object 'C' shape reflection image of the tooling ball, within the two images is the tm^{th} object in I_1 and the tn^{th} object in I_2 . The center position of the target object's fitting circle is utilized for finding dark points.

Substep 3-7: Look for eight dark points within the dark region of the tooling ball for two photos.

Substep 3-8: Find the fitting circle of eight-dark points for two photos.

Substep 3-9: Define the fitting circle's center position of eight dark points as the approximate center position of tooling ball within the photo frame.

4.4.3 Transformation from Photo Coordinate System to World Coordinate System

The position transforming procedure cannot be implemented in this project because of the limitation of equipment. The light source and camera used for the experiment are not set exactly the same as is required. Also, the devices are not able to be mounted on the ABB robot. Therefore, the method for position transformation is described in general without being tested.

Firstly, after analyzing the two photos, the position of the tooling ball's spherical center within the photo frame of the two photos is known as $P_1^{photo} = (px_1, py_1)$ and $P_2^{photo} = (px_2, py_2)$. Also the positions of camera for taking the two photos in the world coordinate system are recorded as $C_1^w = \begin{pmatrix} x_{c1}^w & y_{c1}^w & z_{c1}^w & 1 \end{pmatrix}$ and $C_2^w = \begin{pmatrix} x_{c2}^w & y_{c2}^w & z_{c2}^w & 1 \end{pmatrix}$. The focal length of the camera's lens is also known as f .

Secondly, suppose there is a transformation matrix T_{wt} representing the transformation process from the world coordinate system to the photo coordinate system depending on C_1^w , C_2^w and f . Then, according to homogeneous transformation, we can have two position results for a tooling ball from the two photos represented by $P_{ball1}^w = \begin{pmatrix} x_{ball1}^w & y_{ball1}^w & z_{ball1}^w & 1 \end{pmatrix}$ and $P_{ball2}^w = \begin{pmatrix} x_{ball2}^w & y_{ball2}^w & z_{ball2}^w & 1 \end{pmatrix}$.

Then finally, the position of the ball's spherical center with respect to the world coordinate system can be computed by $P_{ball}^w = (P_{ball1}^w + P_{ball2}^w)/2$.

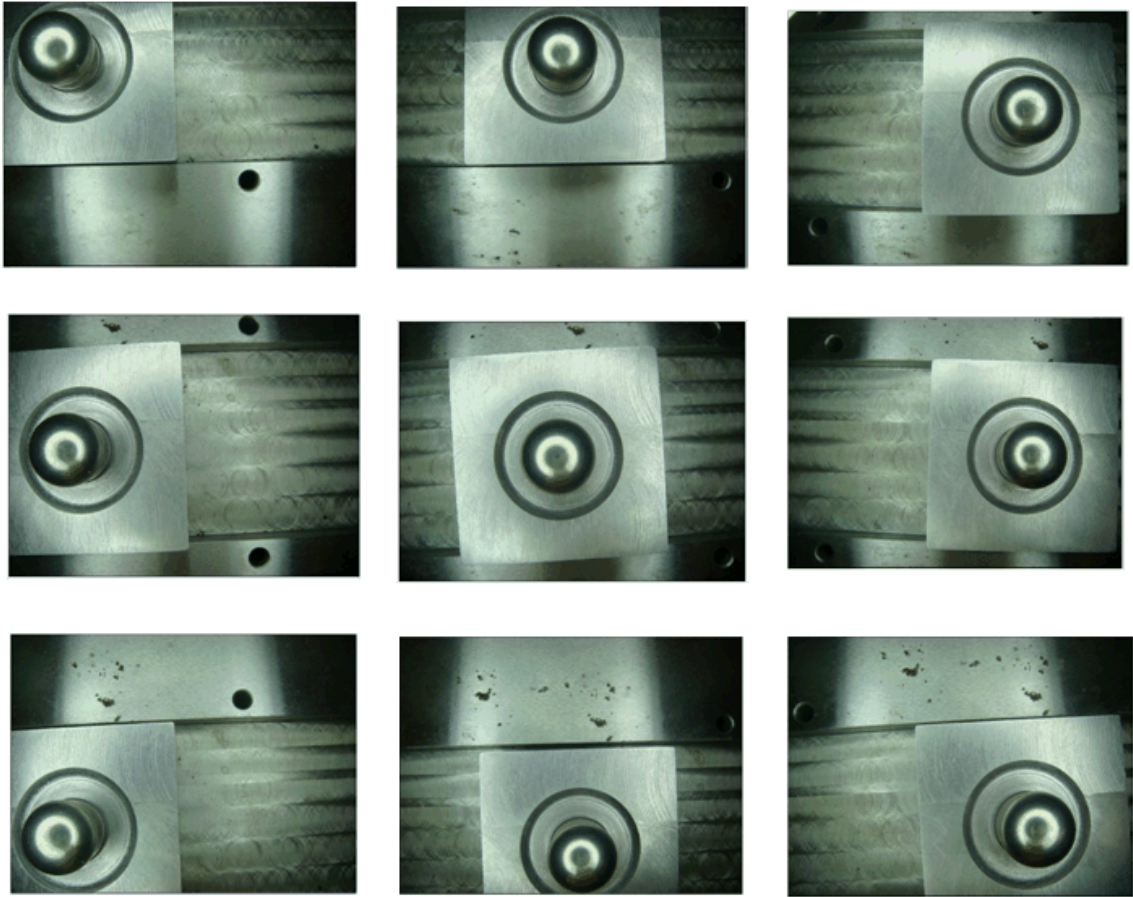


Figure 4.8: 9 Types of Same Photos

4.5 Experiment and Result

- Sample Photos:

There are 50 sample photos taken by camera. The position of the tooling ball within the photos can be separated into nine main types: Center, Up-middle, Up-left, Up-Right, Middle, Middle-left, Middle-right, Down-middle, Down-left and Down-right (Figure4.8).

The background of the photos is a stainless steel block with several holes and edges. Also, the surface of the block is mid-level polished so that it appears to have a similar

optic property as the one of the mould to be calibrated.

- Result: Because there are 50 sample photos in total and any two of them can be selected for each time of detection, there are 1225 combinations for sample photos to be tested. Finally, it was found that all of the 8 dark points within the photos were captured correctly. However, the position of the tooling ball's spherical center in the photo coordinate system is not correct if the center position of the eight dark points' fitting circle is considered as the spherical center. Deviation occurs when the tooling ball locates far away from the middle position of the photo. The reason is that a small part of the dark region (unexpected lightened area) is lightened by the ray which is reflected by the stainless steel block so that the areas of dark region decrease.

Take one of the sample images as an example (Figures 4.9 and 4.10). Eight small white points represent dark points detected. The square white point is the center of the dark points' fitting circle. The round white point is the ideal circle center of the contour of the tooling ball. The position of the tooling ball in the sample image locates at the up-left of the whole image frame and the expected lightened area locates at the bottom-right of the tooling ball. Obviously there is a deviated distance between the actual center of the tooling ball and the circle center of the dark points' fitting circle.

4.6 Chapter Summary

According to the results of the experiment, the target of the course project is achieved, in that the feature of the reflection image is distinguished correctly and the approximate center position of the tooling ball in the photo is detected. Although the position of the tooling ball in the photo coordinate system is detected with some error, the detected

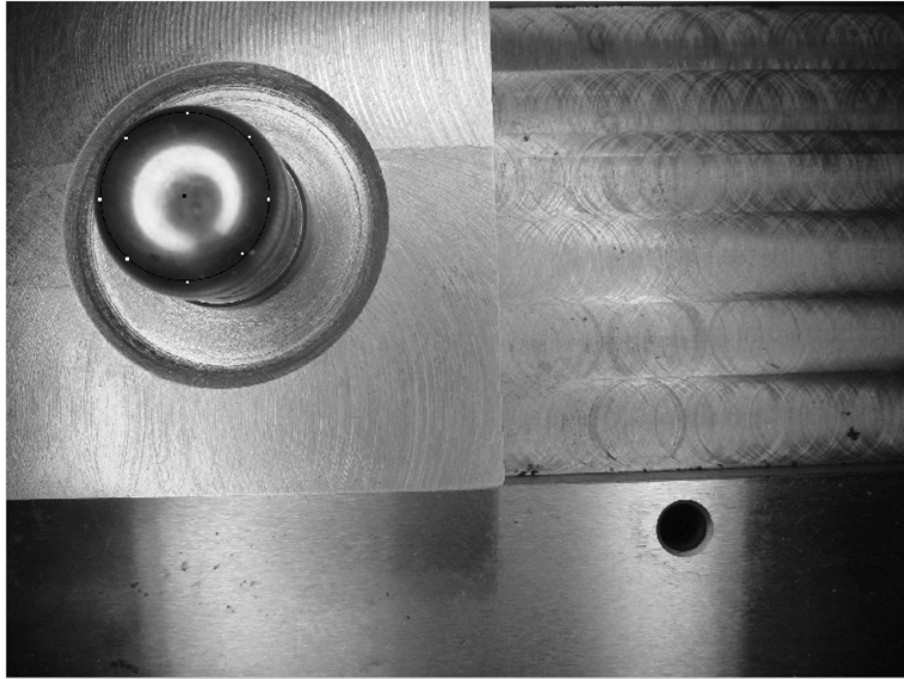


Figure 4.9: A Sample Image for Describing Center Deviation

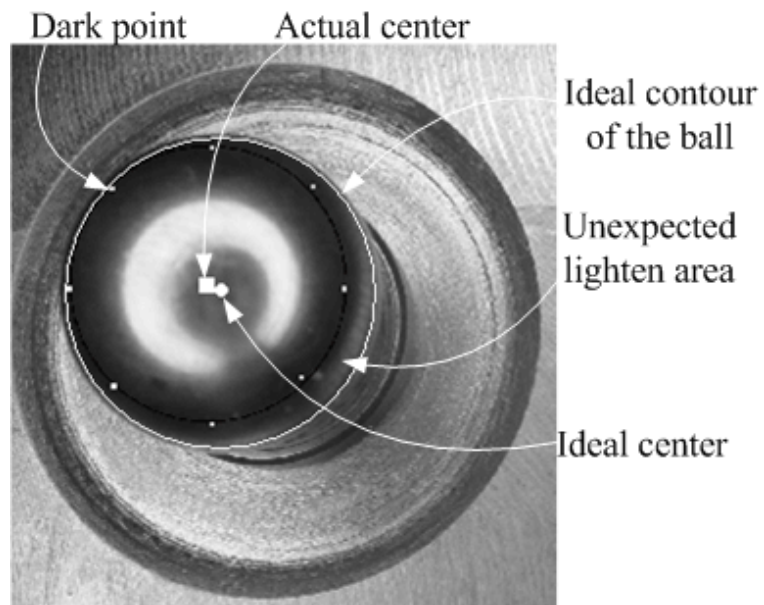


Figure 4.10: Center Deviation

eight dark points are possible to be compensated by doing research on figuring out the relationship between the reflection image and tooling ball's center so that a better fitting circle of compensated dark points can be created to give better results.

The mechanical touching detecting method described in Chapters 2 and 3 have not been tested in the ABB robot system for detecting the tooling ball when the mould is heated up to about $700F^{\circ}$. However, high heat is a potential threat to the durability of the detector. The experiment proves the feasibility of the vision-based detecting method and, as a result, the vision-based detecting method can be applied to compensate for the mechanical touching detecting method.

Divide the mould calibration process into two steps: cold calibration and hot calibration. The tooling ball can be firstly be detected by the mechanical touching method when the mould is cold, obtaining position data in cold status. Since the mould will be extended by the heat when it is heated, the position of the tooling ball will be changed within a certain range. According to the position data in cold status, the camera with a partial ring-shaped light source is carried by the robot arm to the positions tooling ball when the mould is cold. After taking photos and applying the vision-based detecting method designed, the position data of the tooling ball in hot status can be obtained. The whole process can be controlled fully automatically so that dangerous working environment can be avoided.

Chapter 5

Conclusion

5.1 Thesis Summary

The design of a mechanical touch-style tooling ball detecting method for the mould calibration process in the project of automatic TIG welding is described in this thesis from Chapter 1 to Chapter 3. The design includes the mechanical design of the detector (the mechanical component design), the programming design in the microprocessor for signal processing (the electrical component design) and the design of the position computing programmed in the robot controller (the computational component design).

The mechanical component has been implemented and tested base on the NC milling machine as mentioned in Chapter 3. While the feasibility of the detecting method is proven, the accuracy of the position detection of the tooling ball does not satisfy the requirement especially on the Z_w of the milling machine under the present design. The problem may occur during the process of calibrating the joystick, where a good input-output relationship is not obtained. Three deficiencies are thus to be improved for obtaining a better joystick calibration result.

- Changing the connecting method between the bearing housing and the centering shaft in order to obtain an accurate distance for computing the slopes of input-output relationship curves.
- Changing the mechanism of deflecting and rotating the shaft of the joystick or adjusting the material of the shaft extension in order to avoid generating scores on the shaft extension caused by the bearing balls.
- Using multi-meter with a higher accuracy to obtain better voltage measuring results.

Electrical components and computational components have been programmed and tested on a personal laptop without being tested in an actual robot system. Further experiments and improvements are still required:

- Improving the AD conversion process and serial communication process.

For AD conversion and serial communication purposes, an ARM7 microprocessor is not the best choice. However, it is the most convenient choice for testing the feasibility. It is better at selecting better chips for achieving these two processes. The converting accuracy of an AD converter in a microprocessor is just 10 bits and the maximum convertible voltage input is only 2.48V. If we can specialize the AD conversion process by a chip with higher accuracy and convertible voltage value (MAX187 with 12 bits accuracy of conversion, for instance), the electrical component can be designed to be more integrated and more durable.

- Stabilizing the operating voltage supplied to the joystick at 5V by DC stabilizer.

A cell phone charger was used to provide DC power to the joystick. The output voltage is 5.11V which locates within the range of allowance. However, if the voltage was stabilized to 5V (as was recommended in the technical specifications of the

joystick), the input-output relationship of the joystick would not need to be recalibrated. Furthermore, the data from Elobau Sensor Technology regarding the joystick can even be used to evaluate the performance of the design of the joystick calibration.

- More research about error analyzing is required.

Errors exist in the mechanical machining and assembling process, the AD conversion and signal communication process, and the position data of the ABB robot obtaining process. How these errors affects the final result of position computation needs to be analyzed.

- Integrate the tooling ball detecting system with the whole ABB robot system and test the performance.

Though the mechanical component has been tested on the NC milling machine, the settings of the joystick coordinate system, the detecting operation, the calibration of the detector and the working environment all need to be changed if the detecting processes are tested in the robot system.

- Test the detecting method on tooling balls with different dimensions.

The detecting method is tested based on only one tooling ball with a diameter of 15.85mm. It is necessary to test it on a differently dimensioned series of balls to obtain the detecting range and the range of tooling ball sizes that can be detected by the detecting method.

Finally, a vision-based tooling ball detecting method is also taken into consideration to compensate for the performance of a mechanical style touching style detecting method in environments with high temperature. The idea is only roughly proven here and further works is required.

5.2 Future Work

Further developments of the detecting method is described in general by following points.

- Improve the mechanical design of the joystick calibration mechanism and the detector.
- Stabilize the operating voltage of the joystick.
- Increase the convertibility of AD conversion process and the stability of serial communication process.
- Integrate the detecting method with the ABB welding robot system.
- Test the accuracy, repeatability, heat resistance and the durability of the detecting method.
- Analyze the reasons that cause position errors in the tooling ball detecting process.

APPENDICES

Appendix A

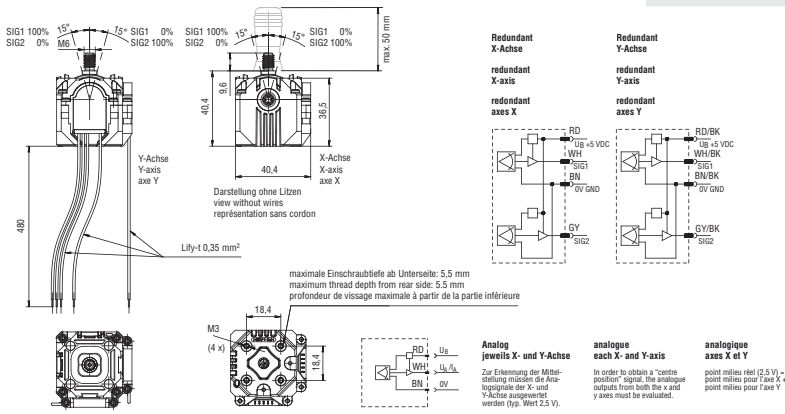
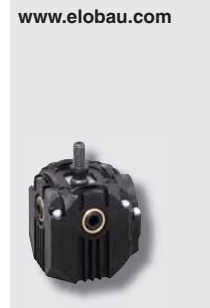
Technical Specifications of Joysticks and Tactile Switch

Joysticks
Joysticks
Joysticks

www.elobau.com

J1

Joystick – kleine Bauform
Joystick – small version
Joystick – version compacte



Der Winkelbereich beträgt $\pm 15^\circ$. Das Messprinzip ist kontaktlos; beim analogen Messprinzip dreht sich ein Magnetfeld um einen Hallsensor. Bei analoger Ausführung ist das System kurzschlussicher (bei unbegrenzter Kurzschlussdauer) gegen Spannungsversorgung. J1 ist mit 6/8/10- oder 12-PIN Molex 5557 Stecker ausgerüstet. Alternativen auf Anfrage.

The angular operating range is $\pm 15^\circ$. The operating principle is non-contacting: – analogue: rotating magnetic field over hall-sensor Short circuit-proof with analogue version (short circuit duration: unlimited) toward power supply. J1 has a 6/8/10 or 12 PIN Molex 5557 connector, alternatives on request.

Le débattement angulaire est $\pm 15^\circ$. Le principe de mesure est sans contact: – analogique: champ magnétique tournant sur détecteur à effet Hall Protégé contre les courts circuits avec version analogique (durée de court circuit: illimitée) en sens alimentation. J1 est équipé avec 6/8/10 ou 12 broches Molex 5557, alternative sur demande.

Technische Änderungen vorbehalten.
We reserve the right to change specifications without notice.
Sous réserve de modifications techniques.

Kabelsätze siehe S. 366 (L2.D001A)
Cable sets see p. 366 (L2.D001A)
Câbles associés voir p. 366 (L2.D001A)

285

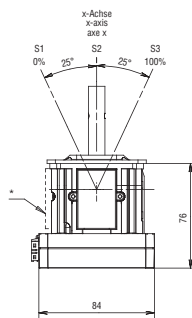
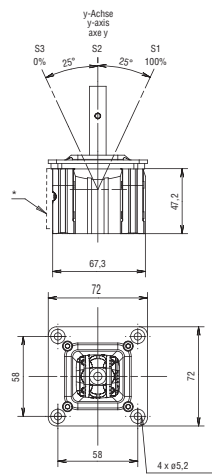
Figure A.1: J1R6AAA00 Copied from: Elobau Sensor Technology

Joysticks
Joysticks
Joysticks

www.elobau.com

J6

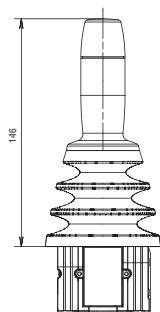
Joystick – kompakte Bauform
Joystick – compact design
Joystick – version compacte



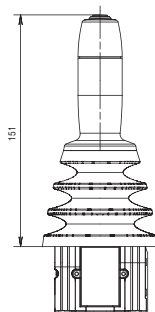
Ausführung Elektronikgehäuse CAN
Construction with electronic case CAN
Construction avec boîtier électronique CAN

* Aufbauhöhe für Ausführung Digital / Redundant
panel thickness for execution digital / redundant
épaisseur pour exécution digital / redondant

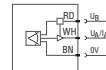
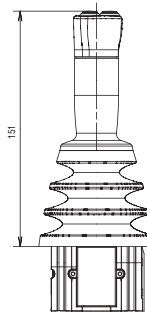
Standardgriff ohne Microtaste
Standard knob without micro button
Poignée standard sans micro-touche



Standardgriff mit Microtaste
Standard knob with micro button
Poignée standard avec micro-touche

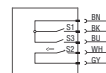


3-Tasten-Griff – max. 3 Microtasten
3-button knob – max. 3 micro button
Poignée à 3 touches – max. 3 micro-touches



Analog jeweils X- und Y-Achse
Zur Erkennung der Mittelstellung müssen die Analogsignale der X- und Y-Achse angeschlossen werden (typ. Wert 2.5 V).

analoge each X- and Y-axis
In order to obtain a „centre position“ signal, the analogue outputs from both the x and y axes must be evaluated.



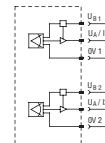
analogische axes X et Y
point milieu réel (2.5 V) = point milieu pour l'axe X + point milieu pour l'axe Y

digital jeweils X- und Y-Achse
Zur Erkennung der Mittelstellung müssen beide Kontakte S1 der X- und Y-Achse UND verküpfelt werden.

digital axes X et Y
point milieu réel = point milieu pour l'axe X + point milieu pour l'axe Y

digital each X- and Y-axis
In order to obtain a „centre position“ signal, contact S1 of both x and y axes must be closed.

— Darstellung in Mittelstellung (S2 betätigt)
shows with knob in centre position (S2 operated)
état des contacts en position milieu



Redundant jeweils X- und Y-Achse
redundant each X- and Y-axis
redundant axes X et Y

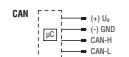


Figure A.2: J6R6AAA00 Copied from: Elobau Sensor Technology

Technical Specification of B3F5000 Tactile Switch


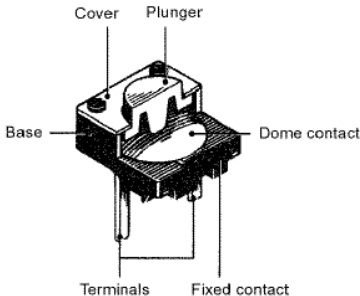
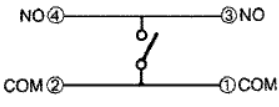
Type	Plunger Type (Color)	Switch height x pitch	Operating force	Model
Long service life	Flat (Blue) 	4.3 x 12.5 mm	General-purpose: 130 g	B3F-5000
Weight	Approx. 0.85 g			
Contact form	SPST-NO			
Switching capacity	1 to 50 mA, 5 to 24 VDC (resistive load)			
Contact resistance	100 M Ω max. (Initial Value, Rated: 1mA, 5VDC)			
Insulation resistance	100 M Ω min. (at 250 VDC)			
Dielectric strength	500 VAC, 50/60 Hz for 1 minute			
Bounce time	5 ms max.			
Vibration	Malfunction durability: 10 to 55 Hz, 1.5 mm double amplitude			
Shock	Mechanical durability: 1,000 m/s ² (approx. 100 G) Malfunction durability: 100 m/s ² (approx. 10 G)			
temperature	-25° to 70°C (with no icing)			
Humidity	35% to 85% RH			
Life Expectancy	10,000,000 operations min			
Pre-travel (PT)	0.3 +0.2/-0.1 mm			
Construction		Contact Form		
				

Figure A.3: B3F5000 Tactile Switch Copied from: Omron Electronic Components LLC

Appendix B

Programs

B.1 Program in Microprocessor

```
#include "config.h"
#define EINT0 14 /* Interrupt NO of EINT0 */
#define EINT3 17 /* Interrupt NO of EINT3 */
#define UART0 6 /* Interrupt NO of UART0 */
extern void DelayNS (uint32 dly)
{
uint32 loop;

for ( ; dly>0; dly--)
for (loop=0; loop<5000; loop++);
}
uint32 ToASCII(uint32 data0)
{
```

```

    uint32 data;
    if (data0<=9) data = data0+48;
    else data = data0+55;
    return data;
}
uint32 GetByte (void)
{
    uint32 RecByte;
    RecByte = UORBR;
    return (RecByte);
}
void GetStr(uint8 *s, uint32 n)
{
    for (;n>0;n--)
    {
        *s++ = GetByte();
        if ( (UOLSR & 0x01)==0 ) break;
    }
}
void __irq IRQ_Eint0(void)
{
    extern ADC_Data[4];
    uint32 ADC_DataM;
    extern SendData[14];
    extern ADCmark;
    uint8 s; //loop counter of UART0 data sending
    uint8 i; //normal used loop counter (including ADC)

```

```

if (ADCmark == 0)
{
    ADCmark = 1;
    /* initialization of ADC process */
    ADCR = (1 << 0) |
        ((Fpclk / 1000000 - 1) << 8) |
        (0 << 16) |
        (0 << 17) |
        (1 << 21) |
        (0 << 22) |
        (1 << 24) |
        (0 << 27);
    DelayNS(10);
    ADC_DataM = ADODR;
    for (i = 0; i < 4; i++)
    {
        ADCR = (1 << i) |
            ((Fpclk / 1000000 - 1) << 8) |
            (0 << 16) |
            (0 << 17) |
            (1 << 21) |
            (0 << 22) |
            (1 << 24) |
            (0 << 27);
        DelayNS(10);
        ADC_DataM = ADODR;
        ADCR = (1 << i) |

```



```

        ((Fpclk / 1000000 - 1) << 8) |
        (0 << 16) |
        (0 << 17) |
        (1 << 21) |
        (0 << 22) |
        (1 << 24) |
        (0 << 27);
DelayNS(10);
    while ((ADODR & 0x80000000) == 0);
    ADC_DataM = ADODR;
    ADC_DataM = ADC_DataM >> 6;
    ADC_DataM = ADC_DataM & 0x000003FF;
    ADC_Data[i] = ADC_DataM;
    IOOPIN = IOOPIN & 0xFFFFF7F;
    DelayNS(100);
    IOOPIN = IOOPIN | (0x01 << 7);
    DelayNS(100);
    IO1PIN = 0x03 << 18 + i*2; //LED Status Display2 -Finished
    DelayNS(100);
    ADC_DataM = 0x00000000;
}

//following program is for data processing
//so that the data can be converted into suitable format to be sent
SendData[0] = (ADC_Data[0] & 0x00000F00) >> 8;
SendData[1] = (ADC_Data[0] & 0x000000F0) >> 4;
SendData[2] = (ADC_Data[0] & 0x0000000F);
SendData[3] = (ADC_Data[1] & 0x00000F00) >> 8;

```

```

SendData[4] = (ADC_Data[1] & 0x000000F0) >> 4;
SendData[5] = (ADC_Data[1] & 0x0000000F);
SendData[6] = (ADC_Data[2] & 0x00000F00) >> 8;
SendData[7] = (ADC_Data[2] & 0x000000F0) >> 4;
SendData[8] = (ADC_Data[2] & 0x0000000F);
SendData[9] = (ADC_Data[3] & 0x00000F00) >> 8;
SendData[10] = (ADC_Data[3] & 0x000000F0) >> 4;
SendData[11] = (ADC_Data[3] & 0x0000000F);

SendData[0] = ToASCII(SendData[0]);
SendData[1] = ToASCII(SendData[1]);
SendData[2] = ToASCII(SendData[2]);
SendData[3] = ToASCII(SendData[3]);
SendData[4] = ToASCII(SendData[4]);
SendData[5] = ToASCII(SendData[5]);
SendData[6] = ToASCII(SendData[6]);
SendData[7] = ToASCII(SendData[7]);
SendData[8] = ToASCII(SendData[8]);
SendData[9] = ToASCII(SendData[9]);
SendData[10] = ToASCII(SendData[10]);
SendData[11] = ToASCII(SendData[11]);
SendData[12] = 0x24;
SendData[13] = 0x26;
for (s=0;s<14;s++) U0THR = SendData[s];
while ((U0LSR & 0x20) == 0);
}
while( (EXTINT&0x01)!=0 )

```

```

    {
        EXTINT = 0x01;
    }
    VICVectAddr = 0x00;
}
void __irq IRQ_Eint3(void)
{
    extern ADCmark;
    ADCmark = 0;
    while( (EXTINT&0x08)!=0 )
    {
        EXTINT = 0x08;
    }
    VICVectAddr = 0x00;
}
uint32 ADC_Data[4];
uint32 SendData[14];
uint8 ReceiveData[14]; // UART0 buffer for receiving data
uint8 ADCmark;
uint8 SendMark;
int main (void)
{
    const uint32 baud = 19200;
    uint32 mid;//mid number for computing baud rate
    uint8 s; //loop counter of UART0 data sending
    //uint8 r; //loop counter of UART0 data receiving
    PINSEL0 = PINSEL0|0x00000005;

```

```

//UART0 and GPIO
PINSEL1 = PINSEL1|0x15400301;
//AD0.0 ~ AD0.3; EINT0(KEY1) and EINT3(KEY5)
PINSEL2 = PINSEL2|0x00000000;
//LED0 ~ LED8 GPIO
IODIR = 0x01 << 7;
DelayNS(200); //BEEP
IOOPIN = IOOPIN | (0x01 << 7); //stop beeping
IO1DIR = 0xFF << 18; //LED
IO1PIN = 0x00 << 18; //Turn on all LEDs
//initialization of UART0
//setting of baud
UOLCR = 0x80;
mid = (Fpclk/16)/baud;
UODLM = mid >> 8;
UODLL = mid & 0xFF;
//UART initialization
UOLCR = (3 << 0) | //3->8Char,
        (0 << 2) | //0-1 stop,1-2 stops,
        (1 << 3) | //0-disable/1-enable odd/even
        (1 << 4) | //odd/even selection
        (0 << 6) | //0-disable/1-enable interval sending
        (0 << 7); //divider lock

//FIFO setting
UOFCR = 0x81;
UOIER = 0x01;
//IRQ Setting

```

```

EXTMODE = 0x00;
//set EINT0 and EINT3 activated by level
EXTPOLAR = 0x00;
IRQEnable();
//Enable the function of IRQ
//open EINT0, EINT3 and UART0
VICIntSelect = 0x00000000;
//set all the interrupt as the IRQ
VICVectCntl0 = 0x20 | EINT0;
//set EINT0 to IRQ0
VICVectAddr0 = (uint32)IRQ_Eint0;
//address assignment for EINT0
//VICVectCntl1 = 0x20 | UART0;
//set UART0 to IRQ1
//VICVectAddr1 = (uint32)IRQ_UART0;
//address assignment for EINT3
VICVectCntl2 = 0x20 | EINT3;
//set EINT3 to IRQ2
VICVectAddr2 = (uint32)IRQ_Eint3;
//address assignment for EINT3
EXTINT = 0x09;
//clear the IRQ mark of EINT0 and EINT3
VICIntEnable = (1 << 14) | (1 << 17);
// Enable EINT0 and EINT3
ADCmark = 0;
SendMark = 0;
while(1)

```

```

{
    IO1PIN = 0x03 << 18;
//LED Status Display3 - Waiting for IRQ
    DelayNS(200);
    IO1PIN = 0x0C << 18;
    DelayNS(200);
    IO1PIN = 0x30 << 18;
    DelayNS(200);
    IO1PIN = 0xC0 << 18;
    DelayNS(200);
    if ( (UOLSR & 0x01) == 1 )
    {
        GetStr(ReceiveData, 14);
        if ((ReceiveData[0] == 0x53) && (ReceiveData[1] == 0x41)) //'SA'
        {
            for (s=0;s<14;s++) UOTHR = SendData[s];
        }
        else if ((ReceiveData[0] == 0x4F) && (ReceiveData[1] == 0x4B)) //'OK'
        {
            for (s=0;s<14;s++) UOTHR = ReceiveData[s];
        }
        else
        {
            for (s=0;s<14;s++) UOTHR = 0x57; //'W'
        }
        ADCmark = 0;
    }
}

```

```
    }  
    return 0;  
}
```

B.2 RAPID Code for Computational Component

```
%%  
    VERSION: 1  
    LANGUAGE: ENGLISH  
%%  
  
MODULE MainModule  
  
    PERS BallNum;  
    VAR num i;  
    VAR string OutStrCL{14};  
    VAR num OutByteCL{14};  
    VAR string OutStrSA{14};  
    VAR num OutByteSA{14};  
    VAR string OutStrOK{14};  
    VAR num OutByteOK{14};  
    VAR iodev channel;  
    PRES bool flag;  
    VAR pos TCPpos;  
    VAR num TCPx;  
    VAR num TCPy;
```

```
VAR num TCPz;

!-----

VAR bool RecChec;
PERS string rec;
VAR string rec1;
VAR string rec2;

!-----

VAR string aVstr1;
VAR num aVnum;
VAR string bVstr1;
VAR byte bVbit;
VAR string bVstr2;
VAR num bVnum;
VAR bool TempChec;
VAR num Vnum{4};

!-----

VAR num k{4};
VAR num Vcx;
VAR num Vcy;
VAR num Amax;
VAR num Ax;
VAR num Ay;

!-----

VAR num L;
VAR num dx;
VAR num dy;
VAR num dz;
```



```

VAR num dt;
PERS num X;
PERS num Y;
PERS num Z;
!-----
PROC main ()
    BallNum := 0;
    FOR i FROM 1 TO 14 STEP 1 DO
        OutStrCL{i} := StrPart ("CL000000000000", i, 1);
        OutByteCL{i} := StrToByte(OutStrCL{i}\Char);
    ENDFOR
    FOR i FROM 1 TO 14 STEP 1 DO
        OutStrSA{i} := StrPart ("SA000000000000", i, 1);
        OutByteSA{i} := StrToByte(OutStrSA{i}\Char);
    ENDFOR
    FOR i FROM 1 TO 14 STEP 1 DO
        OutStrOK{i} := StrPart ("OK000000000000", i, 1);
        OutByteOK{i} := StrToByte(OutStrOK{i}\Char);
    ENDFOR
    Open "com1:", channel \Bin;
    ClearIOBuff channel;                ! Clear input buffer for com1
    flag := TRUE
    WHILE flag = TRUE Do
!Voltage string receiving
        RecChec := FALSE;
        WHILE RecChec = FALSE
            ClearIOBuff channel;        ! Clear input buffer for com1

```

```

rec1 := ReadStrBin(channel,14 \600);           ! Wait for input from com1
rec2 := ReadStrBin(channel,14 \600);           ! Wait for input from com1
IF rec1 <> rec2 THEN
    WriteBin channel, OutByteSA, 14;
ELSE
    rec := rec1;
    WriteBin channel, OutByteOK, 14;
    RecChec := TRUE;
ENDIF
ENDWHILE
TCPpos := CPos(\Tool:=tool0 \WObj:=wobj0);
TCPx := TCPpos.x;
TCPx := TCPpos.y;
TCPx := TCPpos.z;
!Voltage translation
FOR i FROM 1 TO 4 STEP 1 DO
    aVstr1 := StrPart(rec,i*3-2,1);
    TempChec := StrToVal(aVstr1,aVnum);
    bVstr1 := StrPart(rec,i*3-1,2);
    bVbit := StrToByte(bVstr1\Hex);
    bVstr2 := ByteToStr(bVbit);
    TempChec := StrToVal(bVstr2,bVnum);
    Vnum{i} := aVnum*256+bVnum;
ENDFOR
!parameter value assignment
k{1} := 0.5;
k{2} := 0.5;

```

```

k{3} := 0.5;
k{4} := 0.5;
Vcx := 2500;
Vcy := 2500;
Amax := 15;
FOR i FROM 1 TO 4 STEP 1 DO
    Vnum{i} := Vnum{i}/k{i};
ENDFOR
!Angle translation
Ax := ( (Vnum{3}-Vcx)*Amax/Vcx + (Vcx-Vnum{4})*Amax/Vcx )/2;
Ay := ( (Vnum{2}-Vcy)*Amax/Vcy + (Vcy-Vnum{1})*Amax/Vcy )/2;
!Position computation
a := Cos(Ax)*Sin(Ay);
b := Cos(Ay)*Sin(Ax);
c := Cos(Ax)*Cos(Ay);
X := (a*L+TCPx+dx)*Cos(dt)+(b*L-TCPy-dy)*Sin(dt);
Y := (a*L+TCPx+dx)*Sin(dt)-(b*L-TCPy-dy)*Cos(dt);
Z := c*L+TCPz+dz;
BallNum := BallNum + 1;
ENDWHILE
Close channel;
ENDPROC
ENDMODULE

```

Bibliography

- [1] Tool-Tec Welding Inc. Full Proposal Document. 2007. 2
- [2] William H.Minnick. *Gas Tungsten Arc Welding handbook*. Goodheart-Willcox Pub, 1996. 3
- [3] ABB Automation Technologies AB Robotics. *Operating manual, IRC5 with FlexPendant*. 2004. 6
- [4] William W.Melek. *ME547: Robot Manipulators: Kinematics, Dynamics, and Control*. 2009. 6
- [5] R.B. Fisher D.W.Eggert, A.Lorusso. Estimating 3-D rigid body transformations: a comparison of four major algorithms. *Machine Vision and Applications*, 9:272–290, 1997. 10
- [6] Zhang Defen Zhang Cuoxiong. The Optimal Plan for Measuring Center and Radius of a Ball Part by 4-Point Method. *Acta Metrologica Sinica*, 14(4):247–250, 1993. 16
- [7] Timothy J. Gill John A. Hanlon. Machine tool locator. *United States Patent*, 6301007, 2001. 17
- [8] D. Scott Ackerson Robert E. Bridges, Lawrence B. Brown. Retroreflector for use with tooling ball. *United States Patent*, 5861956, 1999. 17

- [9] Tsing-Wong Hsu Louis J. Everett. Method and apparatus for locating physical objects. *United States Patent*, 5177563, 1993. 17
- [10] Hideaki Hashimoto. obot hand including optical approach sensing apparatus. *United States Patent*, 4766322, 1988. 17
- [11] Shinsuke Sakakibara Hajimu Inaba. Gripping device. *United States Patent*, 4423998, 1984. 17
- [12] Hidekazu Araki all of Kadoma Japan Katsuhiko Sasada, Tomoharu Nakahara. Method of Utilizing a Two-dimensional Image for Detecting the Position, Posture, and Shape of a Three-dimensional Objective. *United States Patent*, 5692061, 1997. 17
- [13] Hidekazu Araki Hiroyuki Fujii Haisong Gu, Tomoharu Nakahara. 3-Dimensional object recognition method and bin-picking system using the method. *United States Patent*, 6721444, 2004. 17
- [14] Hua Zhang Ligong Zhou. *Introduction to ARM7*. Beijing University of Aeronautics and Astronautics, 2005. 38
- [15] K. Levenberg. A method for the solution of certain non-linear problems in least squares. *Quarterly of Applied Mathematics*, 2:164–168, 1944. 70
- [16] Help Document of Matlab 7. 82, 101
- [17] Abdul Al-Azzawi. *Light and optics: principles and practices*. CRC/Taylor and Francis, 2006. 98
- [18] Vaughan Pratt. Direct Least-Squares Fitting of Algebraic Surfaces. *Computer Graphics*, 21(4), 1987. 101
- [19] Han Sun Mingwu Ren, Jingyu Yang. Tracing Boundary Contours in a Binary Image. *Image and Vision Computing*, 20:125C131, 2002. 102

- [20] Holbrook L Horton Henry H. Ryffel Christopher J. McCauley Ricardo Heald Erik Oberg, Franklin D. Jones. *Machinery's handbook*. Industrial Press, 2008.